MAPPING DEEP STRUCTURE IN NESS COUNTY, KANSAS
FOR CO_2 STORAGE CHARACTERIZATION

A Thesis

Presented to

the Faculty of the Department of Natural Sciences and Mathematics

University of Houston

In Partial Fulfillment

of the Requirements for the Degree

Master of Science

By

Shannon Nicole LeBlanc

May 2011

MAPPING DEEP STRUCTURE IN NESS COUNTY, KANSAS

FOR CO_2 STORAGE CHARACTERIZATION

_____
Shannon Nicole LeBlanc

_____
Dr. Chris Liner

_____
Dr. Robert Stewart

_____
John Smythe

_____
Dean, College of Natural Sciences and Mathematics

MAPPING DEEP STRUCTURE IN NESS COUNTY, KANSAS
FOR CO_2 STORAGE CHARACTERIZATION

An Abstract of a Thesis

Presented to

the Faculty of the Department of Natural Sciences and Mathematics

University of Houston

In Partial Fulfillment

of the Requirements for the Degree

Master of Science

By

Shannon Nicole LeBlanc

May 2011

ABSTRACT

This project uses 3D seismic data and sparse well control from the Dickman field to map pre-Pennsylvanian formations in the Dickman Field area. This study focuses on formations in the lower Mississippian (Osage and Gilmore City) and in the Ordovician (Viola). The primary storage candidate in the Dickman field is a deep saline aquifer located in the Osage formation. Deep saline aquifers are excellent potential CO2 storage candidates, but significant pre-storage characterization is required to determine suitability.

The main objective is to investigate possible CO_2 migration pathways. Both time and depth structure maps of the Osage, Gilmore City and Viola formations were produced and interpreted. Several seismic attributes were interpreted to highlight small faults and fractures. Seismic attributes such as coherence, variance, curvature, SPICE, and ANT play a vital role in validating the interpreted discontinuities. Discontinuities were classified as probable, possible, or doubtful.

Allowing for data quality, there are 4 out of the 17 discontinuity picks considered to be probable small faults or fractures; 3 of the 4, trend northeast-southwest in agreement with the orientations reported by Nissen et al. (2010). According to Nissen et al., these northeast-southwest trending lineaments are likely to block fluid flow. Therefore, our Osagian aquifer, the primary storage candidate in the Dickman field, seems to be promising for CO_2 storage.

CONTENTS

INTRODUCTION.....1

BACKGROUND.....3

Geology.....3
CO_2 Storage.....5
Study Area.....10
Description of the data.....11

METHODOLOGY.....14

Work Plan.....15
Synthetic Generation.....17
Horizon tracking and picking discontinuities.....23
Structure Maps.....27
Isopach Maps.....34
Attribute analysis 37

RESULTS.....45

Amplitude.....45
Coherence.....52
Variance.....56
Curvature.....61
SPICE.....67
ANT (from Variance) Tracking.....71

DISCUSSION.....76

CONCLUSION.....84

INTRODUCTION

The focus of this study is to map deep structure in Ness County, Kansas and determine if a deep saline aquifer has the potential to be a CO_2 storage candidate. The primary method of testing this hypothesis is by locating and quantifying faults and fractures in and around the saline aquifer. Many seismic attributes are analyzed in order to aid fault/fracture identification. The DOE-funded Carbon Capture and Storage (CCS) group at the University of Houston is investigating the potential for CO_2 storage in the Dickman Field. The Dickman 3D seismic survey is approximately 3.325 square miles (Figure 1) and the field has produced about 1.7 million barrels of oil since its discovery in 1962. My work is based on 3D seismic data from the Dickman field and SMT KINGDOM software was used for interpretation. Previous Dickman studies include depth structure of the Permian Stone Coral (Califf, 2010), and the value of seismic attributes in geologic modeling of the Fort Scott formation (King, 2010, in preparation). Ongoing studies include structure of the Mississippian unconformity (B. Flynn), rock properties and amplitude on the Mississippian unconformity (J. Parker), and other detailed geologic investigations. I focus on deeper formations in the lower Mississippian and Ordovician.

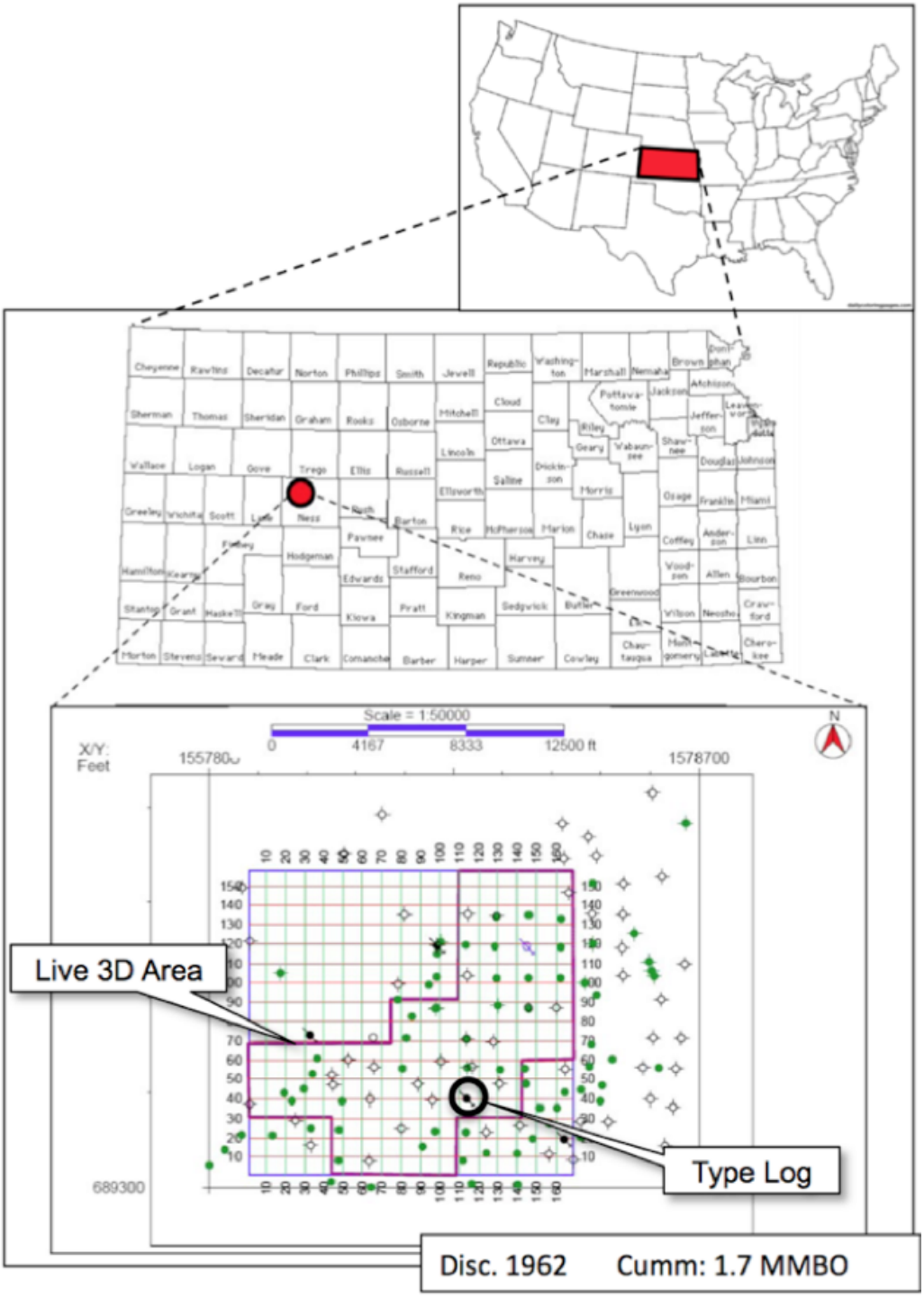

Figure 1: Location map of 3D Seismic area (3.325 sq. mi.), 142 wells: 54 in 3D area, 45 with digital logs [GR (43), Resistivity (25), Neutron (27), P-Sonic (6), Density (3)], 7 with core [porosity and permeability], 3 full deep saline aquifer penetration (Liner et al., 2010).

BACKGROUND

Geology

The storage target being investigated in this study is a porous saline aquifer that lies above the Gilmore city (lower Mississippian) formation and at the base of the overlying Osage formation. This aquifer is a primary sequestration target whereas the upper Mississippian is a secondary target. Above the area of this study is a slight structural closure in the fractured Mississippian unconformity, a section of porous and solution-enhanced shelf carbonate that produces oil. The oil/water contact is at approximately 1981 ft. (603.8 m) subsea and there is an oil column of about 35 ft. (10.7 m). At the Mississippian/Pennsylvanian boundary there is a prominent incised channel (observed on 3D seismic). Between the Mississippian and the overlying Pennsylvanian shale and conglomerates of the Cherokee Group there is a regional unconformity contact which is a karst surface. There is also an oil reservoir made up of sandstones from the Lower Cherokee group that are locally deposited on the sub aerial karst (Liner et. al., 2010).

The stratigraphic column of Kansas is shown in Figure 2. Starting with the deepest formation of interest, the Viola formation mainly contains a mixture of dolomite and limestone with some cherty beds also present throughout the strata. The dolomite is dominant in the North Kansas basin but in some areas of the basin more “earthy and granular limestones are present, especially at the base” (Jewett et al., 1968). Overlying the Viola is the Gilmore City formation, separated by the Gilmore City

(GMC) unconformity which has NW and NE fractures as sinkholes (Liner, 2010). Jewett et al. (1968) states, "The Gilmore City Limestone consists of noncherty, soft, chalky limestone enclosing granules of broken calcareous fossils...The Gilmore City Limestone of Kansas occurs northeast and west of the Central Kansas uplift."

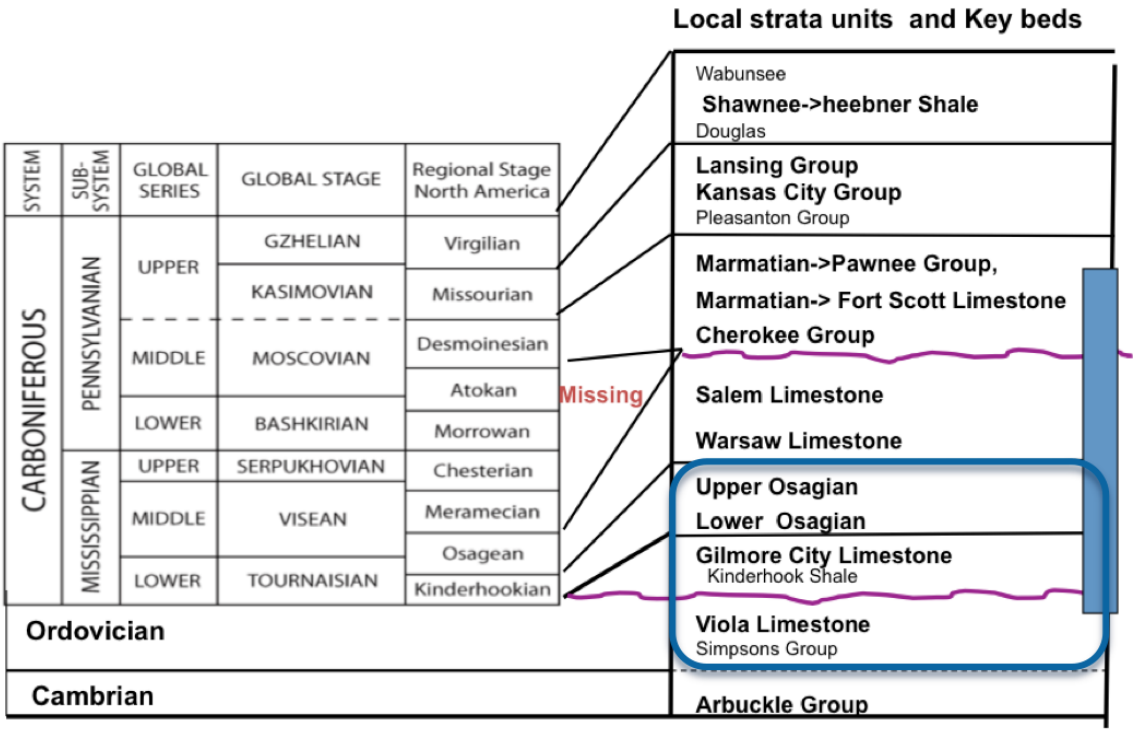

Figure 2: Stratigraphic chart of the Dickman area. Chart to the left is the stratigraphic rank, chart to the right is the correlatable local stratigraphic units. The bolded names were recognized with better confidences in the subsurface of the studied area, and the vertical blue bar indicate the target for the geological model and flow simulation grid (Modified from Sawin et al., 2008).

Above the Gilmore City carbonate is the Osage formation. The Osage includes a deep saline aquifer in the Dickman Field and is the prime focus of study in determining if this aquifer is a suitable CO_2 storage candidate. Shallower formations in the Dickman area include the Warsaw-Salem carbonate strata above the Osage which is speculated to affect the distribution of primary porosity within the reservoir as well

as somewhat resisting diagenesis, fracturing, and erosion (Liner, 2010). Prolonged post Mississippian exposure of the Warsaw-Salem and karst development associated with fractures resulted in fractured zones, pressure solution zones and karst breccia zones, which increase hydraulic conductivity of the reservoir. The Lower Cherokee was deposited on the unconformity surface resulting in sandstone reservoirs. Overlying the Lower Cherokee is the Fort Scott Limestone, possibly acting as a hydrocarbon seal. Post Pennsylvanian folding and fracturing formed a NE35-oreineted fold normal to the axis of the Central Kansas Uplift (CKU) which resulted in 20-40 ft. (6-12 m) closures in the NE direction. There was post-Pennsylvanian faulting on the NW side of the fold, which leaves us with a sealing NE Boundary Fault in the Dickman project area (Liner et. al., 2010). Nissen et al. (2010) concludes that there are two primary fault/fracture orientations, one northeast and the other northwest. Based on the geology and production data from nearby fields they suggest "the northeast-trending lineaments appear to be barriers to fluid flow, and may represent fractures filled with low-permeability clay and silt, while the northwest-trending lineaments appear to represent open fractures, which serve as conduits into the underlying aquifer."

CO_2 Storage

In the United States alone, there is an estimated 5,600 million metric tons/year of greenhouse gas emissions from fossil fuel combustion, mostly carbon dioxide (National Energy Technology Laboratory, 2010). These numbers give the U.S.

incentive to research and fund Carbon Capture and Storage (CCS) studies. As this is not only a concern in the U.S., CCS was first formally addressed at the international level in 1992 at the First International Conference on Carbon Dioxide Removal in Amsterdam (Sawyers and Wilson, 2010). Statoil first applied CCS technologies in 1996 at the Sleipner gas field in the North Sea, (Sawyers and Wilson, 2010) with CO_2 storage in a saline sandstone aquifer. Carbon Capture and sequestration (CCS) involves mitigating greenhouse gas emissions by first capturing the CO_2 at a plant/industrial facility, compressing it, transporting it (via pipeline), then injecting the CO_2 back into the earth (Fang et. al., 2010). CO_2 can also be injected into diminishing oil fields to enhance recovery (Figure 3, Plasynski et. al, 2007).

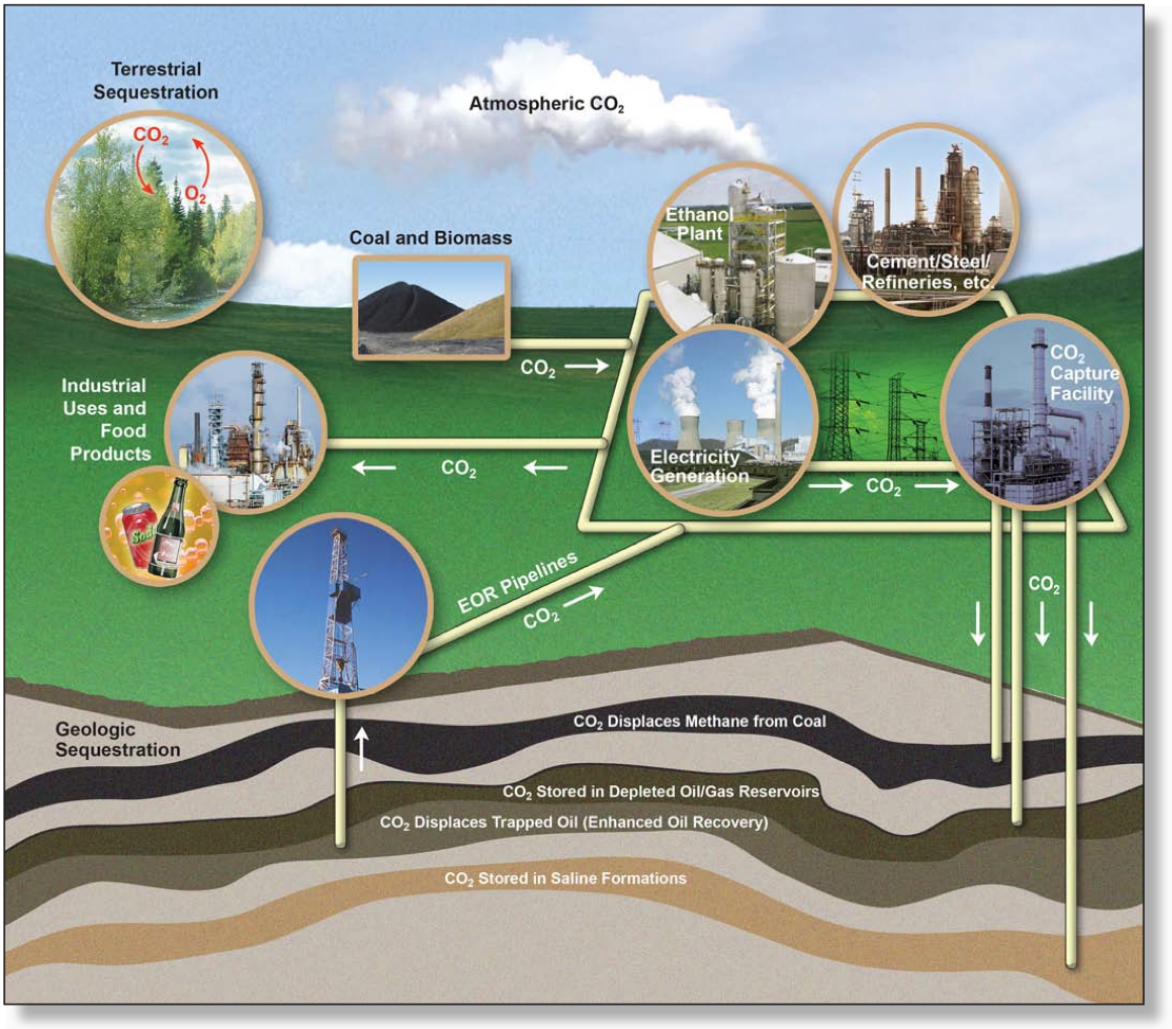

Figure 3: Overview of CO2 sequestration concepts and targets (Plasynski et al., 2007).

Some of the primary requirements for CO_2 storage include appropriate size, depth, geologic structures, porosity and permeability, and the absence of drinking water. The size of the potential storage reservoir must be large enough to store significant quantities of CO_2 (megaton range). Depth of the reservoir must be sufficient for CO_2 to become a supercritical fluid (Figure 4). Geologic structures also have to be considered. An important requirement for storage is absence of faults and fractures

that might serve as possible CO_2 migration pathways. There must also be a permeable overlying seal (cap rock) so that CO_2 cannot migrate upwards. Porosity and permeability in the potential storage reservoir must be high so that a sufficient volume of CO_2 can be injected into the reservoir. And lastly, the CO_2 must not be injected into or near a site of aquifers intended for human consumption or activities. Retention of injected CO_2 is vital, with current U.S. DOE standards calling for, "the amount of CO_2 retained in appropriately selected and managed reservoirs is very likely (probability of 90-99 percent) to exceed 99 percent over 100 years and is likely (probability of 66-90 percent) to exceed 99 percent over 1,000 years" (Plasynski et. al., 2007).

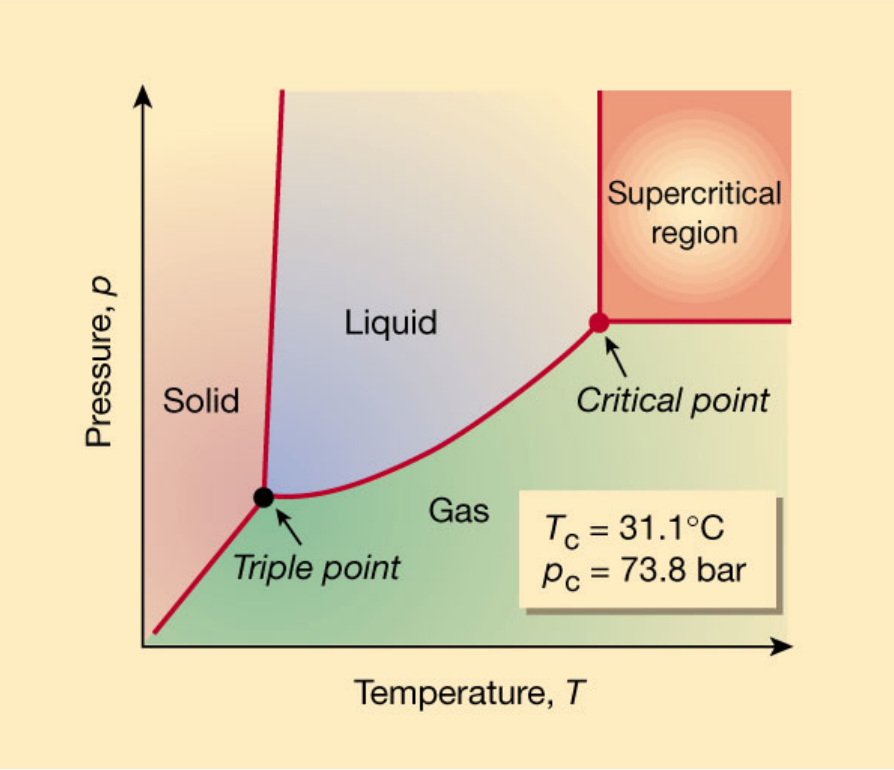

Figure 4: CO_2 phase diagram (Leitner, 2000). The Dickman Osage aquifer maps to the supercritical region.

The proposed storage candidates for CO_2 are deep geological formations such as depleted oil reservoirs, deep saline aquifers and unmineable coal seams. Deep saline aquifers are large, have high CO_2 storage capacity and few well penetrations, all properties of the aquifer associated with the Osage, Gilmore City and Viola formations in the Dickman area. In a saline aquifer, CO_2 becomes a supercritical fluid beyond 31.1 °C and 7.38 MPa as shown in Figure 4, corresponding to a depth of 4,081 ft. (1.24 km). These are preferred conditions (supercritical fluid) for CO_2 storage candidate because the CO_2 will have a high density like a fluid but it will be mobile like a gas (Yang et. al., 2010). Quick development of supercritical fluids can ultimately lead to a precipitation of solids. Depending on the pressure and temperature, the supercritical CO2 can have a density ranging from 150 kg/m^3 to over 800 kg/m^3 in a saline aquifer. Figure 5 shows that "considering normal conditions with a surface temperature of 15 °C and a geothermal gradient of 30 °C/km, CO2 density increases rapidly with depth and then remains stable" (Yang et. al., 2010).

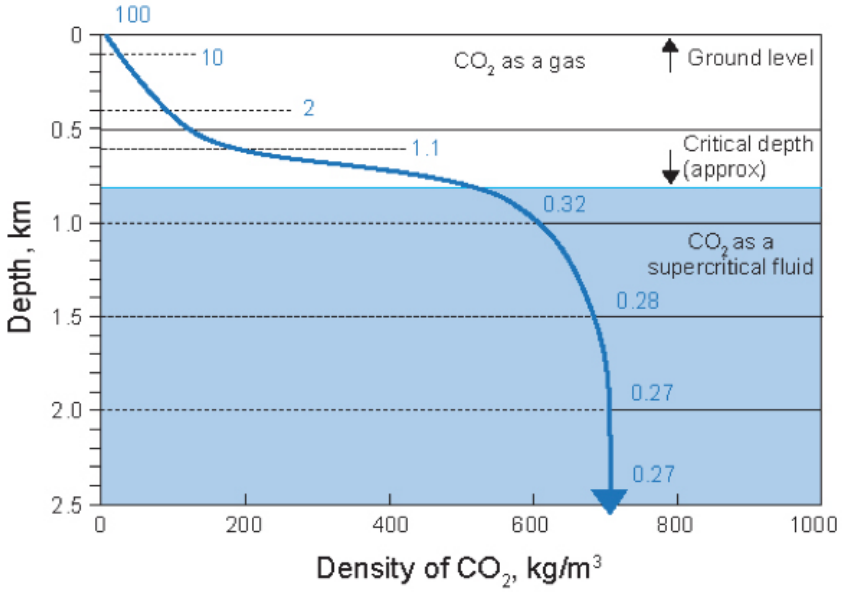

Figure 5: Density of CO2 vs. depth under normal conditions, 100 m^3 of CO_2 at surface would occupy 0.32 m^3 at 1 km (Yang et. al., 2010).

Study Area

The saline aquifer in the Dickman field is the primary storage candidate. It is part of the Western Interior Plains and Ozark Plateau aquifers that extend for several hundred thousand square miles. In our study area the thickness of the saline aquifer is about 70 ft. (21 m) thick. It has a water flow velocity of about 40 ft. (12.2 m) per million years meaning that injected CO2 will not migrate to the surface by means of aquifer water flow (Liner, 2010). Deep saline aquifers are ideal storage candidates because after injection, the supercritical CO2 first dissolves, then it ultimately precipitates carbonate minerals. "The reactions among CO2, brine and formation minerals play an important role in formations with a large number of proton sinks, such as feldspar and minerals…some reactions may be beneficial to storage, but others may result in migration pathways" (Yang et. al., 2010). Therefore, depending

on the geological, geochemical and hydrological conditions, these reactions must be thoroughly investigated in order to guarantee safe storage of the carbon dioxide. Investigation of CO2 sequestration involves the use of simulation models and numerous monitoring techniques in order to have a better understanding of how CO2 flows.

Description of the data

In 2001 a 3D seismic survey, approximately 3.325 square miles, was conducted in the Dickman Field. Survey acquisition parameters are shown in Table 1 and acquisition geometry is shown in Figure 47. Figure 48 shows shallow evidence of acquisition footprint (0.428 sec timeslice).

Source	Vibroseis
Sweep	20-128 Hz, 12 s
Shot interval	165 ft, 45 deg NW-SE
Shot line interval	880 ft
Receiver interval	220 ft
Receiver line interval	660 ft
Time sample rate	2 ms
Interpolated bin size	82.5 x 82.5 ft
Inlines, Crosslines	158, 169

Table 1: Acquistion parameters of the Dickman 3D seismic survey.

Original data processing was by Sterling Seismic Services, but we worked with a prestack time migration volume generated at the U of Houston Allied Geophysical

Lab (processing workflow in Figure 6). Dominant frequency in the data is around 35 hertz giving vertical resolution ($\lambda/4$) in our area of interest is approximately 113 ft. (34 m) and the lateral resolution ($\lambda/2$) is about 226 ft. (69 m).

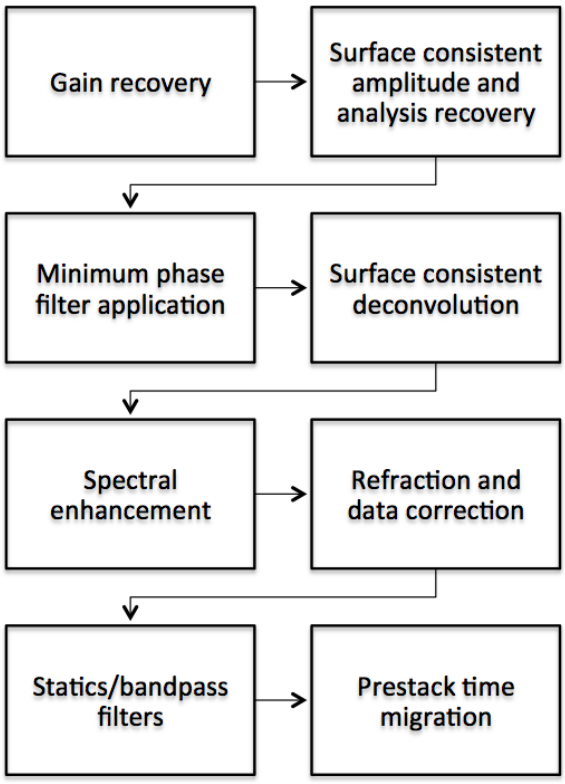

Figure 6: Seismic data processing workflow.

There are 142 wells in the Dickman Field but only four wells that penetrate the deep horizons of this study as shown in Figure 7. The Humprey 4-18, Stiawalt 3 and Sidebottom 6 wells have picks for the Osage, Gilmore City and Viola formations (Table 2). The Schaben 4 well only penetrates the Osage and Gilmore City formations.

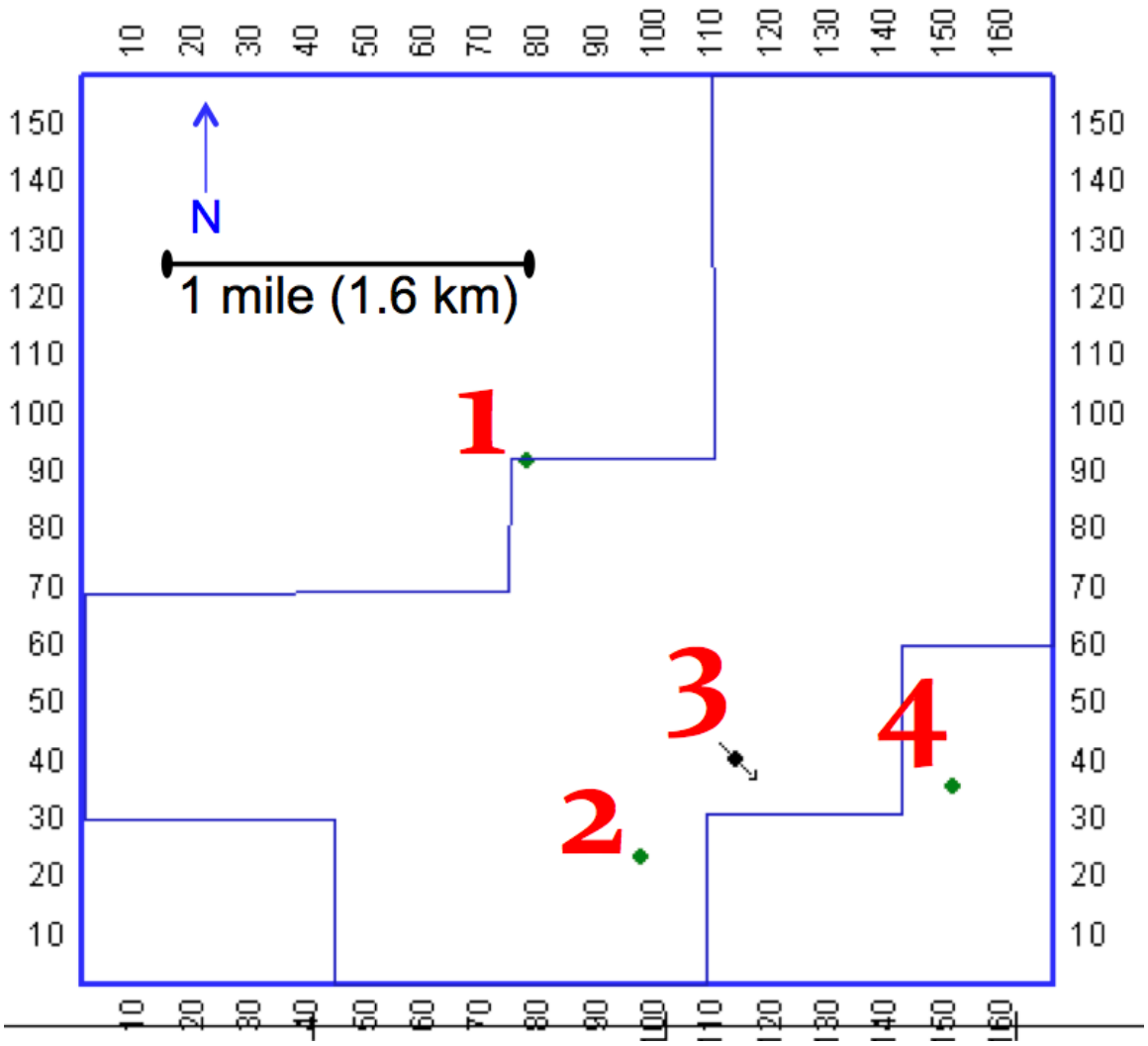

Well	Formation	Top (SS ft)
1. Humphrey 4-18	Viola	-2163
2. Schaben 4	Gilmore City	-2135
3. Stiawalt 3	Viola	-2260
4. Sidebottom 6	Viola	-2239

Figure 7: Deep penetrations in Dickman area and detail table.

METHODOLOGY

Investigation of the deep saline aquifer is primarily seismic due to minimal well control. The purpose of this investigation is to use seismic attributes to map fractures and yield contributing evidence that this deep saline aquifer can be an adequate storage candidate for CO_2. It has already been confirmed from previous studies by that there are indeed fractures beneath the Mississippian unconformity. Nissen et al. uses a map of dip magnitude (figure 8a) to show major regional structural trends computed from the top of the Mississippian surface.

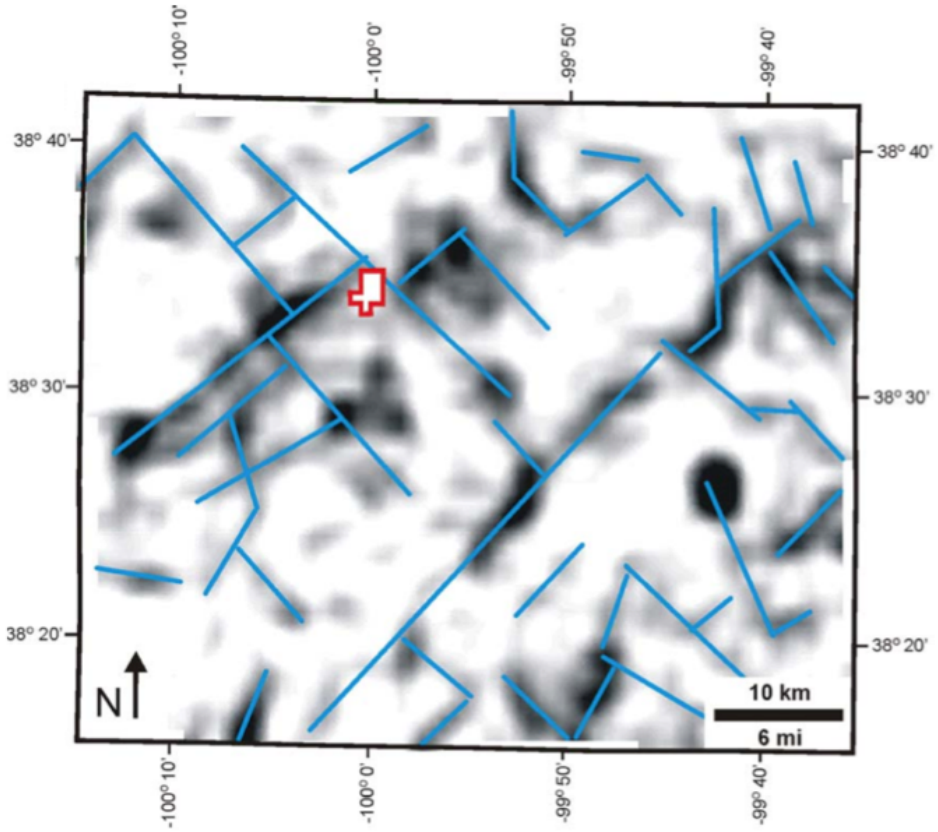

Figure 8a: "Dip map of the top of Mississippian surface (from well tops) for Ness County. Black indicates high dip. Interpreted lineaments are shown in blue. High dip magnitude lineaments are likely to represent either faults or sediment drape over deeper faults. Location of the Dickman Field 3-D seismic survey is outlined in red." Current survey outline is larger than the survey in this figure. Nissen et al. (2009).

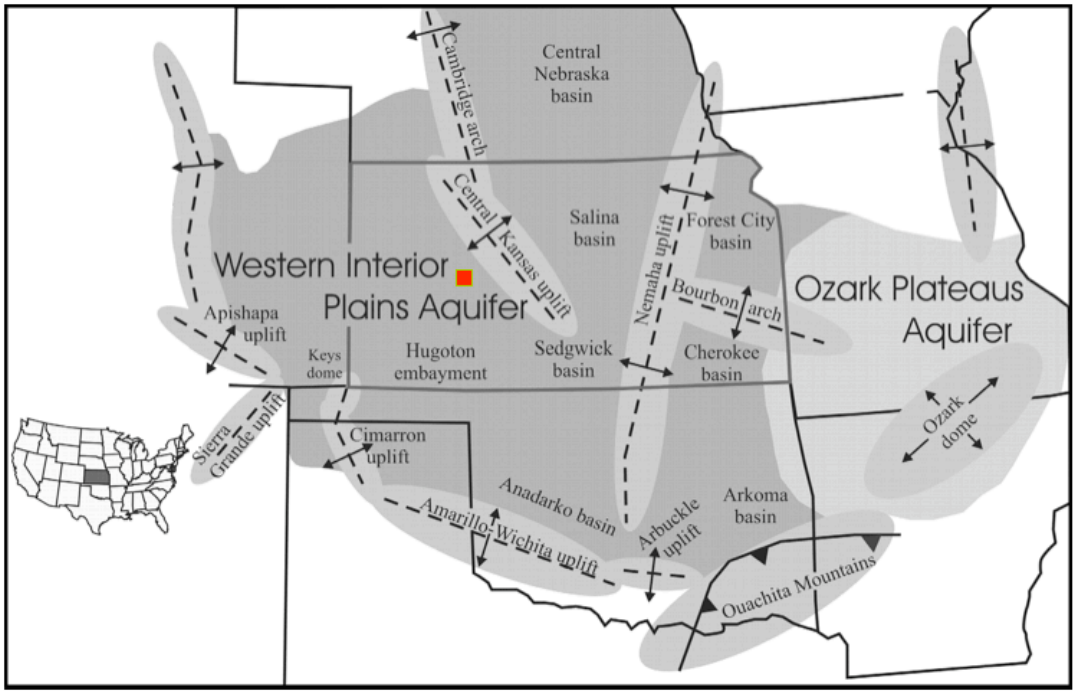

Figure 8b: "Deep saline aquifer system under the state of Kansas (From Carr et al, 2005), with red square indicating location of the Dickman project simulation area" Liner (2009). Major structural trends labeled.

The orientations of these underlying fractures are most likely directly related to the fault orientation above (Nissen et. al., 2009). Although the saline aquifer (storage target) is located at the Osage formation it is still essential to map formations below as they may have an association with the structure above. Figure 8b displays the deep saline aquifer system under the state of Kansas and highlights the major structural trends in Kansans to indicate main directions of regional stress.

Work Plan

Figure 9 shows a workflow of mapping deep structure for the Dickman Field in Ness County, Kansas. The Dickman field geology was first tied to the 3-D seismic volume by creating synthetic seismograms using the two wells that have sonic and density logs (Humphrey 4-18 and Sidebottom 6). This confirms the time/depth relationship of the Osage, Gilmore City and Viola formations in the seismic, which then allows horizon picking throughout the volume. After finalizing the synthetics, Osage, Gilmore City and Viola horizons were tracked throughout the 3D image area to create time and depth structure (using T-D curve from Elmore 3 well) maps. Isopach maps were created subsequent to structure maps. Small faults and fractures were picked throughout the seismic volume first on amplitude data, then SPICE for better visualization of discontinuities. No fault/fracture picks were made in horizontal view, they were only made in vertical section (amplitude and SPICE). Several different attributes were then used for surface mapping and validation of discontinuity picks made in amplitude and SPICE to further classify them as probable, possible or doubtful.

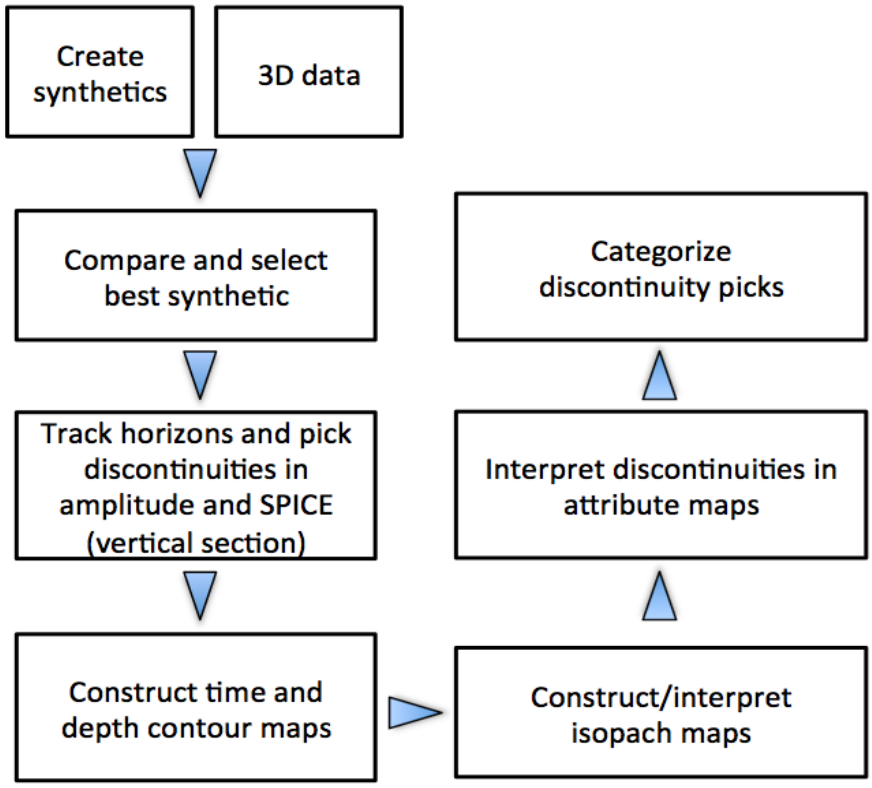

Figure 9: Project workflow.

Synthetic Generation

The conclusion was made that only two out of the four deep wells (Tables 2 and 3) were viable for synthetic seismogram generation, specifically Sidebottom 6 and Humphrey 4-18. Synthetic seismograms were created for each of these wells, but there were a few problems:

1) The Humphrey 4-18 is on the edge of the 3D seismic area

2) The Sidebottom 6 is ~750 ft. (229 m) outside the 3D seismic area

3) Both synthetics had a correlation coefficient well below 0.1

4) Humphrey 4-18 has questionable density and sonic logs

Well	Osage Top	GLC Top	Viola Top	Total Depth	Sonic Coverage (MD)	Density Coverage (MD)
1) Sidebottom 6	**-2063 ft. SS** 4460 ft. MD 1359 m MD	**-2119 ft. SS** 4516 ft. MD 1376 m MD	**-2239 ft. SS** 4636 ft. MD 4313 m MD	4976 ft. MD 1517 m MD	255-4980 ft. 78-1518 m	3500-4957 ft. 1067-1511 m
2) Humphrey 4-18	**-2033 ft. SS** 4470 ft. MD 1362 m MD	**-2105 SS** 4542 ft. MD 1384 m MD	**-2163 SS** 4600 ft. MD 1403 m MD	4604 ft. MD 1403 m MD	186-4594 ft. 57-1400 m	0-4579 ft. 0-1396 m
3) Schaben 4	**-2028 ft. SS** 4406 ft. MD 1343 m MD	**-2135 ft. SS** 4513 ft. MD 1376 m MD	**N/A**	4551 ft. MD 1387 m MD	N/A	N/A
4) Stiawalt 3	**-2055 ft. SS** 4450 ft. MD 1356 m MD	**-2128 ft. SS** 4523 ft. MD 1378 m MD	**-2260 ft. SS** 4655 ft. MD 1419 m MD	4900 ft. MD 1494 m MD	N/A	N/A
DH 4-18 (Relocated Well)	**-2033 ft. SS** 4470 ft. MD 1362 m MD	**-2105 SS** 4542 ft. MD 1384 m MD	**-2163 SS** 4600 ft. MD 1403 m MD	4604 ft. MD 1403 m MD	186-4594 ft. 57-1400 m	0-4579 ft. 0-1396 m
DS-6 (Relocated Well)	**-2055 ft. SS** 4450 ft. MD 1356 m MD	**-2128 ft. SS** 4523 ft. MD 1378 m MD	**-2260 ft. SS** 4655 ft. MD 1419 m MD	4976 ft. MD 1517 m MD	255-4980 ft. 78-1518 m	3500-4957 ft. 1067-1511 m

Table 2: Deep wells in Dickman Field showing sonic and density log intervals SS = subsea, MD = measured depth, DH 4-18 = "Dummy" Humphrey 4-18, and DS-6 = "Dummy" Sidebottom 6.

Sidebottom 6	Humphrey 4-18
• Density (errors) • RHOB (errors) • RHOB_CLIP • Sonic	• DT (errors) • DT_CLIP • RHOB (errors) • RHOB_CLIP

Table 3: Logs Available for synthetics.

To address problems 1 and 2, the Humphrey 4-18 and Sidebottom 6 were 'moved' about 0.5 mile (0.8 km) so that they now lie inside the 3D seismic area by creating mock (dummy) wells DH-4-18 and DS-6, see Figure 10. This is justified since most horizons are laterally continuous (layer cake geology). These dummy wells were placed inside the survey area, away from edge effects, but as near as possible their

original locations. They also contained all the same well parameters as their original well, except the DS-6 used tops from the Stiawalt 3 since it is slightly closer than the original Sidebottom 6 well.

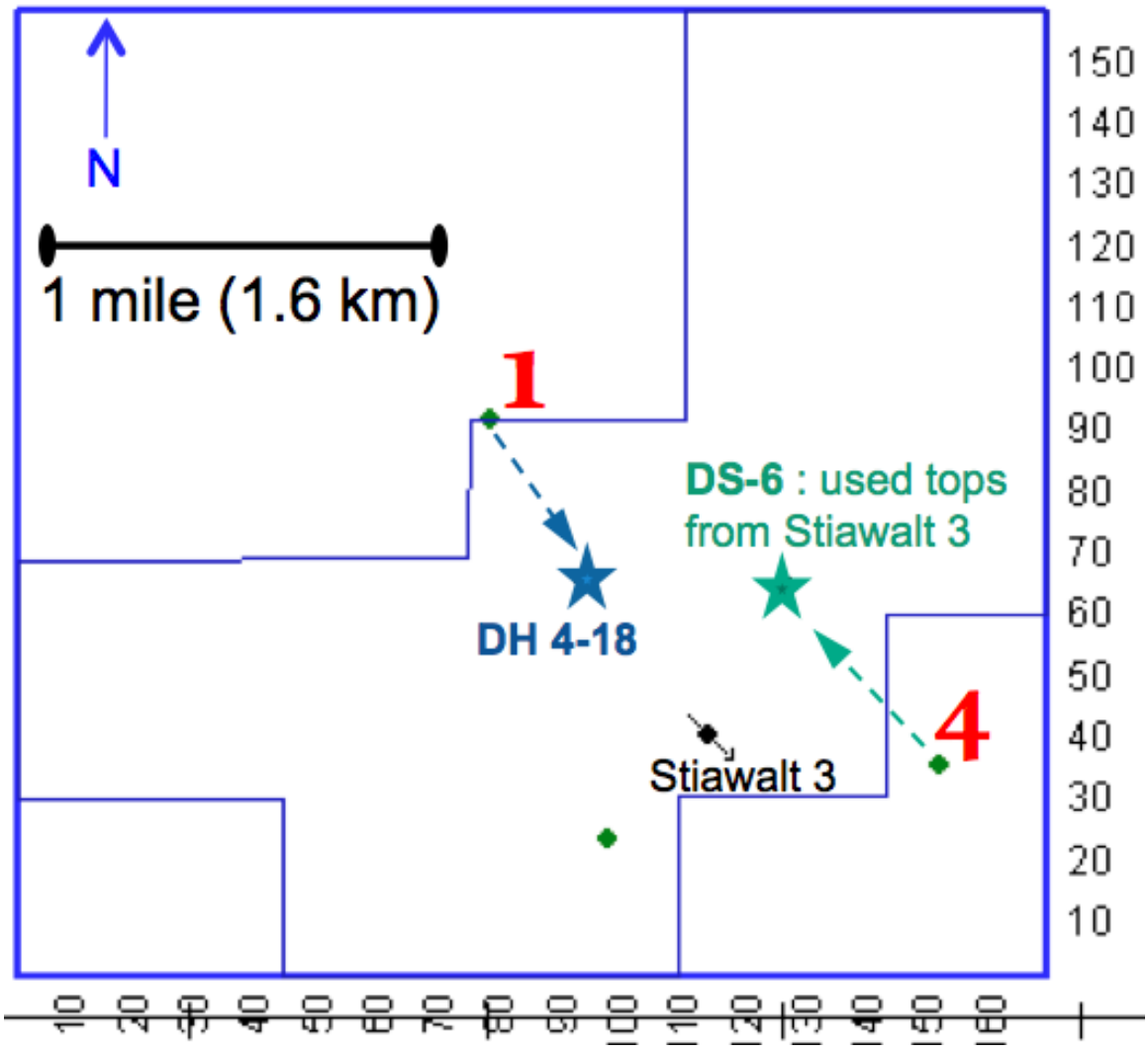

Figure 10: Key wells Humphrey 4-18 and Sidebottom 6 were located on the edge or outside survey area. To create synthetics these were relocated about a half mile into survey to "dummy" well locations.

Synthetic parameters for both DH-4-18 and DS- 6 include a wavelet extraction using a 500 ft. (152 m) radius at the dummy location, sample interval of 2 milliseconds, wavelet length of 0.1 seconds, and time interval 0.75–1.25 s.

The DH-4-18 synthetic used both a clipped density and a clipped sonic log to avoid unrealistic spikes in the log data. The field wavelet was extracted from 116 3D seismic traces and the synthetic correlation coefficient was R=0.115 before any phase shift was attempted. The phase shift (PS) that produced the best visual match was -180 degrees. Unfortunately the R-value (correlation coefficient) dropped even lower leaving a value of R = 0.112, see Figure 11.

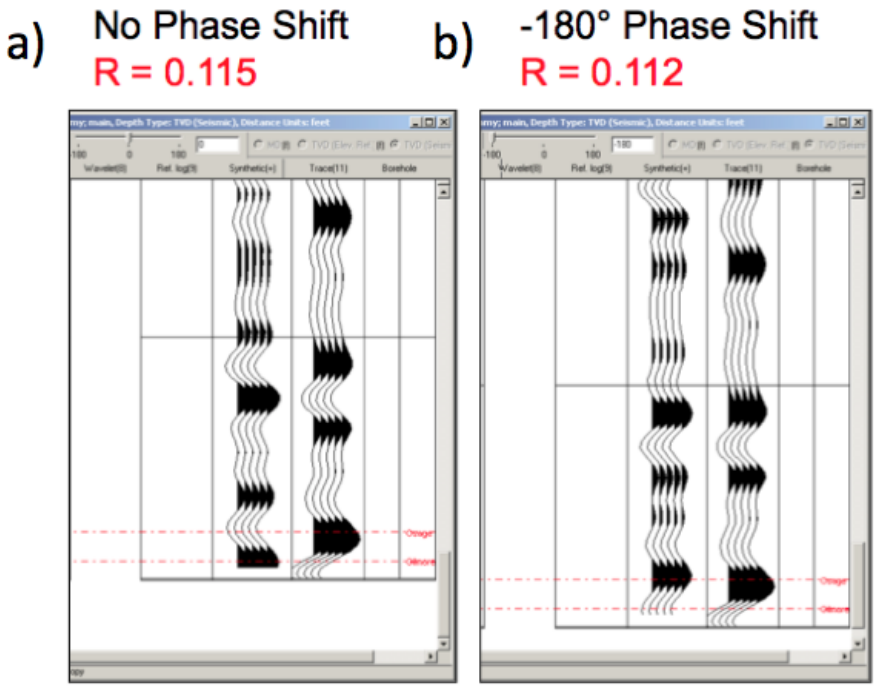

Figure 11: Dummy Humphrey 4-18, synthetic wavelet before (a) and after (b) phase shift. Constructed using clipped logs. In each plot, traces on left are synthetic and traces on right are extracted field traces. Note that, after phase shift the synthetic shows a better visual match to 3D seismic trace but it has a lower correlation coefficient.

DS-6 used the original sonic log and a clipped density log. The field wavelet was extracted from 112 traces and had the synthetic had a correlation coefficient of R = 0.362. A PS of 53 degrees gave the best visual match and a much better value of R = 0.648, see Figure 12.

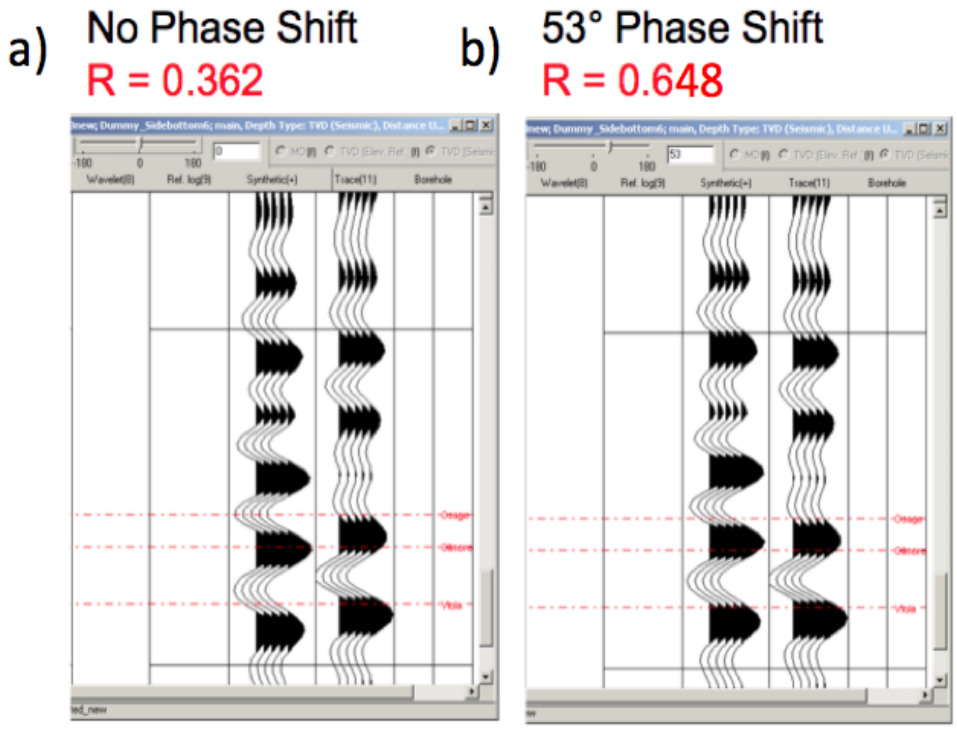

Figure 12: Dummy Sidebottom 6, synthetic wavelet before (a), and after (b) phase shifts. Constructed using original sonic log and clipped density log. In each plot, traces on left are synthetic and traces on right are extracted field traces. Note higher correlation coefficient after phase shift.

After a comparing the DH 4-18 and DS-6 synthetic seismograms (see Figure 13a and 13b), a decision was made to move forward using only the DS-6 well to tie the geology to the seismic. A complete synthetic seismic display of DS-6 is shown in Figure 13c. To confirm the geological accuracy of the DS-6 synthetic seismogram, I

verified that my formation tops as well as shallow formation tops (Fort Scott, Cherokee, etc.) aligned with the formation tops in several other wells throughout the 3D survey area. Horizon tracking and picking discontinuities was initiated subsequent to this verification.

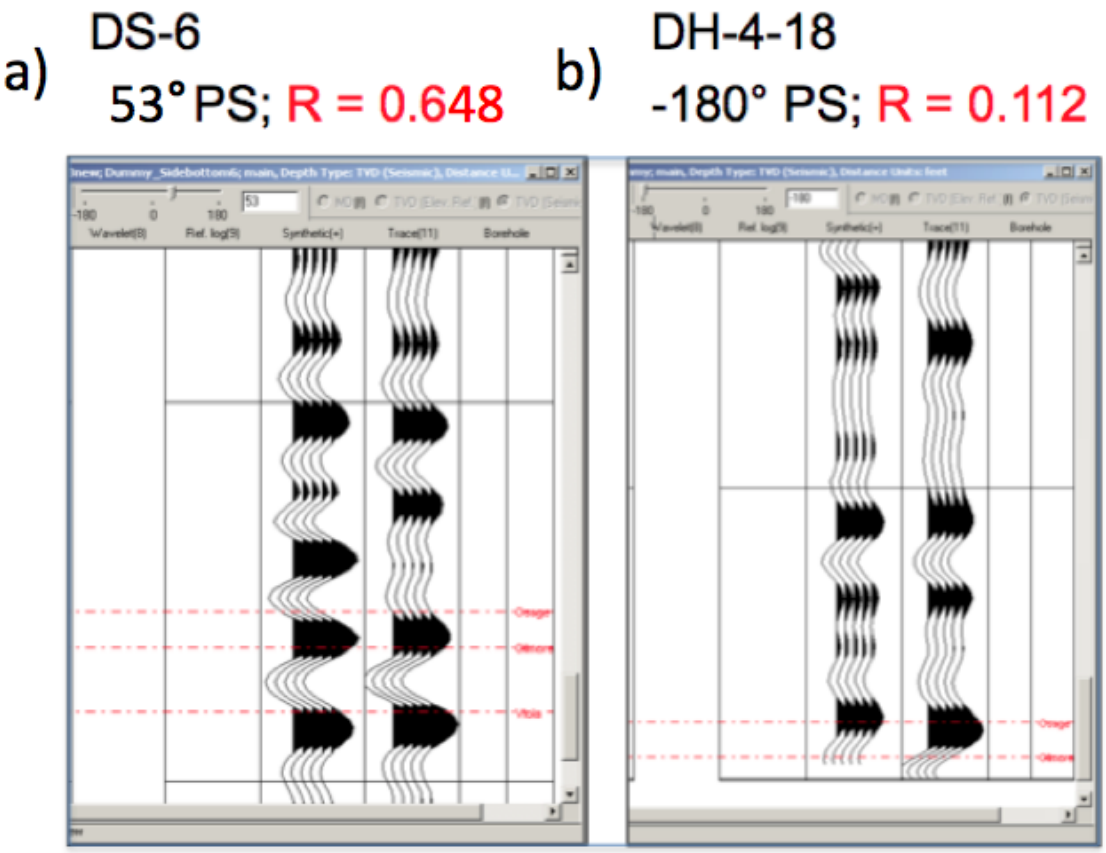

Figure 13: Comparison between synthetic seismograms from each well. DS-6 (a) shows a better match and yields a much better R-value.

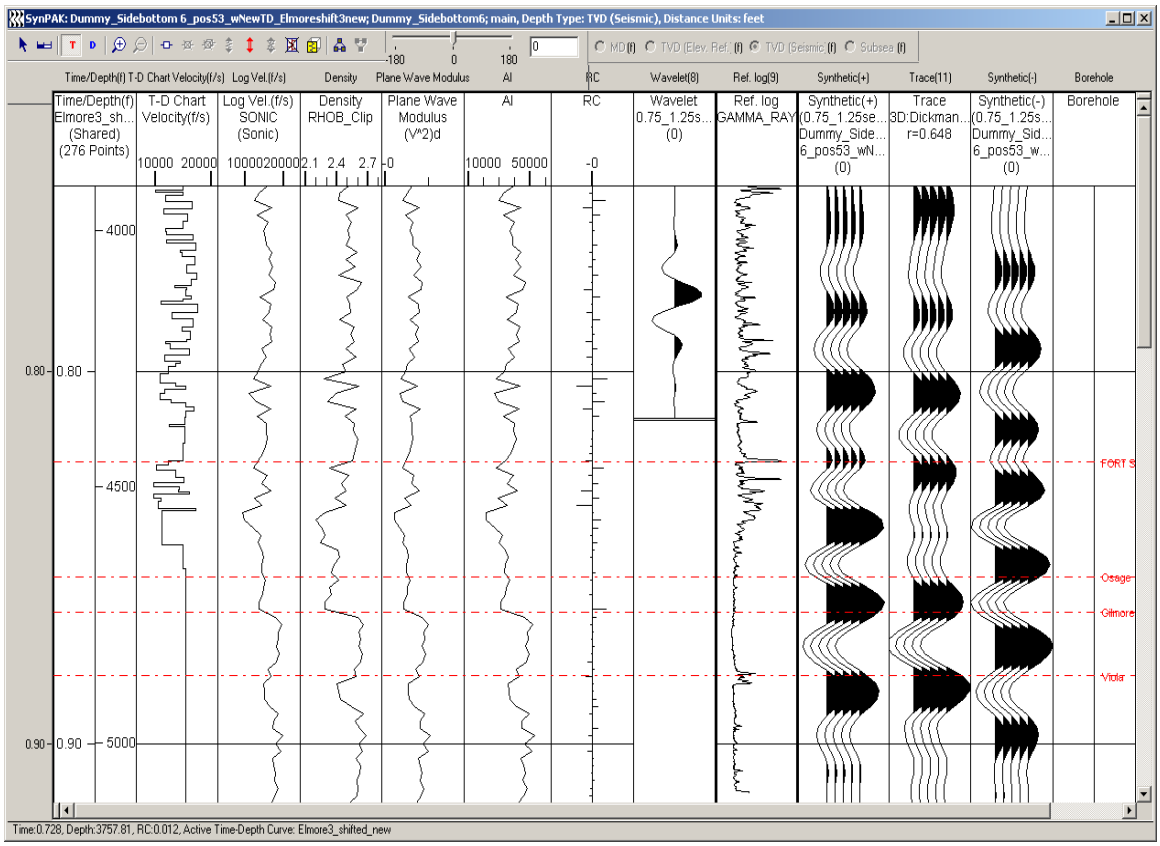

Figure 13 c: Shows a complete synthetic seismic display of DS-6.

Horizon tracking and picking discontinuities

Following detailed consideration of the phase shifted DS-6 synthetic [in a vertical section, crossline 126] (Figure 14), it was noted that the Osage lies at the base of a trough (near zero crossing), Gilmore City lies at the base of a peak, and Viola lies at a zero crossing. Therefore, the Osage was picked at a trough and attributes extracted from the horizon. The Gilmore City was picked at a peak and Viola at the peak

directly below the zero crossing in order to extract amplitude attributes from the horizon.

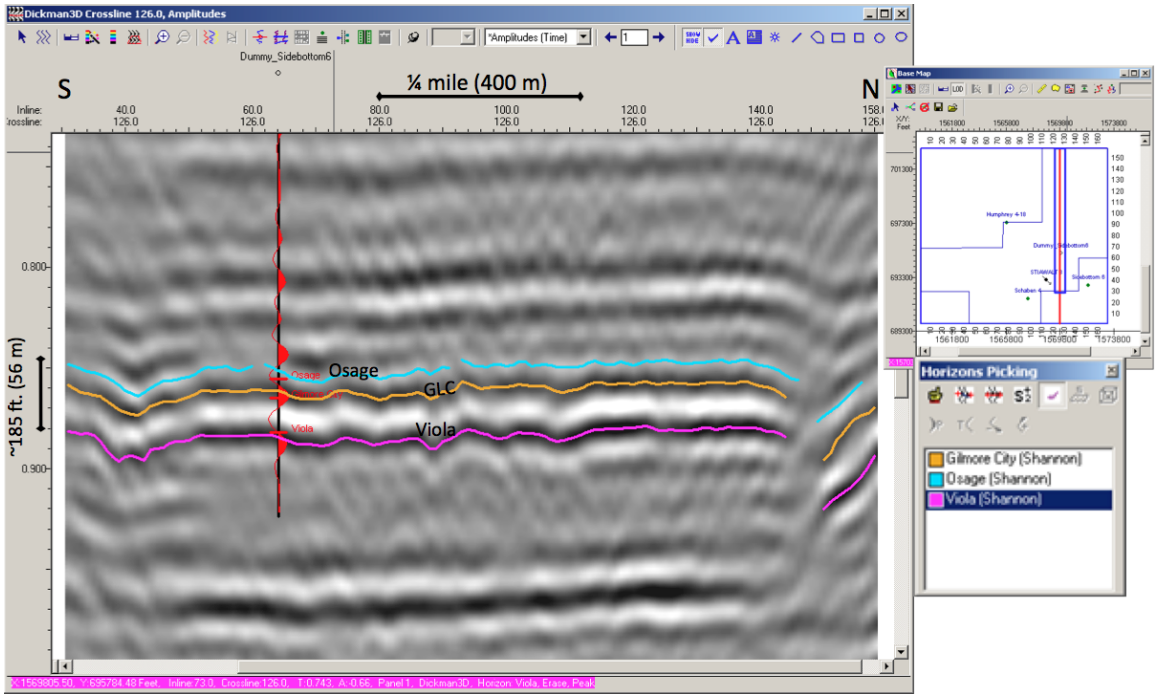

Figure 14: Dummy synthetic (DS-6) shown in vertical section Osage picked at trough, Gilmore City at peak, Viola at peak.

Each horizon was tracked on every inline and every crossline in order to capture fine detail and small discontinuities. Some discontinuities were easily seen on amplitude in vertical section, for example the NE-SW trending fault in the NW corner of the survey (Figure 14). This normal fault (downthrown to the North) is seen through each of the three horizons investigated. Other discontinuities required the SPICE attribute (vertical section), which better highlights discontinuities in a vertical section as seen in Figure 15. Several faults/fractures were visible both on the time and depth horizons, while some were better highlighted with SPICE as well

as other attributes (discussed later). Discontinuities that were more easily recognized with SPICE had minimal to zero throw.

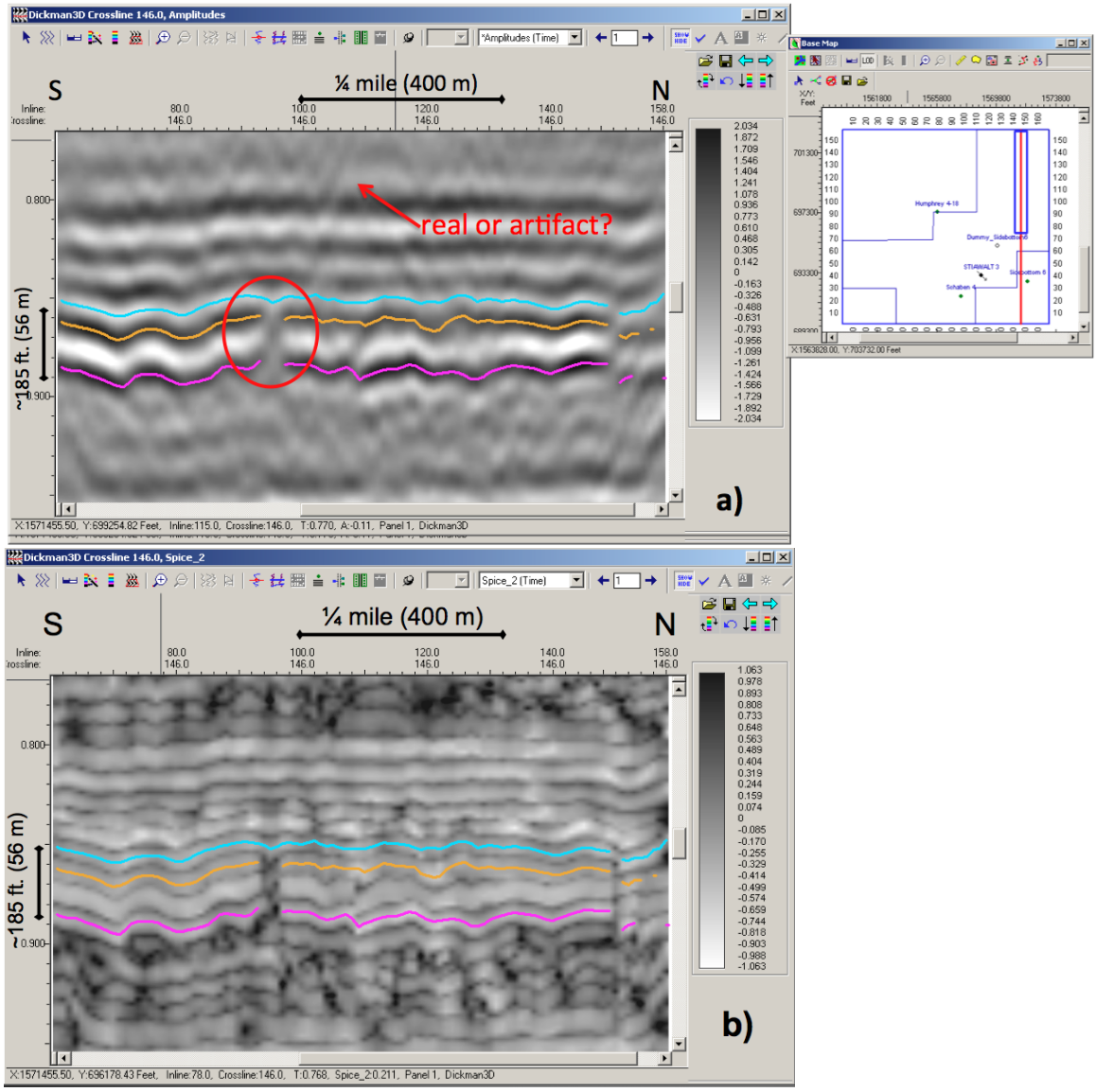

Figure 15: Discontinuities observed on amplitude (a) and SPICE (b). SPICE highlights discontinuities better than amplitude in most cases. This particular example could be an artifact or noise induced.

There were 17 fault/fracture picks (all displayed in Figure 16) in the area of interest between 0.8-0.9 seconds. Discontinuities 2, 4, and 9 were deleted due to

interpretation errors. All fault/fracture picks were made in vertical section using amplitude and SPICE data.

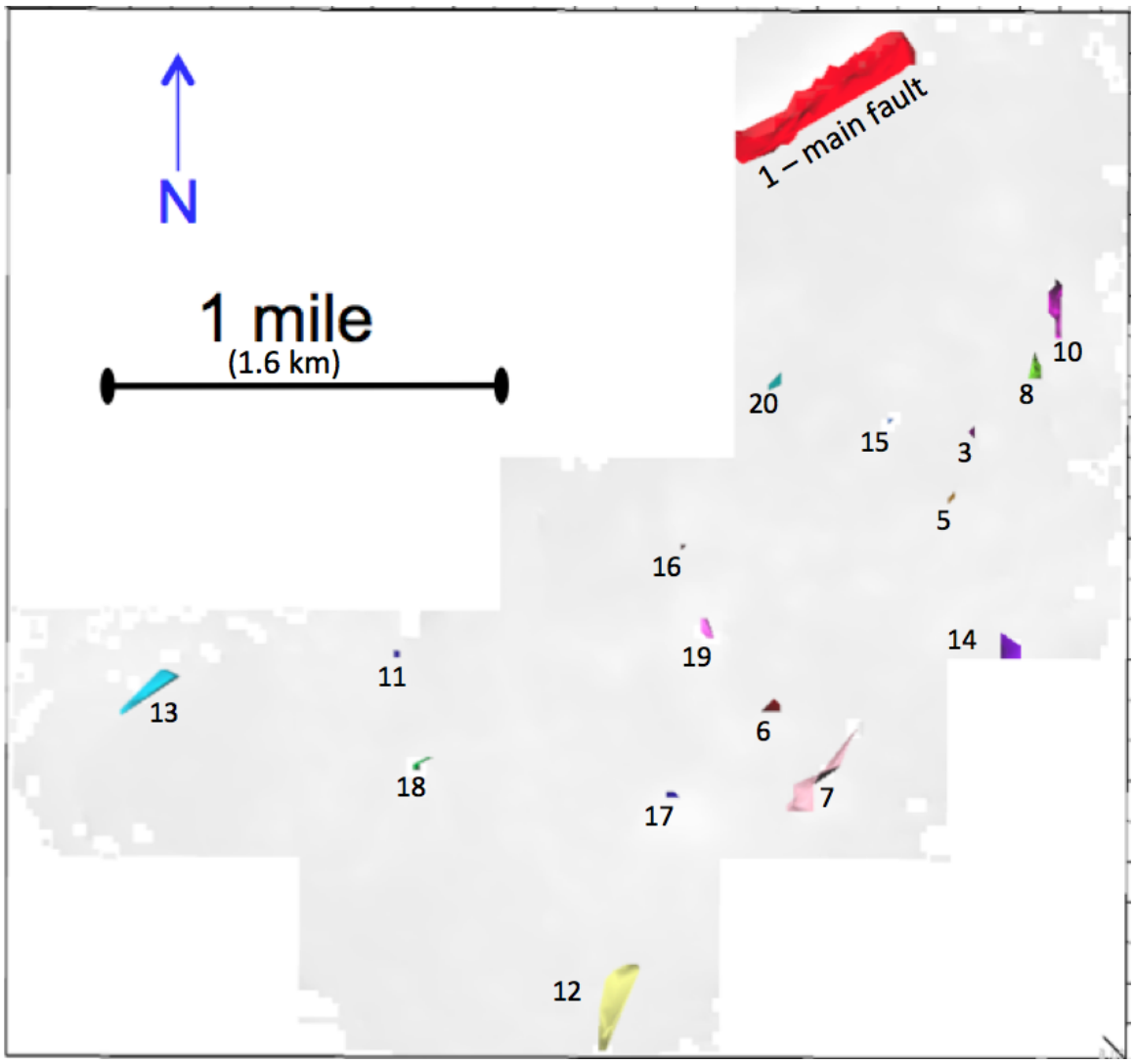

Figure 16: All fault/fracture picks (surfaces) displayed in darker color, VuPack.

The discontinuity features are categorized into probable, possible or doubtful based on several criteria (Table 4). These fault/fracture picks are observed in the Viola (6), in the Gilmore City (9) and in the Osage (9). The criteria for classification of discontinuities were based on the extent of the fault/fracture, if it was visible/aligned with anomalies on amplitude, SPICE, ANT, coherence, variance and

curvature. Discontinuities induced by noise or affected by edge effects decrease the credibility of these being actual faults/fractures. All horizons were observed in VuPack in order to have a better idea of the extent of discontinuities (Figures 17a, 17b, and 17c). If the discontinuity had extent it significantly increased the credibility of being an actual small fault/fracture.

Probable	Possible	Doubtful
• **Has significant extent** • Corresponds with amplitude and SPICE data (vertical section) • Corresponds well with most attributes • Not noise induced	• Corresponds with amplitude and SPICE data (vertical section) • Corresponds with most attributes • Not noise induced	• No significant extent • Corresponds with ≤ 3 attributes • Is noise induced and/ or near edge of the survey

Table 4: Classification criteria for discontinuities.

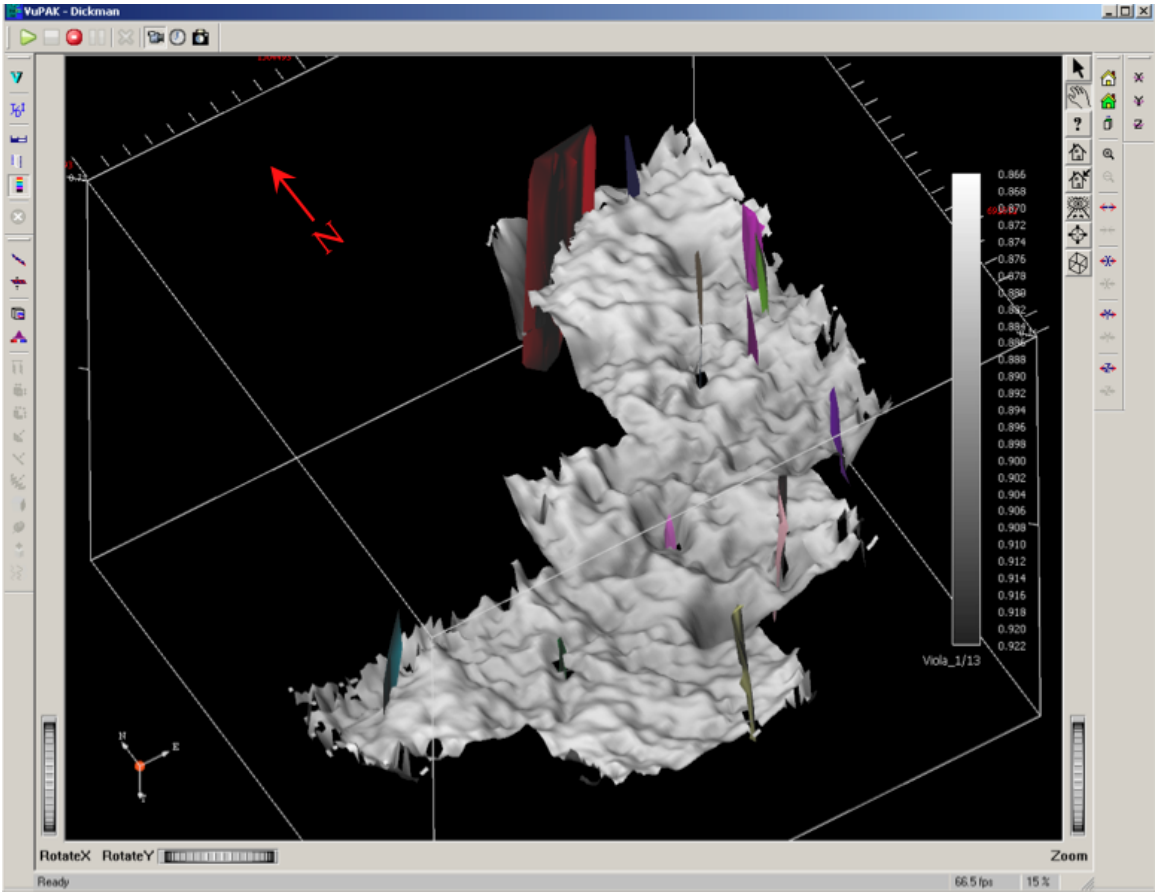

Figure 17 a: Viola discontinuities observed in 3D visualization, deep to shallow horizons. Dark/colored areas highlight faults.

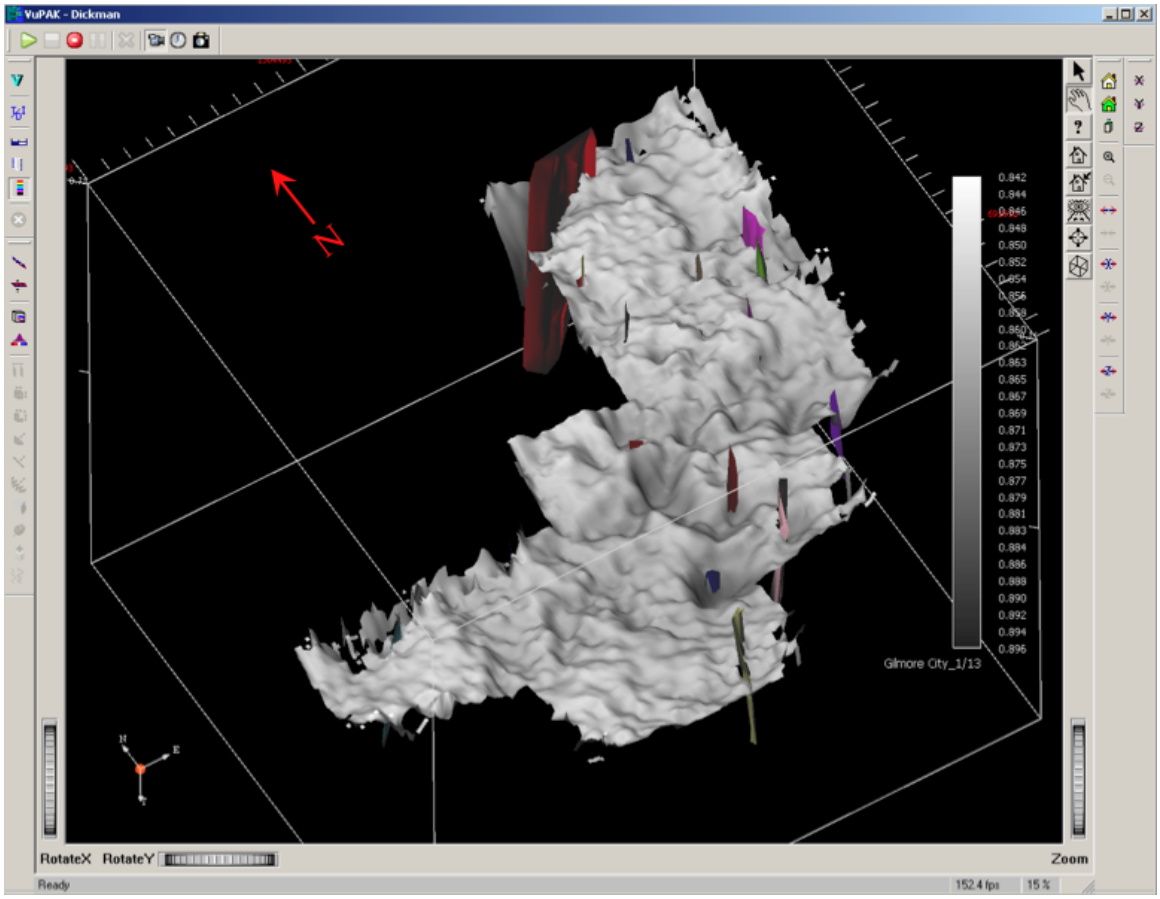

Figure 17 b: Gilmore City discontinuities observed in 3D visualization, deep to shallow horizons. Dark/colored areas highlight faults.

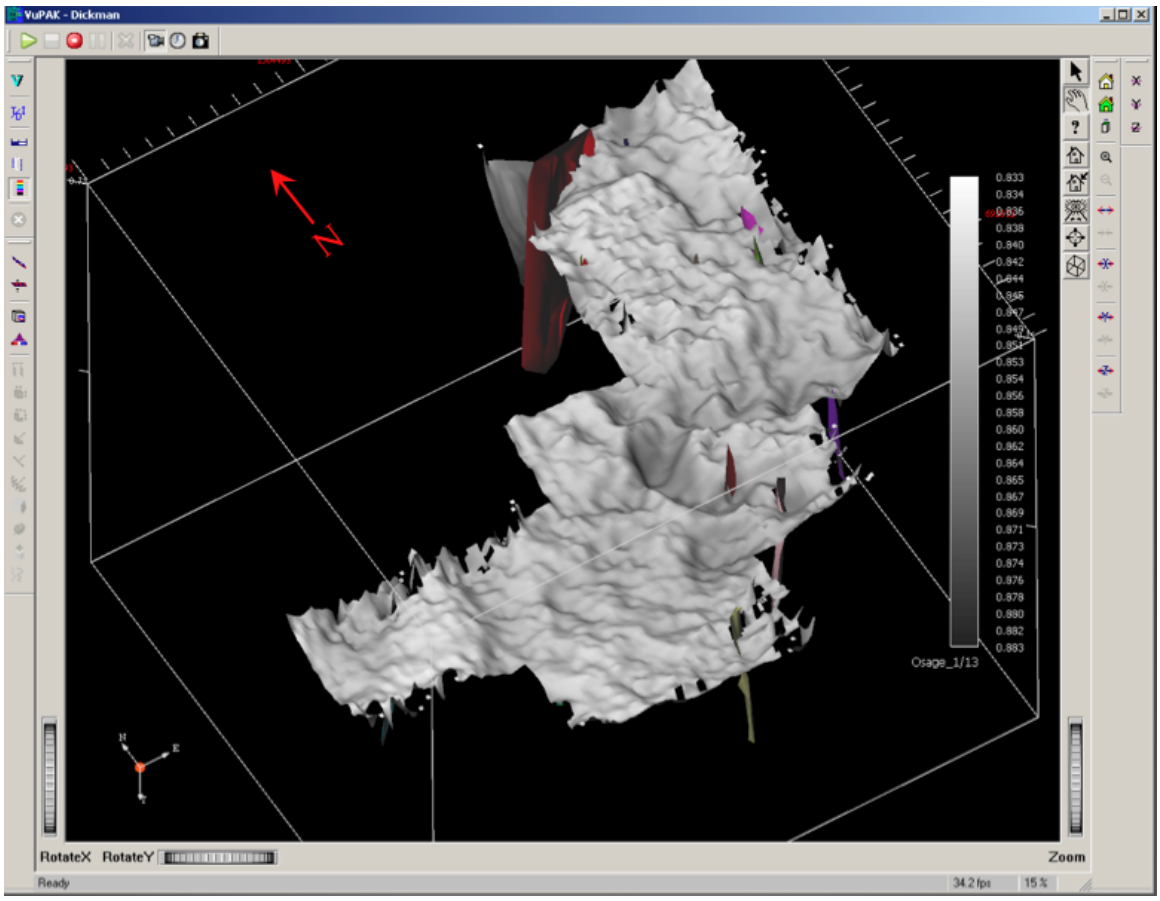

Figure 17 c: Osage discontinuities observed in 3D visualization, deep to shallow horizons. Dark/colored areas highlight faults.

Finally, SMT's 3D hunt was applied for horizon interpolation. Contoured time structure maps (from gridded time) are displayed in Figures 18a, 19a, and 20a. Depth structure maps of these horizons are also displayed in Figures 18b, 19b, and 20b. The depth structure maps were constructed using the Elmore3_shifted_new time-depth curve (T-D). Other T-D curves were available in the dataset but the Elmore3_shifted_new T-D curve was used for all wells in this project to maintain data consistency.

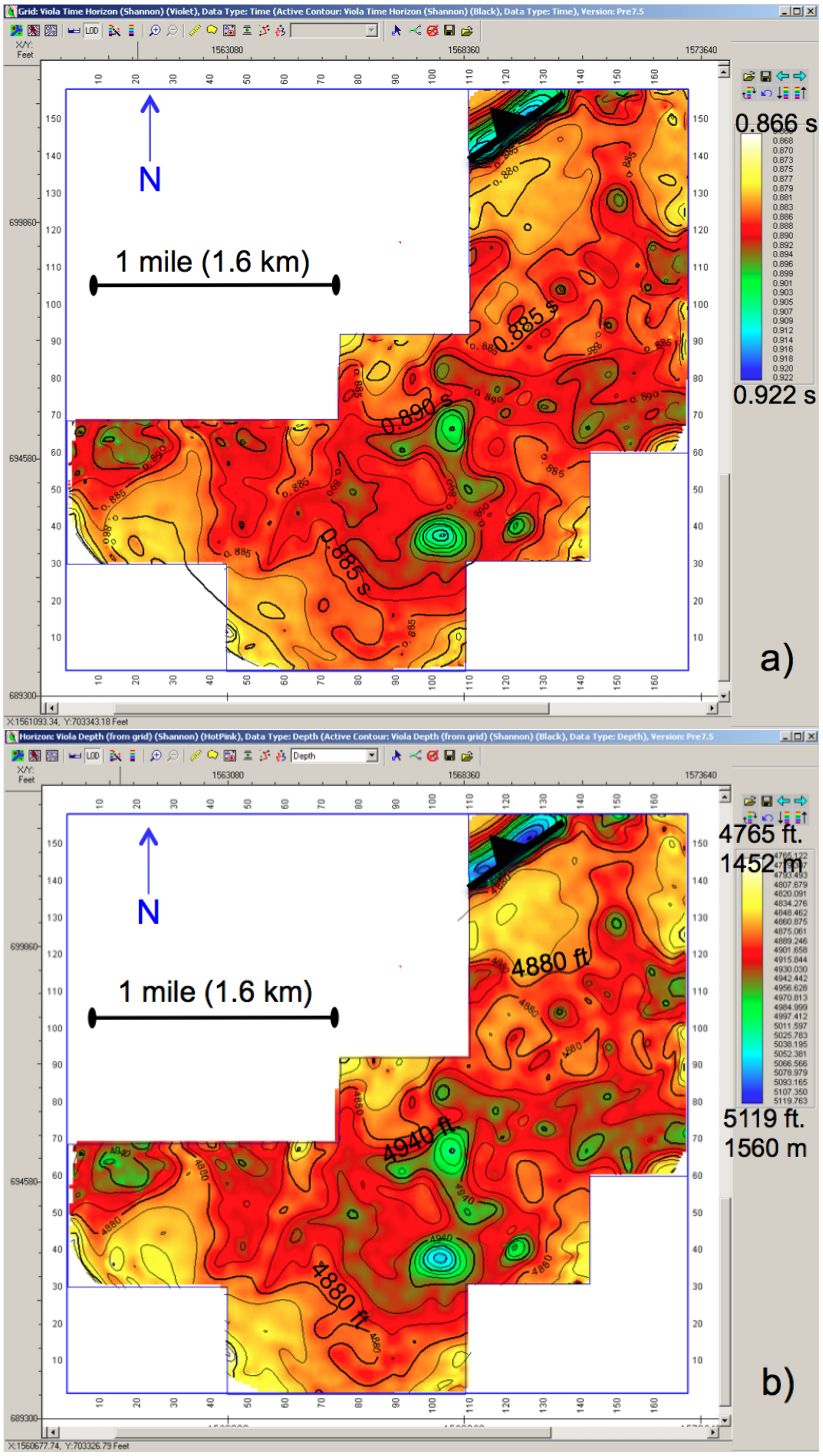

Figure 18: Viola structure maps (gridded). (a) Time structure with 2.5 ms contours. (b) Depth structure with 20 ft contours. Note bulls-eyed features are representative of karst geology.

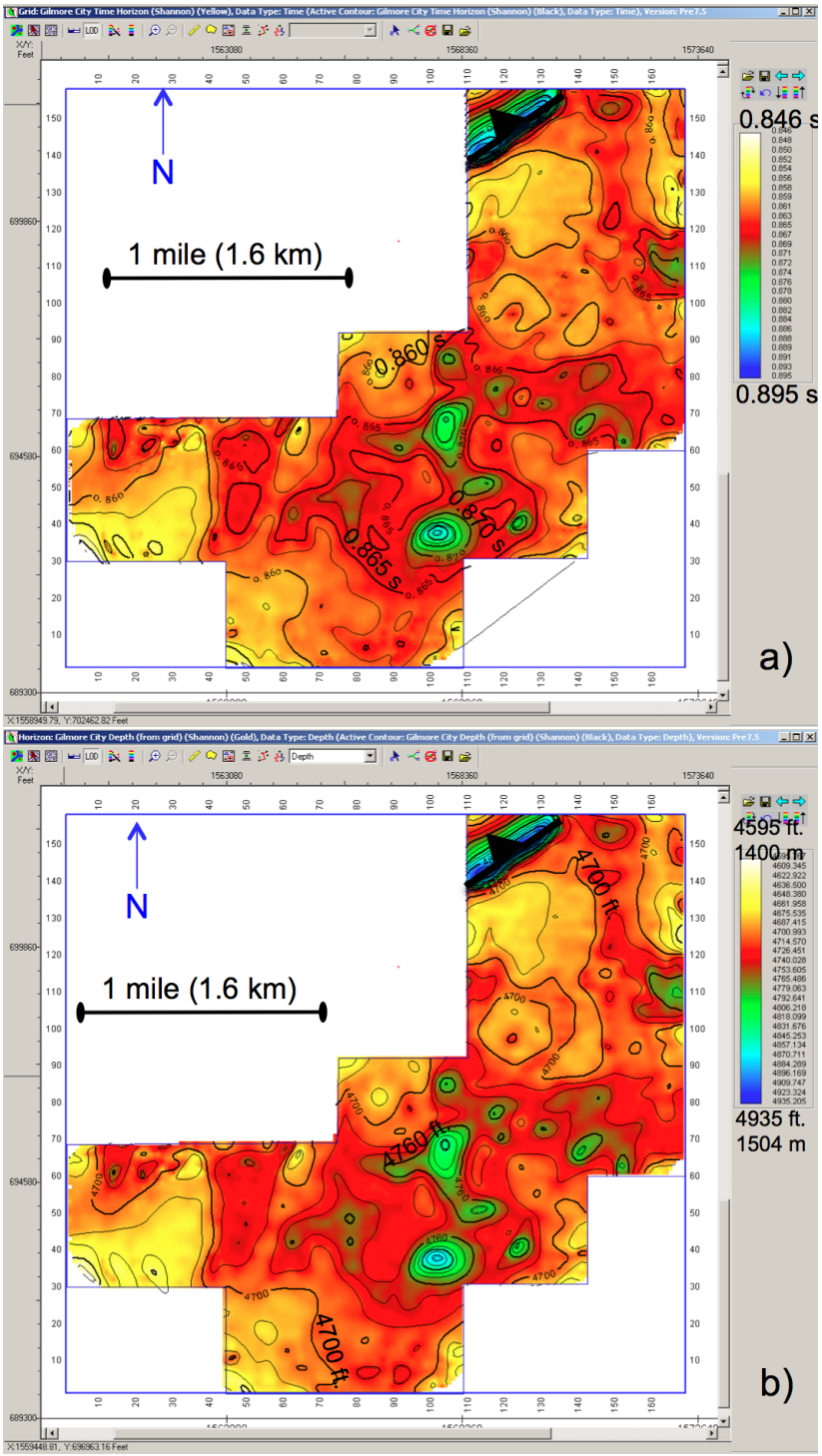

Figure 19: Gilmore City structure maps (gridded). (a) Time structure with 2.5 ms contours. (b) Depth structure with 20 ft contours. Karst features become well connected as we move shallower to Gilmore City time/depth.

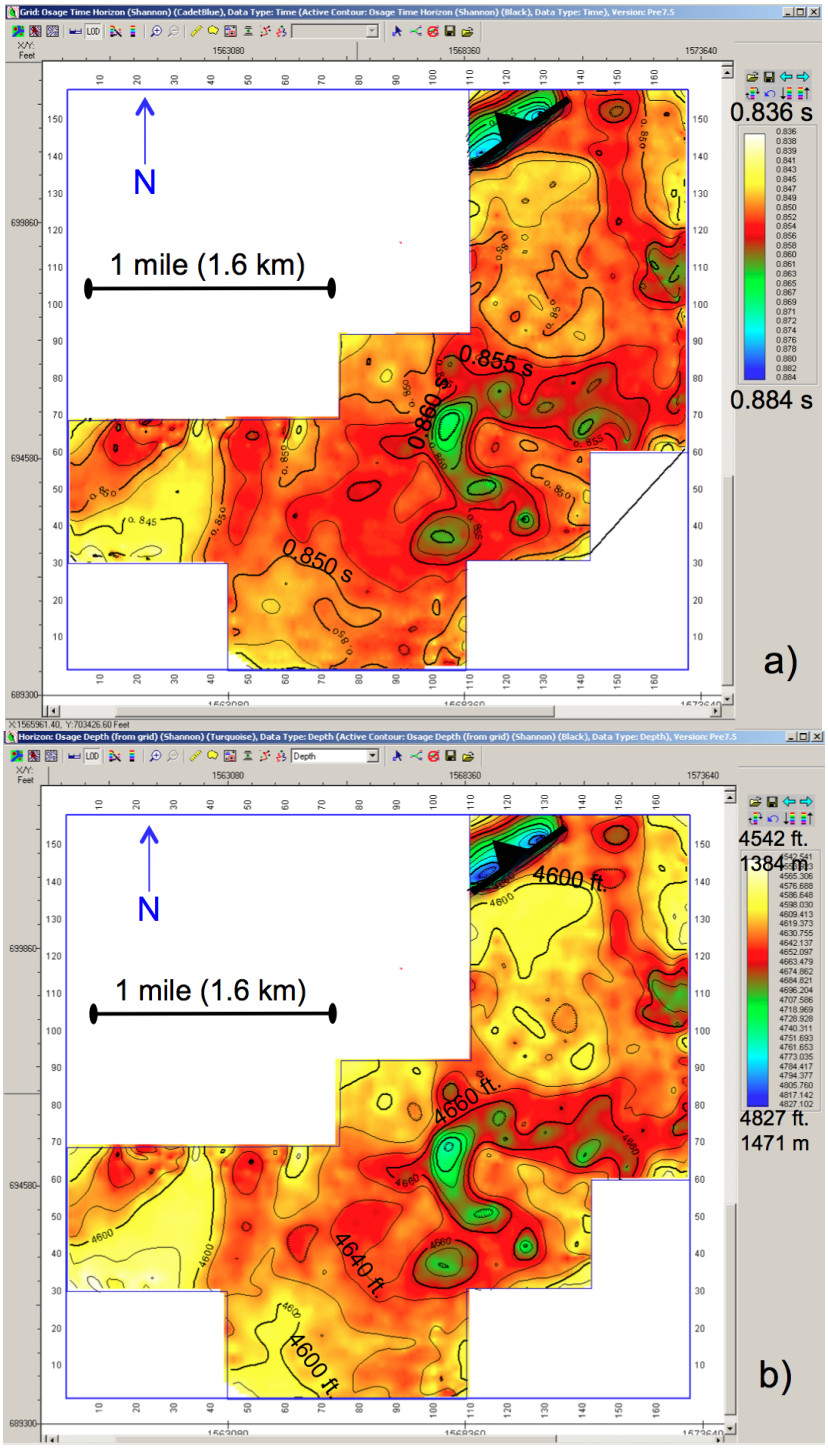

Figure 20: Osage structure maps (gridded). (a) Time structure with 2.5 ms contours. (b) Depth structure with 20 ft contours. Connection of karst features mimic the overlying Miss./Penn. channel, easily observed in Osage time and depth maps.

The karst features are easily observed (darker, deeper topography) in all three time and depth horizons. The only differences observed between the time and depth structure maps is that the area of karst features is slightly larger in the depth maps and there is somewhat of a sharper contrast in topography in the depth maps. All three horizons (especially Viola and Gilmore City) display a bulls-eye feature (blue) near the southeast portion of the map and this is interpreted as a possible sinkhole. Karst features in the Viola are slightly more abundant than those in the Gilmore City horizon. Likewise, the karst features in the Gilmore City are slightly more numerous than those in the Osage. Although, it seems these karst features become more connected and portray a trend as one moves from the deep Viola (Figure 18) up to the shallower Osage horizon (Figure 20). I believe the reason for this observed connectivity in the Osage is due to the overlying incised channel that occurs in the Miss./Penn. boundary as mentioned earlier. The trend of karst features observed in the Osage aligns with the orientation of the incised channel.

Isopach Maps

Three isopach maps were constructed; one taken from the Viola to the Gilmore City (Figure 21a), the second was taken from the Gilmore City to the Osage (Figure 21b), and the third was taken from the Viola to the Osage (Figure 21c). The isopach map for the Viola to Gilmore City depth (21a) had a maximum thickness of 288 feet and a minimum thickness of 67 feet. The thickest areas are located in the vicinity of the overlying Miss./Penn. channel location and in the western portion of the map.

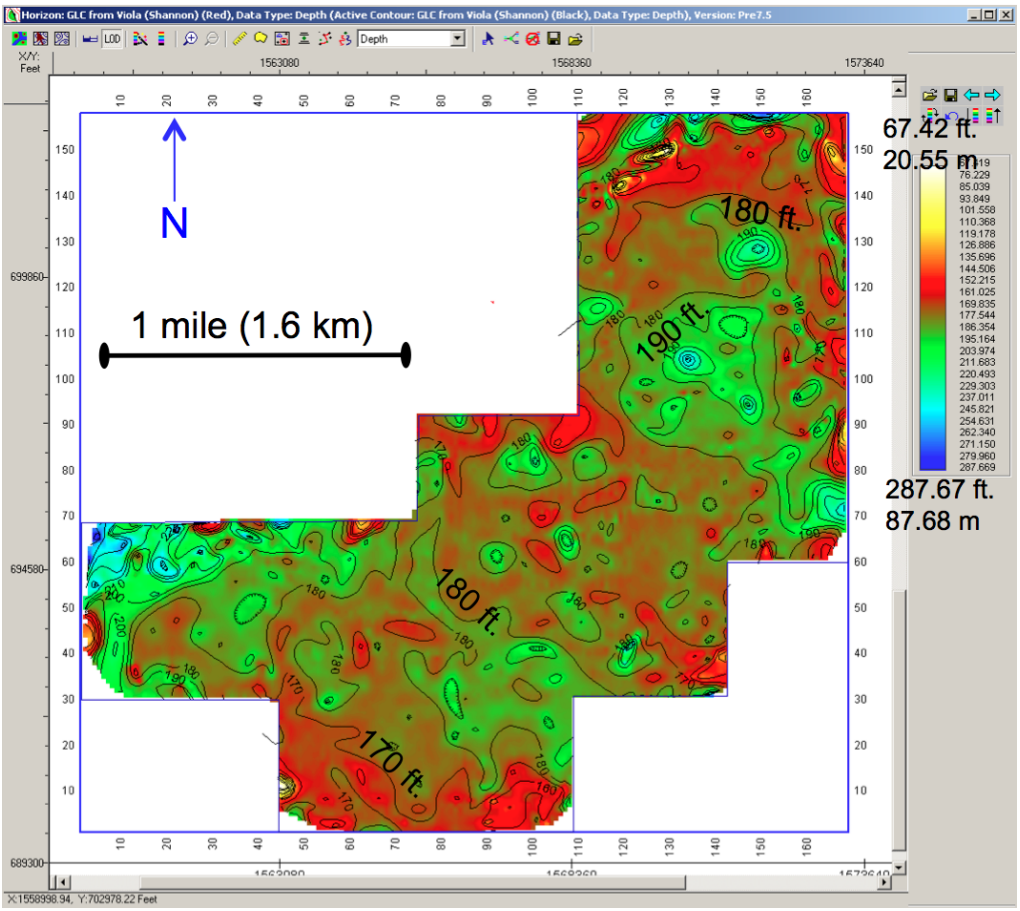

Figure 21 a: Isopach map. Viola depth to the Gilmore City depth, thickness increases in vicinity of Miss./Penn. channel.

The Gilmore City to Osage isopach map (Figure 21b) had a maximum thickness of 178 ft. (54.3 m) and a minimum thickness of 7.6 ft. (2.3 m) therefore the thickness between the Gilmore City depth and Osage depth is less than the thickness between the Viola and Gilmore City. Although, we must take into consideration that the Viola was actually picked on the peak below the zero crossing it was located on in the synthetic. The thickest area in this map (Figure 21b) is located in the mid-south portion of the map; the area previously interpreted as karst from several attribute maps. This area is most likely representative of a sinkhole

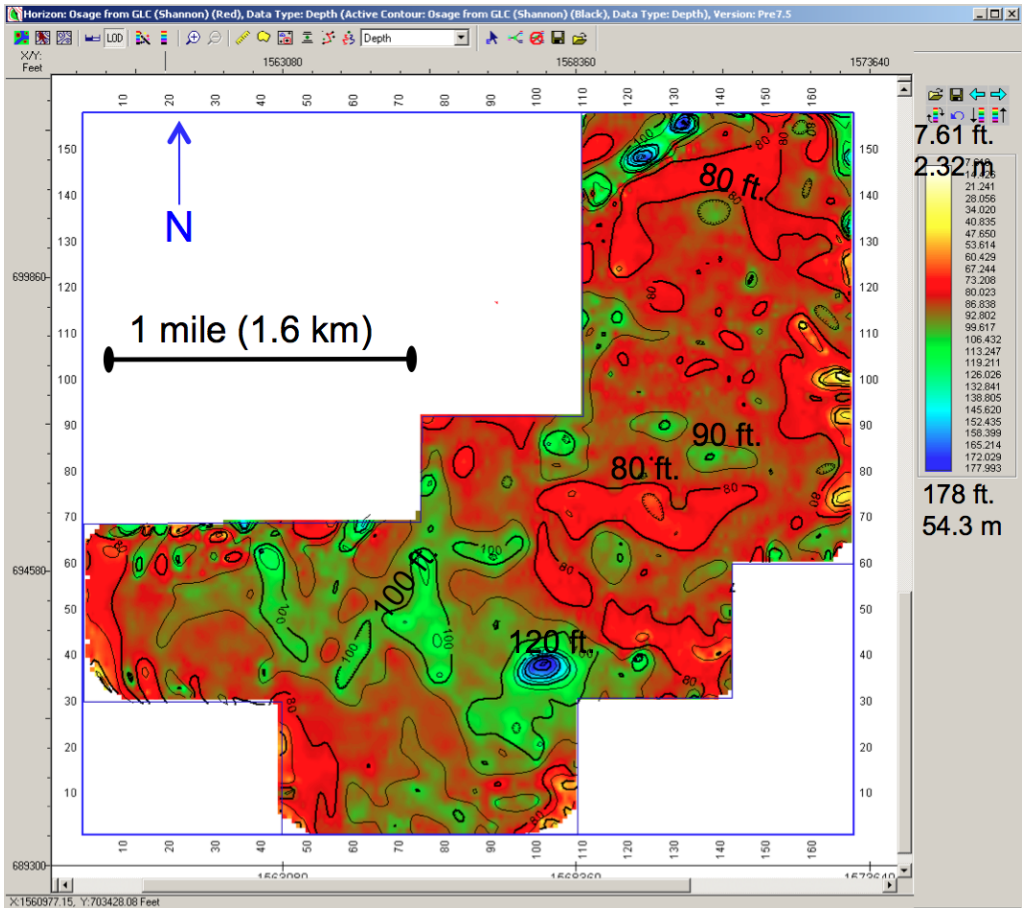

Figure 21 b: Isopach map. Gilmore City depth to Osage depth, thickest area in mid-south portion of map, interpreted area of karst and/or possible sinkhole.

The isopach map for the Viola to the Osage depth (Figure 21c) had a maximum thickness of 368 ft. (112 m) and a minimum thickness of 150 ft. (45.7 m) and this isopach was expected to be the thickest because it was taken from the shallowest horizon of investigation to the deepest. We see the interpreted sinkhole is the thickest area of the map and thicker than it was in the Gilmore City-Osage isopach map. The thicker areas in this map also reside in the vicinity of the Miss./Penn.

channel meaning that the areas below the channel have more sediment accumulation.

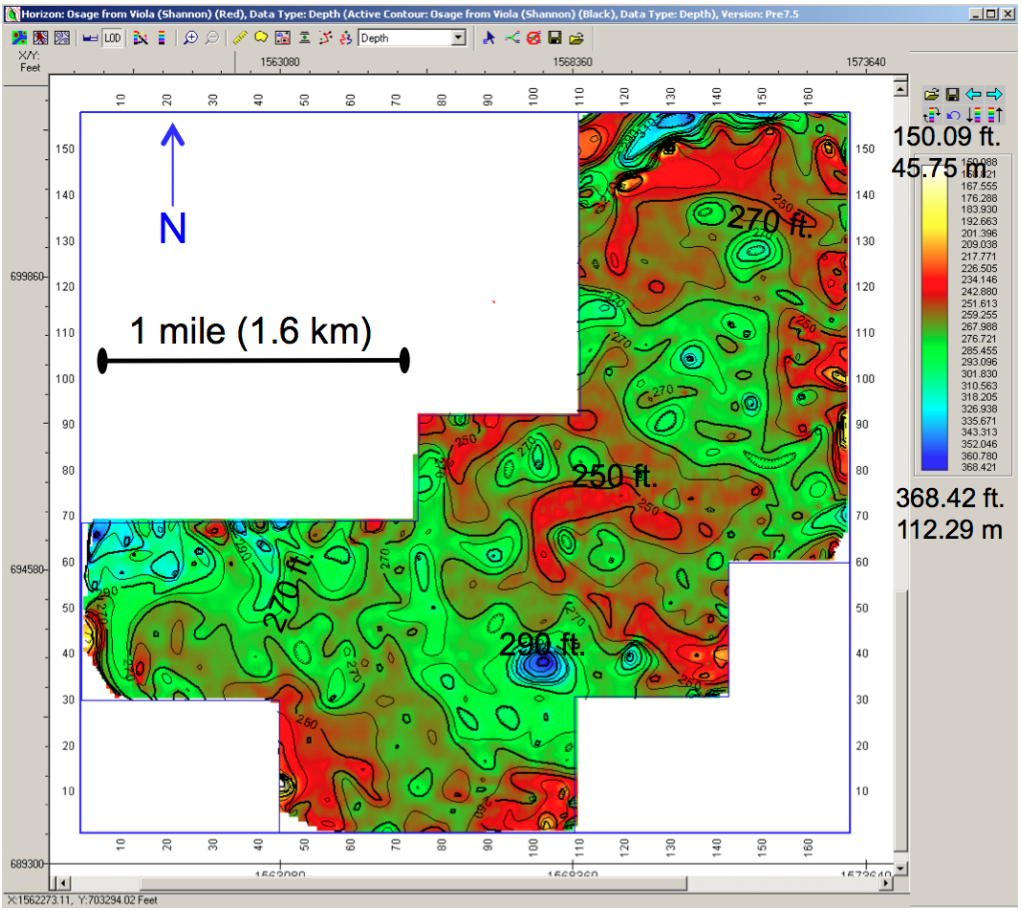

Figure 21 c: Isopach map. Viola depth to Osage depth, thickness increases in vicinity of Miss./Penn. channel. Thickest bulls-eye feature (blue) is interpreted as a possible sinkhole.

Attribute analysis

After Mike Forrest discovered that amplitude anomalies or bright spots were direct hydrocarbon indicators, the time of the so-called Digital Revolution emerged (Castagna, 2011). With this, so did the development of a multitude of seismic attributes. Digital recording not only yielded seismic data of better quality but it also

brought about awareness of the significance of preserving relative amplitudes. The essential seismic data for attribute analysis includes time, amplitude, frequency, and attenuation. Alistair Brown's diagram (Figure 22) helps to understand attribute classification. This study investigates time-derived attributes, which help with structural identification, and amplitude-derived attributes, which are useful for stratigraphy issues and reservoir properties. Furthermore, horizon attributes are the main focus of this study where the attribute is extracted along the horizon. Windowed attributes, alternatively, use a particular time interval to extract the attributes (Brown, 2001).

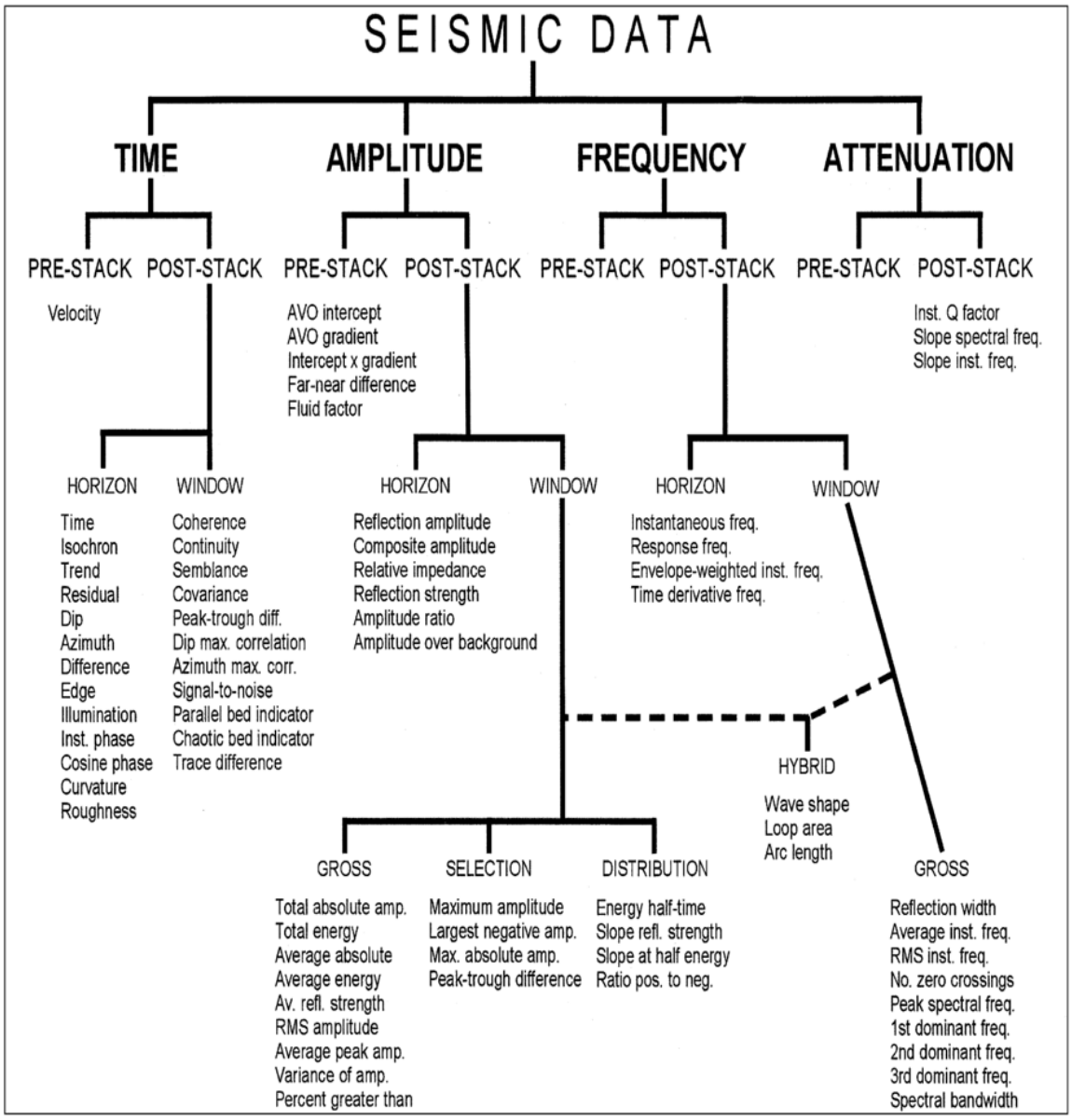

Figure 22: "Seismic attributes derived from or related to the basic seismic information of time, amplitude, frequency, and attenuation. The window can be a constant time interval, a constant interval hung from one horizon, or the interval between two horizons" Brown, (2001).

The attributes used in this study focus on identifying the locations of faults and fractures. One attribute that draws attention to these discontinuities is **coherence**. This attribute uses a crosscorrelation method to calculate a coherence coefficient

from seismic amplitudes on neighboring traces. Using crosscorrelation reduces influence of variability in source amplitude and phase, allowing the geoscientist to measure waveform continuity. In other words, it measures waveform similarity, allowing the interpreter to easily recognize faults, buried deltas, river channels and dewatering features. **Variance** (or semblance) is a definition of coherence that relies on lateral amplitude but the crosscorrelation and eigenstructure definitions rely on full waveforms (Chopra and Marfurt, 2007). Energy ratio and outer product are other attributes analyzed in this investigation and are very similar to coherence.

Curvature is another attribute that highlights horizon geometry using reflector dip and azimuth to measure curvature, or the shape of a reflector. The mathematical definition of curvature is "the inverse of a circle's radius which is tangent to that surface at that point" (Blumentritt et. al., 2006). Chopra and Marfurt (2007, p. 16) define curvature as "a three-dimensional property of a quadratic surface that quantifies the degree to which the surface deviates from being planar." Using curvature, the interpreter can eliminate the effects of regional dip, which with therefore allow a closer interpretation of the small-scale features. Usually the most positive (anticline) and the most negative (syncline) curvature are used for seismic interpretation (Figure 23).

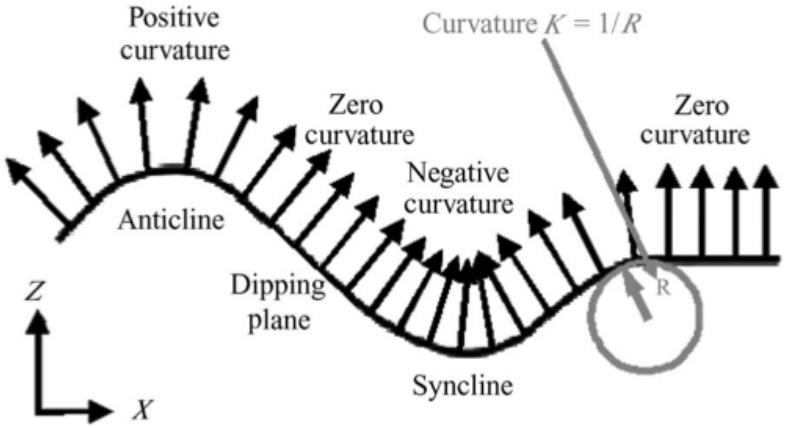

Figure 23: Definition of curvature. Positive curvature usually highlights anticlines while negative curvature highlights synclines. Blumentritt et al. (2006).

Curvature may aid with fracture identification but is still being researched as how to distinguish if the fractures are opened or closed. There are various curvature attributes used in this study developed by Kurt Marfurt (Chopra and Marfurt, 2007, 2008). A table of attributes used in this study and their origin can be found in Table 5.

Attributes	From Liner	From June (Geoframe and Petrel)	From Marfurt and/or Geokinetics	Window Size (ms)
Coherence		√		~30
Variance		√		~50
Curvature (I)			√	~50
SPICE	√			n/a
ANT		√		n/a
Curvature (II)			√ (smaller window)	~30
Energy Components			√	~50
Dip Components			√	vary
Gradient Components			√	vary
Fractional Derivative			√	~50
Edge & Outer Product			√	~50
Confidence			√	n/a

Table 5: Table of attributes; those in red are discussed in detail. Attribute acquired from Chris Liner, Jianjun Zeng (June), Kurt Marfurt and/or Geokinetics.

SPICE (spectral imaging of correlative events) is a general attribute that will help identify fractures. This is a recent attribute based on wavelet transform decomposition and singularity analysis of migrated seismic data. "The physical basis of SPICE relates to spectral shaping during wave propagation and reflection" (Liner et. al., 2004). Smythe computed the SPICE attribute from the acoustic impedance (AI) log, reflection coefficient (RC) log, then, the sonic/density (geology) data. All plots (Figure 24) show a nearly identical appearance with SPICE therefore justifying that what we see in the SPICE attribute is similar to what we would see in the geology (Smythe, 2004).

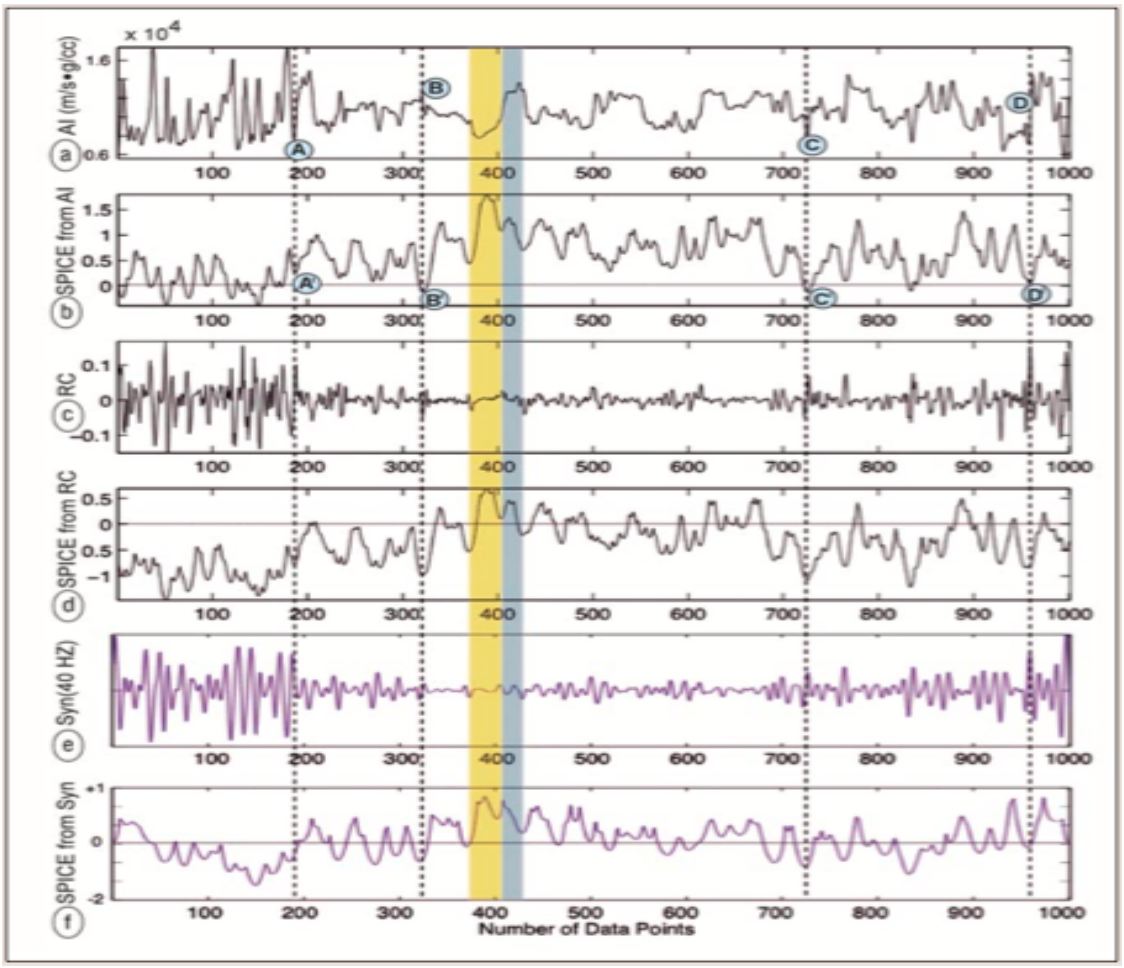

Figure 24: "SPICE demonstrated on well data: (a) acoustic impedance (AI) log (sample interval is 0.5 ft. or 0.15 m); (b) spice computed from AI; (c) reflection coefficients (RC) calculated from AI; (d) spice computed from RC; (e) 40-Hz synthetic; (f) spice computed from synthetic" Smythe et al. (2004).

This study also uses **Ant Tracking**, an automatic fault extraction technique available in the Petrel interpretation system. Minimal noise in the volume is preferred and preliminary enhancement of spatial discontinuities using any edge detection algorithm is a required preprocessing step, followed by generation of the Ant Track Volume. The Ant Tracking algorithm mimics the ants we know of in nature and their ability to track pheromones to find the shortest path between the colony and food. It

gives us a picture of the seismic volume's so called plumbing system by sending these electronic "ants" into the data so they can detect the fault/fracture surfaces highlighted by edge detection methods (i.e. SPICE, variance, coherence, etc.). Both **ANT from SPICE** and **ANT from variance** were used in this study.

Other attributes considered in this study include coherent energy and total energy (useful for multiattribute display), confidence measure (useful for subsequent filtering), multiple dip components (required for subsequent curvature), multiple gradient components (good for mapping changes in high amplitude reservoirs) and fractional derivitive (similar to sobel filter 'coherence') (Marfurt Shell script notes). Only the most significant attributes are discussed in detail for the purposes of this study (Table 4).

RESULTS

Amplitude

Starting with the deepest horizon of interest, the Viola amplitude map (Figure 25) displays unstructured high amplitude clusters.

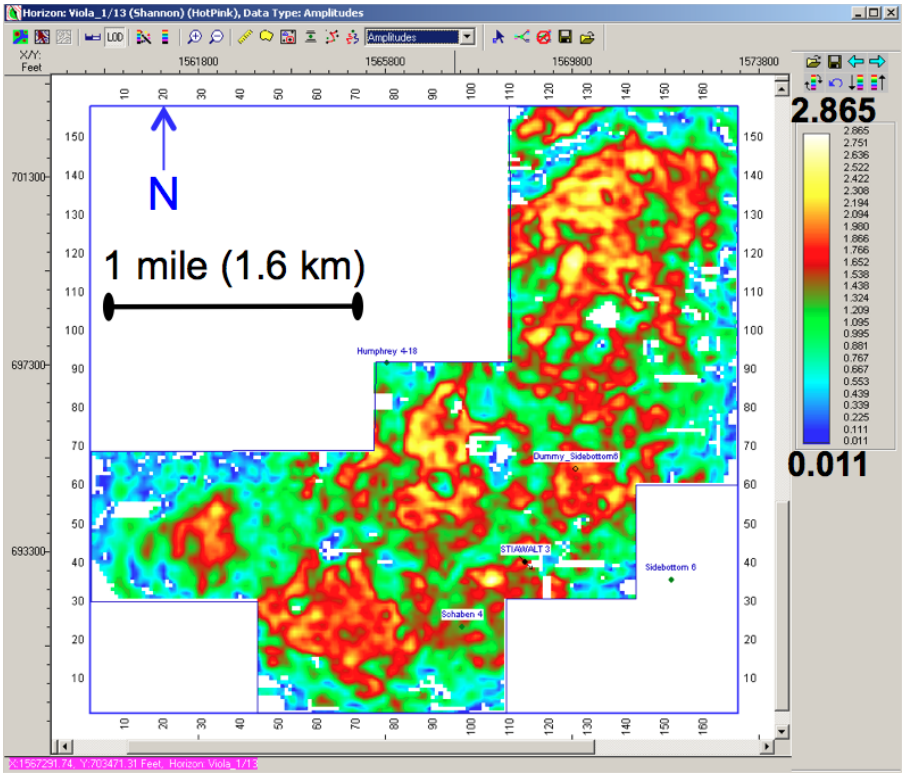

Figure 25: Viola amplitude map. Unstructured random clusters of high amplitudes are representative of karst geology.

These higher amplitudes are abundant and cover almost half of the map. They are likely representative of either higher zones of porosity and/or karst features. Furthermore, no particular trend of amplitude was observed excluding the most prominent fault in the northwest corner of the map (observed in all amplitude maps). There is a relative amplitude difference of about 33 percent from the average high to low amplitudes. All amplitudes in the Viola range from positive (+) 0.01

(lowest) to (+) 2.87 (highest). Furthermore, in all three amplitude horizon maps there are holes present near the edges of the map. These are areas where horizon tracking lacked confidence due to edge effects.

Figure 26 shows high amplitude values in the Gilmore City amplitude map tend to be grouped together in the southern half of the map and there is only one smaller cluster of high amplitudes in the northern portion.

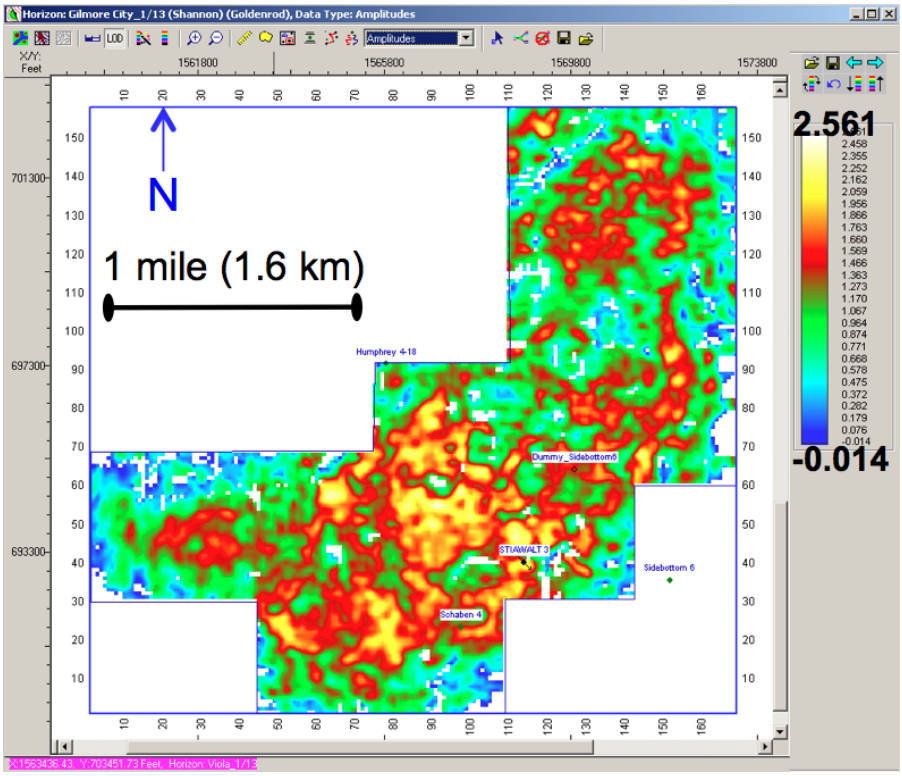

Figure 26: Gilmore City amplitude map. Higher amplitudes grouped together in southern portion of map and a smaller group in the northern portion of the map.

There is a relative amplitude difference of about 46 percent from the average high to low amplitudes. The high amplitudes in the Gilmore City horizons seem to dominate over half of the map. These higher amplitudes are well connected in

contrast to those of the Viola horizon. The scale of the Gilmore City amplitudes ranges from a low of negative (-) 0.01 to positive (+) 2.56.

The Osage amplitude map (Figure 27) differs significantly both the Viola and the Gilmore City maps in that, rather than a group or clusters of high amplitudes, we instead have lower amplitudes dominating the map with a background of higher amplitudes.

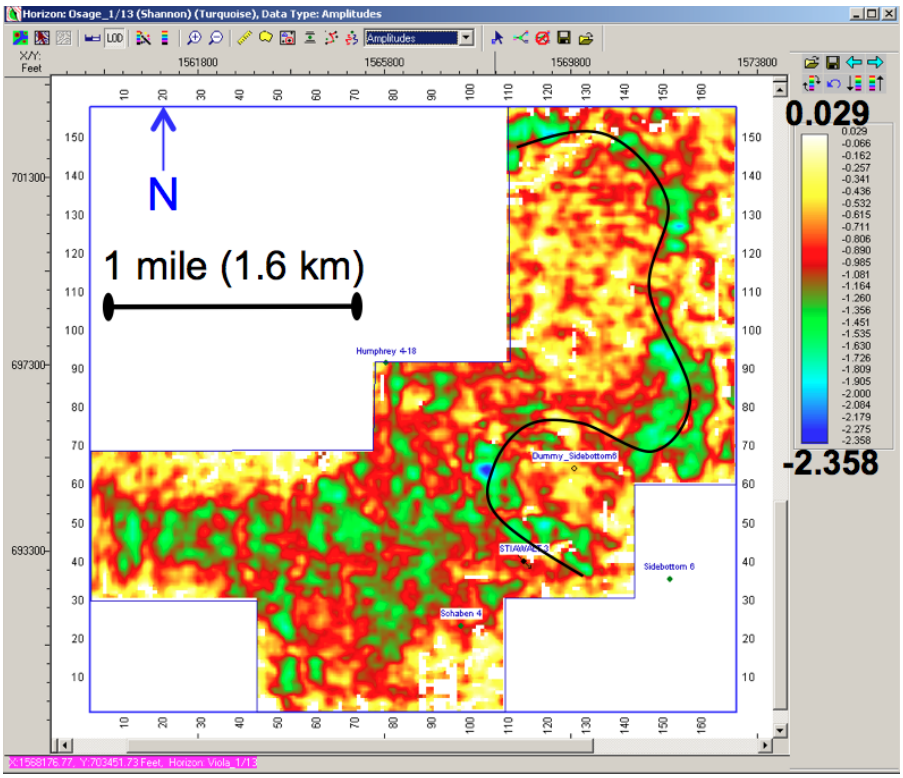

Figure 27: Osage amplitude map, note the highlighted channel, lower amplitudes. Subtle acquisition footprint (E-W) in the northern portion of the survey was observed. Figure 48 shows better evidence of acquisition footprint at timeslice 0.428 seconds.

There is a relative amplitude difference of about 34 percent from the average high to low amplitudes. The scale of the Osage amplitudes ranges from a low of negative

(-) 2.36 to positive (+) 0.03. The low Osage amplitudes interestingly enough, align almost perfectly with the trend of the incised channel at the Miss./Penn. boundary. There was also an observed extreme low sitting inside the curve of the channel in the center of the map. Lower amplitudes are dominant in the southwest portion of the map as well as in the center to northern portion following the trend of the incised channel above.

The wire-line logs we have for the four deep wells can give us information and a partial explanation as to the nature of our amplitude maps. We must recall that only two of the deep available logs (Tables 2 and 3) in our project have significant lithological logs, Humphrey 4-18 and Sidebottom 6. Observing the lithology log of DS-6 in Figure 28, there is a slight decrease in the density reading from the Mississippian oil/water contact (OWC) down to the Osage. This explains why Osage amplitude map displays negative values. The acoustic impedance shows a decrease as well. Also, the Osage has a low photoelectric (PE) reading relative to the surrounding limestone, which indicates the presence of dolomite.

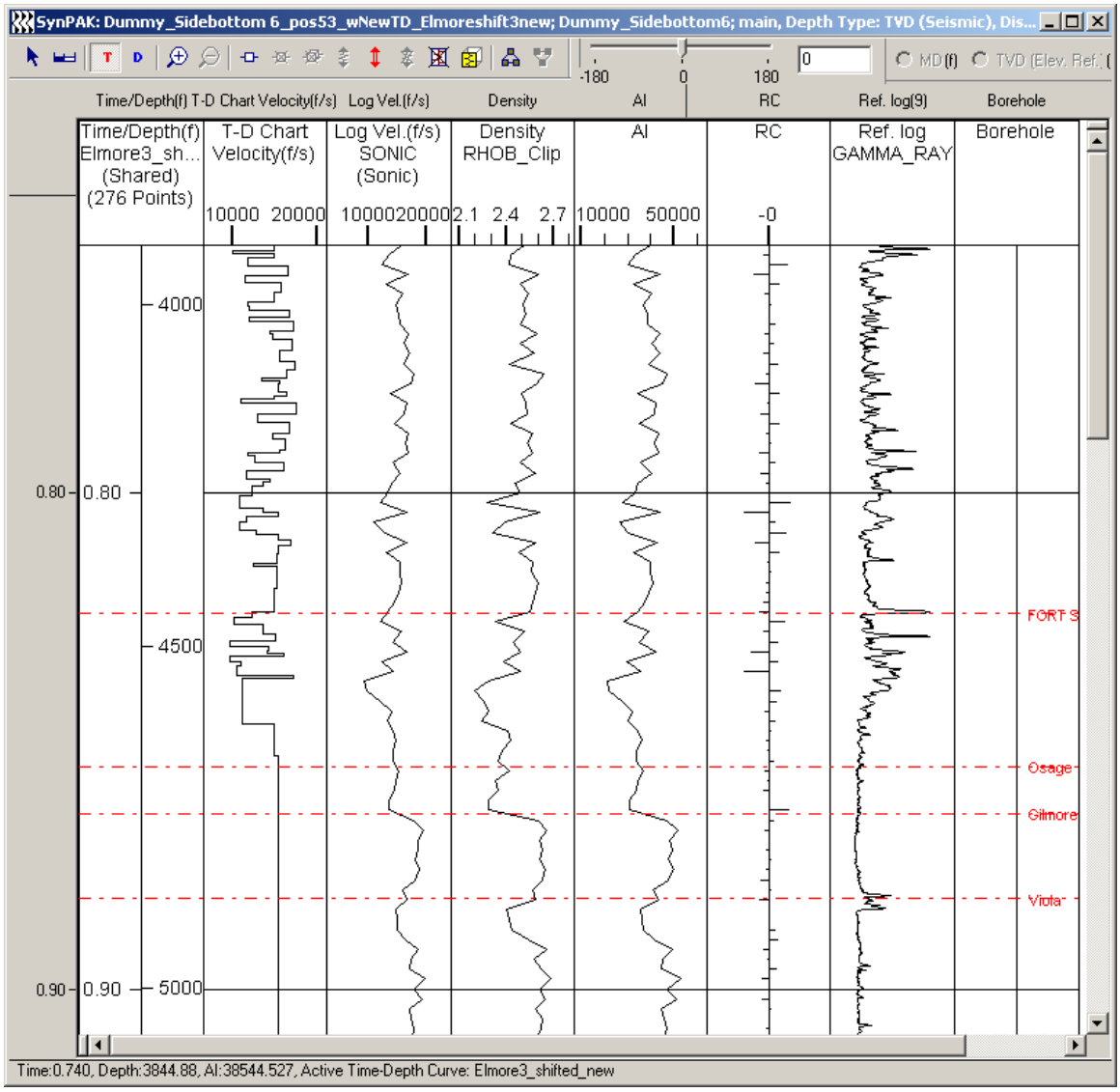

Figure 28: DS-6 lithology logs (sonic, density, and gamma ray), acoustic impedance, and reflection coefficient displayed.

The density log values for the underlying Gilmore City have a substantial increase while the sonic log (Figure 28) has a slight increase when moving from the Osage to the underlying Gilmore City. This explains why we now see more positive amplitudes in the Gilmore City amplitude map. The lesser density reading in the overlying Osage is not only a lithology indicator but also implies a higher presence

of porosity than in the Gilmore City. The Gilmore City has a higher PE reading (not shown in Figure) than the Osage and is relatively pure limestone.

The Sidebottom 6 (and DS-6, Figure 28) is the only well that contains lithology logs penetrating the Viola formation. Both the density and sonic logs (Figure 28) have a minor decrease when going from the Gilmore City down into the Viola formation but we see positive values in the Viola amplitude map. This is attributed to the fact that I mapped the Viola horizon on the peak below where its actual pick was located (at the above zero crossing).

One observation with amplitude needed further investigation, the channel trend of low amplitudes in the Osage amplitude map. One would not expect to see an imprint of the Miss./Penn. incised channel almost 100 ft. (30.5 m) below at Osage depth. A possible hypothesis explaining this observation is velocity sag due to the channel therefore affecting the information below. Velocity sag (or velocity push-down) is defined by Sheriff, (1991), as "a velocity anomaly resulting form local shallower material of exceptionally high (or low) velocity. It has the effect of pulling up (or pushing down) horizons under the shallower high (or low) velocity." Though it is unlikely for velocity sag to directly affect the amplitudes, this matter must be considered to confirm that what we are seeing is geology and not data corrupted by velocity sag. To test this hypothesis I computed the average velocity in two wells from 4412 ft. (1345 m) (~Miss top) to 4492 ft. (1369 m) (Figure 29).

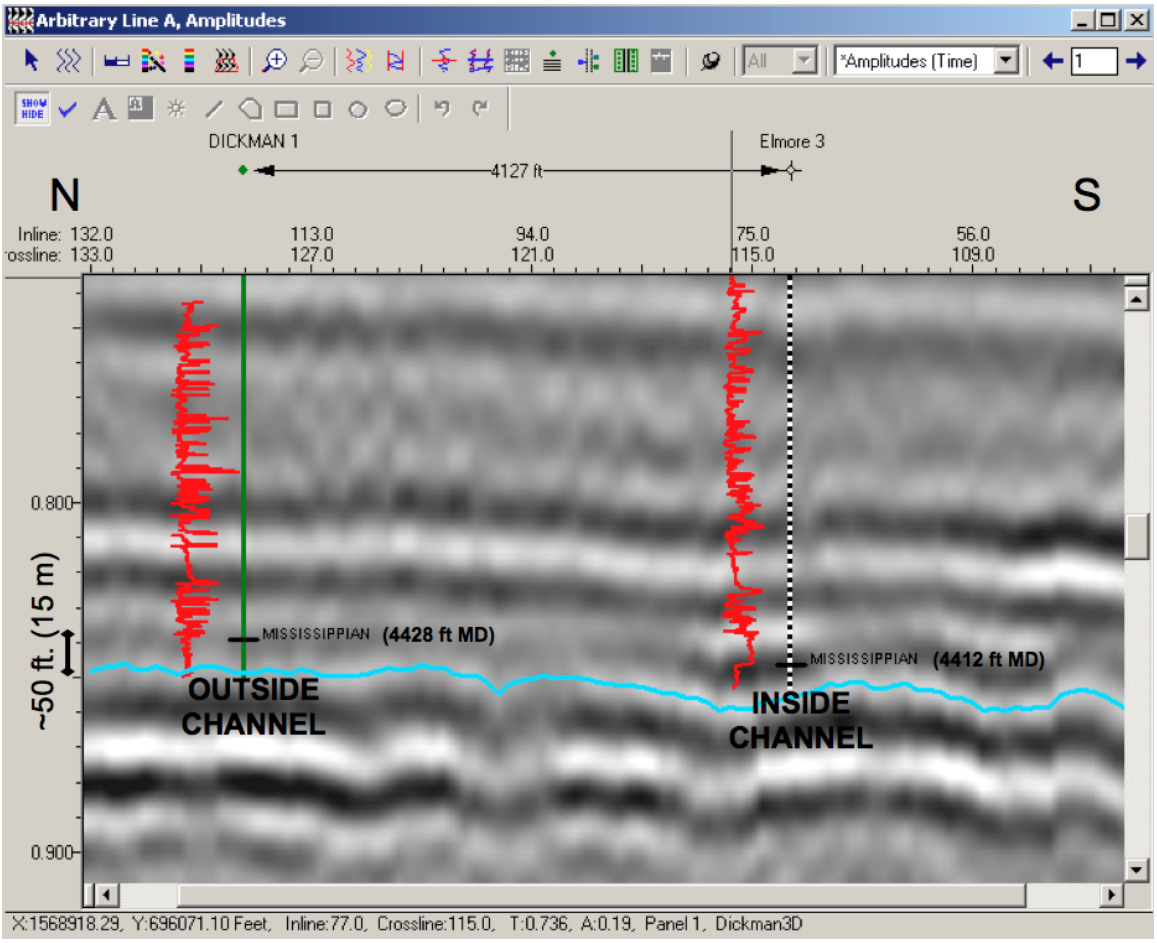

a)

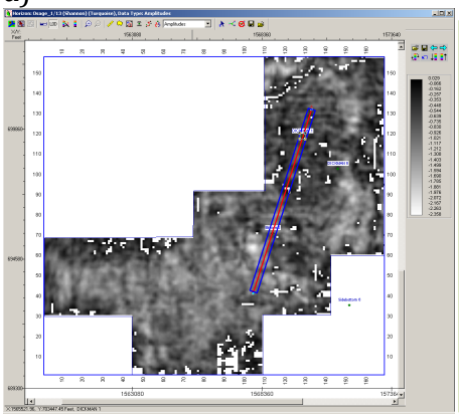

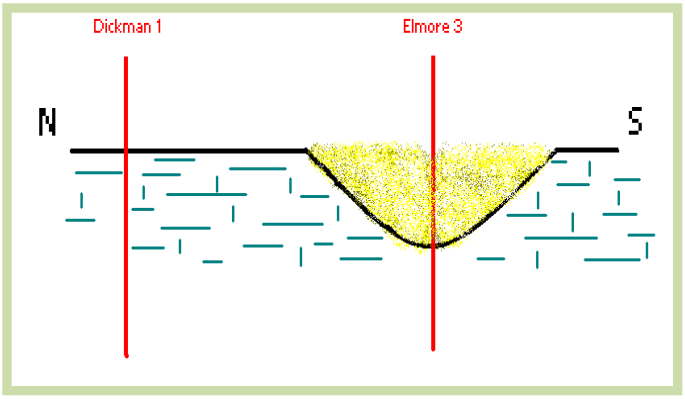

b) c)

Figure 29: Channel sag estimation (a) Vertical section. (b) Base map with location of arbitrary line. (c) Schematic diagram displaying location of wells for velocity sag calculation. Resulting time difference was 0.135 milliseconds, less than one time sample (2 ms) so not large enough to be considered channel sag.

One of the wells, Dickman 1, was outside the channel and the other, Elmore 3, was inside the channel. With the average velocity from sonic at each well (V_1 and V_2) and the target depth interval (Δz) we can calculate the time difference to the top of the Mississippian between the two well locations (Figure 29). The resulting time difference of 0.135 milliseconds is less than one time sample (2 ms) and not large enough to be observable. Therefore, the channel imprint at Osage depth is indeed real geology.

Coherence

Coherence is an attribute that highlights discontinuities by measuring waveform similarity. Figure 30 shows the Viola coherence map has a maximum value (lighter in color) of 127 and a minimum (darker) of 101. The high values are areas where the waveform and it's surrounding waveforms are very similar. The darker anomalous areas indicate rapid lateral change in reflectivity. These darker areas in the coherence map are probably representative of the karst features throughout the Viola formation. They also have the tendency to be more concentrated near/around the vicinity of the shallower channel (Miss/Penn boundary) and the western most portion of the map. Furthermore, most Viola fracture/fault picks align perfectly with the dark anomalous features but there are many dark areas that have no fault/fracture picks that align with them.

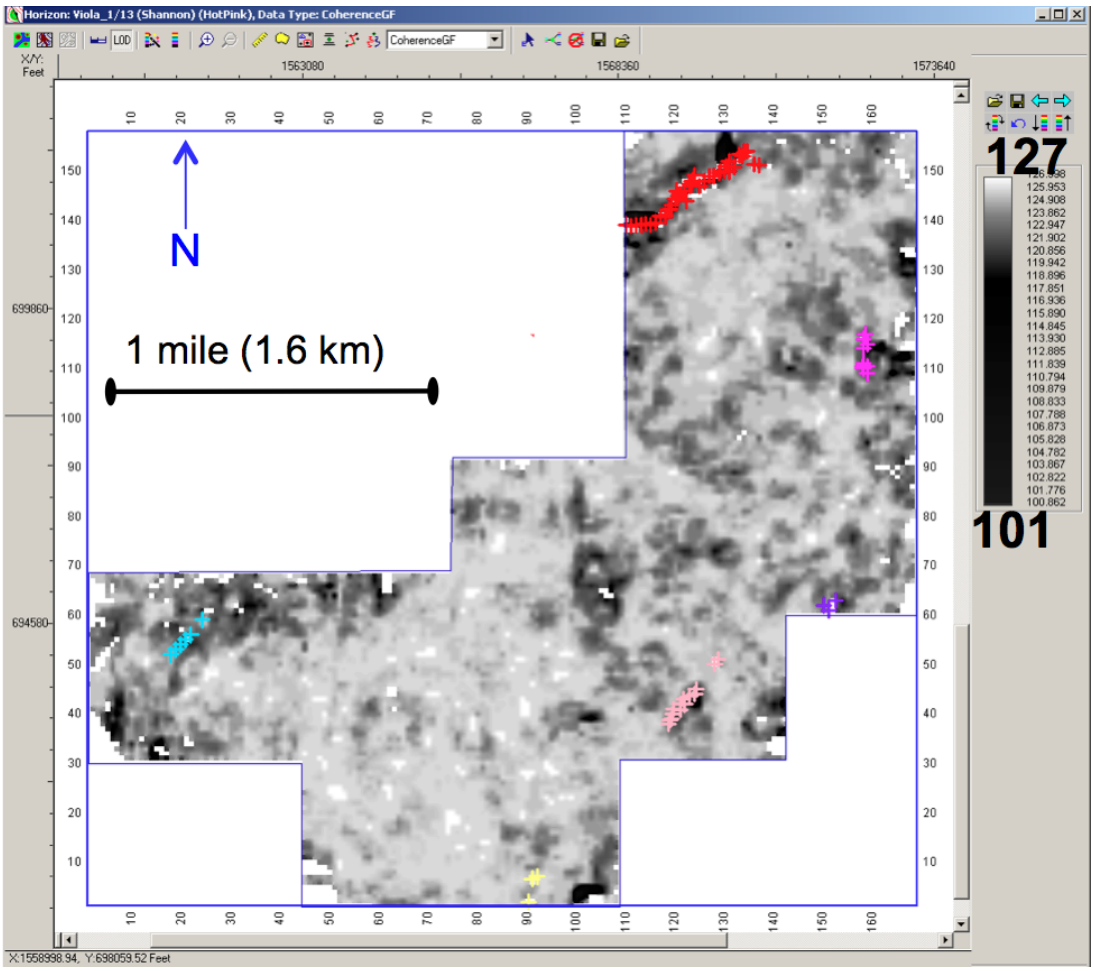

Figure 30: Viola horizon coherence map. Dark anomalous areas are representative of karst geology. Most discontinuity picks align with anomalous areas.

The coherence map of the Gilmore City horizon (Figure 31) is not as pronounced as the Viola in that there is less of a contrast and fewer anomalous features. It has a maximum value of 127 and a minimum of 82, which is a larger range than the scale of the Viola. The anomalous features that are present in the Gilmore City coherence map were also in the Viola. The difference is that these features have a greater (lighter in color) value than the Viola features. Also, there are more fault/fracture picks (9 picks as seen in Figure 31) displayed in the Gilmore City map than in the

Viola (6 picks), but not all of them have the obvious alignment with the anomalous features like those in the Viola. One interpreted karst feature stands out in this map and does not have a corresponding fault/fracture pick. This feature looks like a circular depression and is located between inlines (west to east) 30-40 and crosslines (north to south) 95-110. This area was seen as an anomalous feature in the Viola coherence map but it did not have the distinct circular shape. It is also analogous to one of the deepest parts of all structure maps and is interpreted as a possible sinkhole.

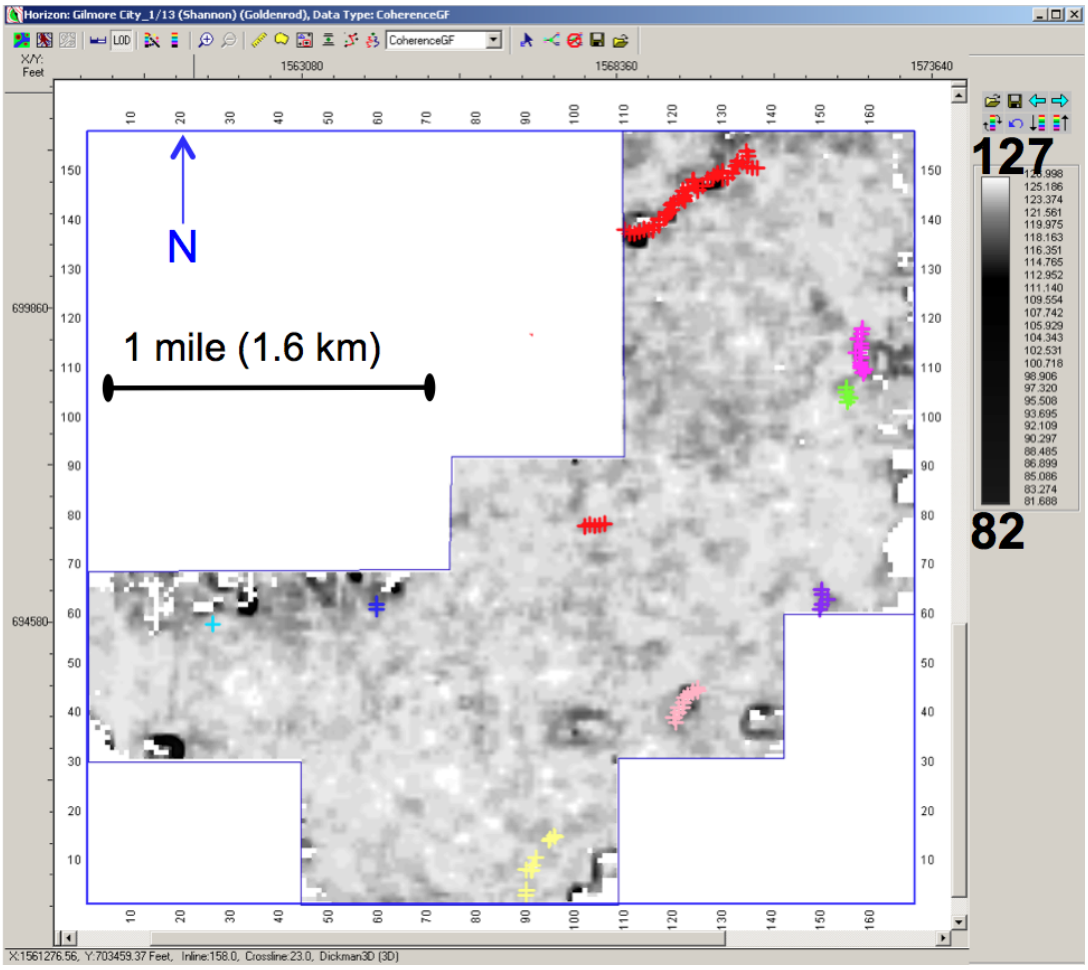

Figure 31: Gilmore City horizon coherence map, note circular feature between inline 30-40.

When observing the Osage coherence map in Figure 32, more anomalous features are seen than in the Gilmore City but still not as abundant as in the Viola coherence map (Figure 30). The Osage's anomalous coherence features, like the Viola, are most concentrated near/around the vicinity of the overlying Miss/Penn channel.

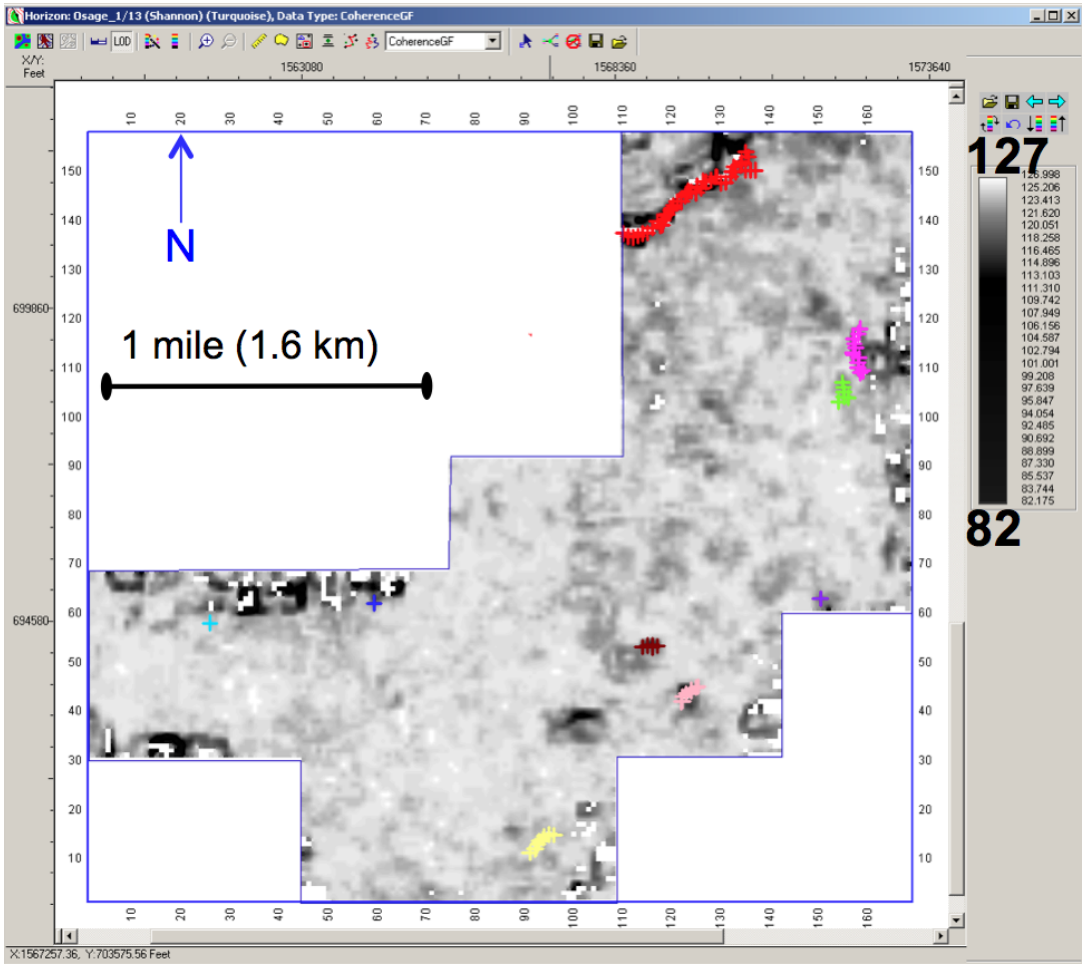

Figure 32: Osage horizon coherence map, note circular and U-shaped features (depressions).

The maximum value in the Osage coherence map is again 127 and the minimum is 82. This scale has about the same range as the underlying Gilmore City but still exhibits more anomalous features. The Osage coherence map contains 9 visible

fault/fracture picks (Figure 32) and most of them align with the anomalous features present. There are anomalous features within the map that do not have corresponding fault/fracture picks. Two particular features standout in this map, the circular depression that was in the underlying Gilmore City map and the other is a U-shaped depression in the middle of the map. This U-shaped feature was also an extreme low observed in the Osage amplitude map. I am confident that these features are indeed depressions because the time and depth map confirm that these are areas of lower topography. The U-shaped depression was also a noted feature in the Viola coherence map but it did not have the unique U-shape.

Variance

Variance is a definition of coherence that relies on lateral amplitude so it is not too surprising that the Viola variance map (Figure 33) has some similarities to the coherence map. There are differences observed as well. For instance, there is a much sharper contrast in the variance map than there was in the coherence map. Anomalous features are much darker and more abundant than those in the coherence. There are features present in areas of the variance map where no coherence features were present and these features have no particular trend. The Viola variance map's scale has a minimum value (light in color) of 0.000 and a maximum (dark) of 0.959, which means the variance map scale is much different from that of the coherence map scale. Variance scales portray a much smaller range than the coherence scales and this might be due to the differing methods of

calculation for variance and coherence. Most anomalous features in the Viola variance map have a curved or circular signature. There are 6 different fault/fracture picks in the Viola variance map (Figure 33) and every one of them is aligned with a dark anomalous feature. 3 out of these 6 feature lie on or very near to the edge of the map and this has to be considered when categorizing the fractures.

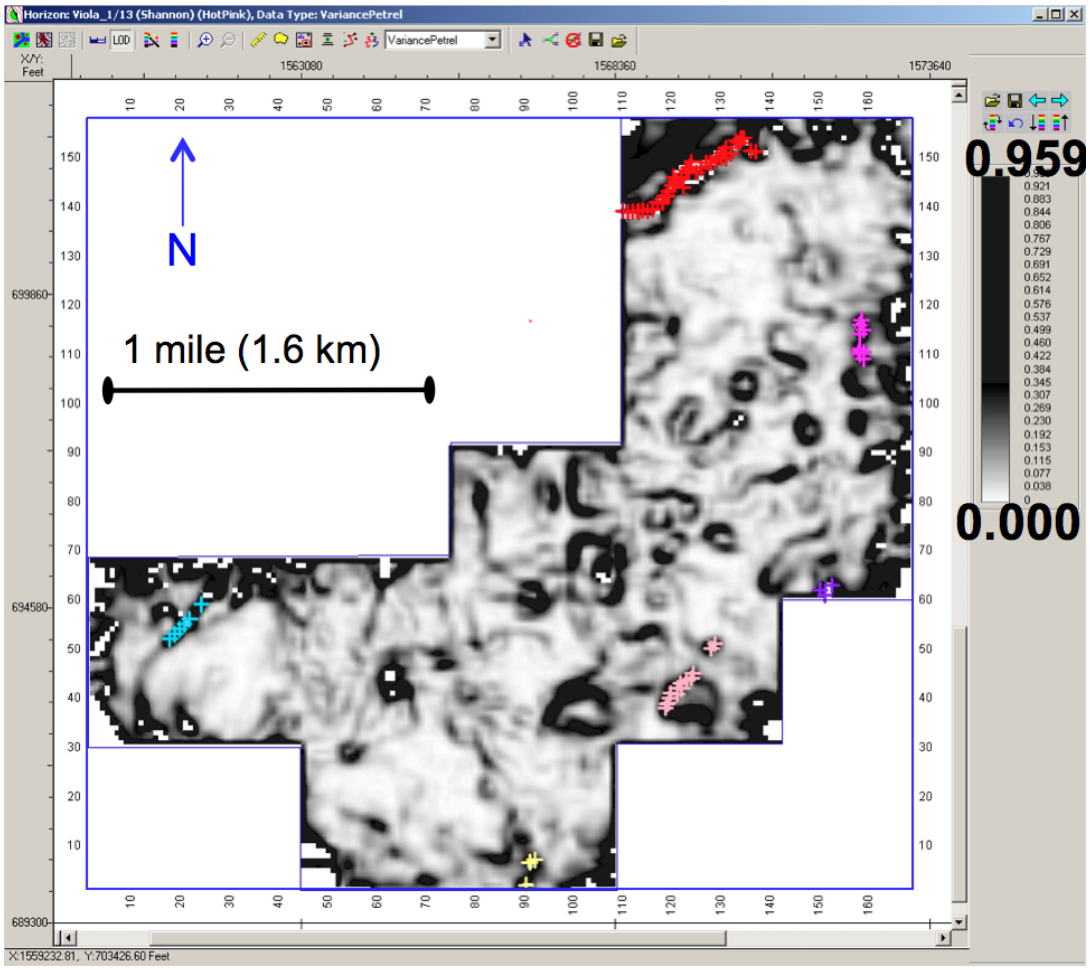

Figure 33: Viola horizon variance map, circular features represent karst. All discontinuities align perfectly with anomalous features so this attribute was used as the input for Viola horizon ANT map.

One of the circular features (southeast portion of map) has a fault/fracture pick that aligns with almost half of the circumference of the circle. I believe these circular features are representative of karst features in the Viola formation.

The Gilmore City variance map (Figure 34), like coherence, exhibits fewer anomalous/dark features than the Viola variance map. Although, the features that are present seem to be more abundant on the middle-northeastern portion of the map, which is in the vicinity of the above channel (Miss/Penn). These features still have a curved or circular shape like those in the Viola variance map and most have the same standout, size, and locations. In fact, some of these features are somewhat grouped together in such a fashion that mimics the outline of the above channel trend (previously highlighted in Figure 26).

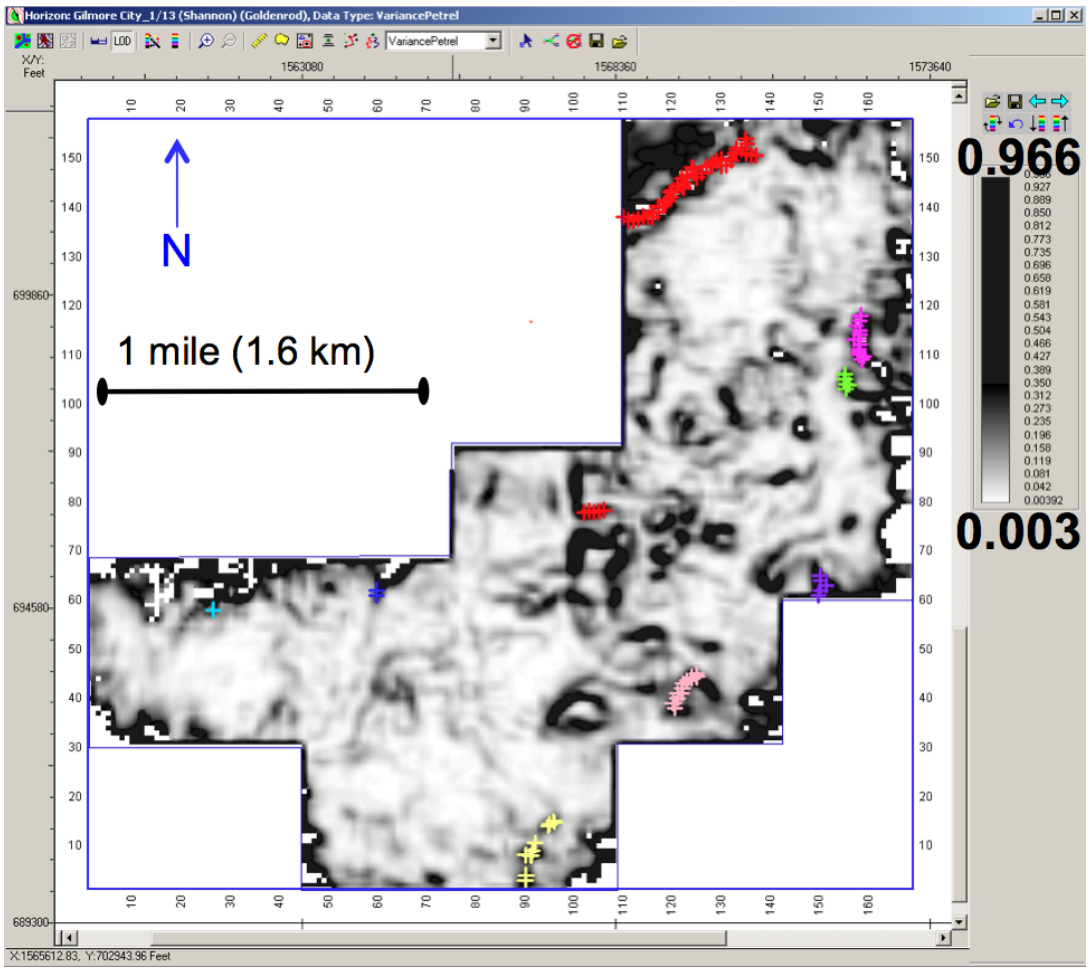

Figure 34: Gilmore City horizon variance map, most karst (circular) features in vicinity of overlying Miss/Penn channel. All discontinuities align perfectly with anomalous features so this attribute was used as the input for Gilmore City horizon ANT map.

The minimum value in the Gilmore City variance scale is 0.003 and the maximum is 0.966. There are 9 different fault/fracture picks in the Gilmore City variance map and again every one of them aligns almost perfectly with these karst features. Also, as before we must take into account that some of these fault/fracture picks lie on or near the edge of the map. The same fault/fracture pick that aligned with the circular karst feature in the Viola variance map (southeast portion of the map), is also present in the Gilmore City variance map. In the most eastern portion of the map

there is a curved feature that is less extensive than seen at the Viola level. The fault/fracture pick that aligns with this feature also has more picks for that particular discontinuity in the Viola than it does in the Gilmore City. This confirms accuracy of highlighting discontinuities in the Dickman Field with variance.

Figure 35 shows the Osage variance map reveals about the same quantity of anomalous features as the Gilmore City but these features have a slightly different distribution. There are little to no features in the southwestern portion of the map. Like the two horizons below, the Osage variance features also have a curved signature. The grouping of these features in the center portion of the map is even more evident in the Osage variance map than in the Gilmore City map. These features are also better connected in the Osage map and better mimic the nature of the overlying Miss/Penn channel. The scale of this map ranges from a minimum of 0.003 and a maximum of 0.932. As with the previous two variance maps (Viola and Gilmore City), every discontinuity pick displayed in the Osage variance map aligns perfectly with the anomalous features and their orientation.

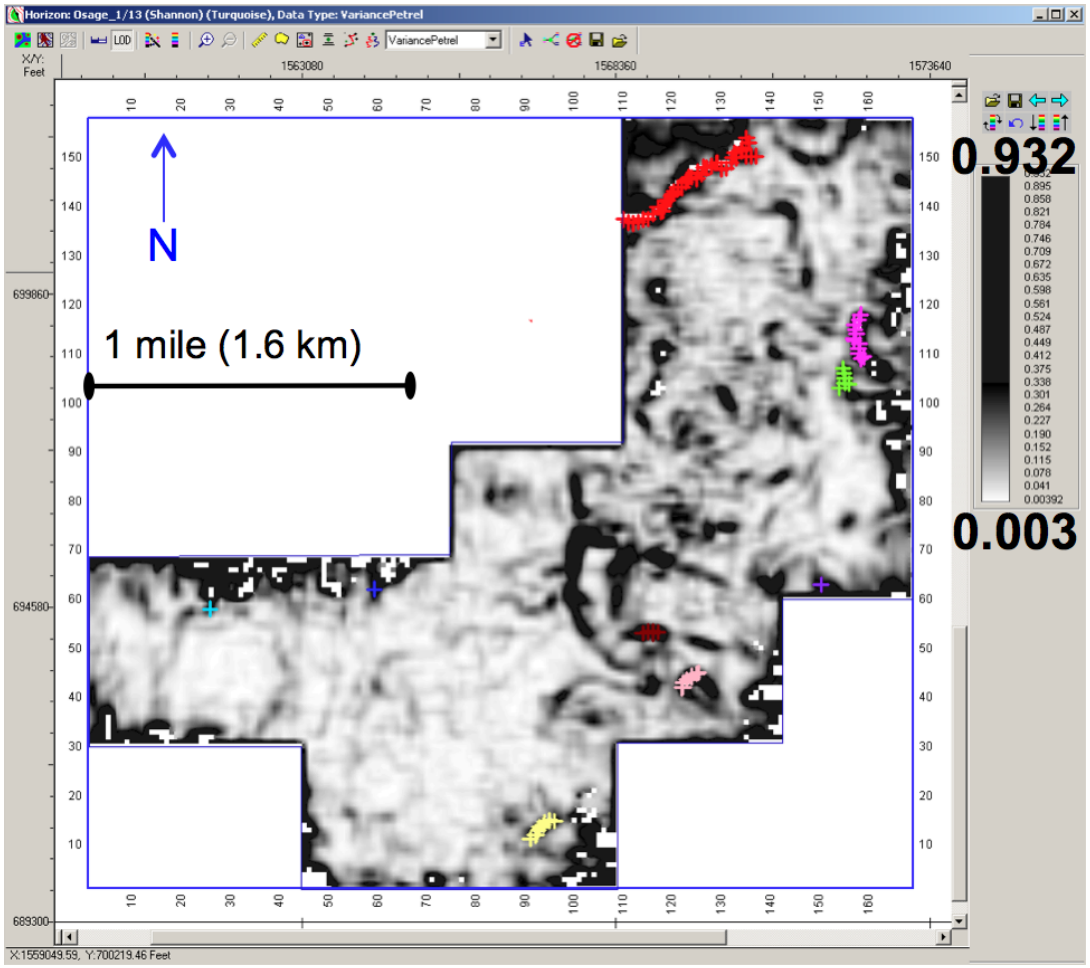

Figure 35: Osage horizon variance map, most karst (curved) features in vicinity of overlying Miss/Penn channel. All discontinuities align perfectly with anomalous features so this attribute was used as the input for Osage horizon ANT map.

Curvature

Curvature measures reflector dip and azimuth to estimate the shape of a reflector. This attribute is useful for detecting discontinuities as well. In Figure 8, recall Nissen et. al. studies a regional dip (required for subsequent curvature) map of the top of the Mississippian surface to interpret lineaments. One lineament right outside northwest corner of the survey (different shape in Figure 8, current survey size has increased) has a northeast-southwest orientation. This area of high dip (dark)

corresponds with the northeast-southwest fault in the northwest corner of our survey. Also, there are a few more discontinuity picks within the survey with a northeast-southwest orientation. The dip map assists with fault/fracture identification so even more detail should be seen when we take azimuth into account as well.

There were two curvature attributes examined in the Dickman project. One curvature attribute had a 50-millisecond window and the other had a 30-millisecond window. After comparing the two curvature maps, it was observed that the curvature using the smaller window showed a little more detail. On the contrary, this detail was so abundant that it was somewhat difficult to recognize analogous features. The main trends were still discernable in both the large and smaller windowed curvature attributes. Therefore, I only found it necessary to interpret the 50-millisecond curvature attribute. Both the negative and positive curvature were investigated for each horizon. They had very similar maps so only negative curvature will be displayed.

The Viola negative (Figure 36) and positive curvature maps, unlike the previous attributes analyzed do not exhibit anomalous features more so in one portion of the map than another. These maps more or less show us the orientation of lineaments. The lineaments are representative of areas of high curvature. The common orientations seem to be trending north to south and west to east but we must keep

in mind that geophone array (Figure 47) was also oriented from north to south which could bias the validity of the observed lineaments. The most prominent of these features is located in the center of the map. This is the same location in which a connection of features was observed in the Variance maps.

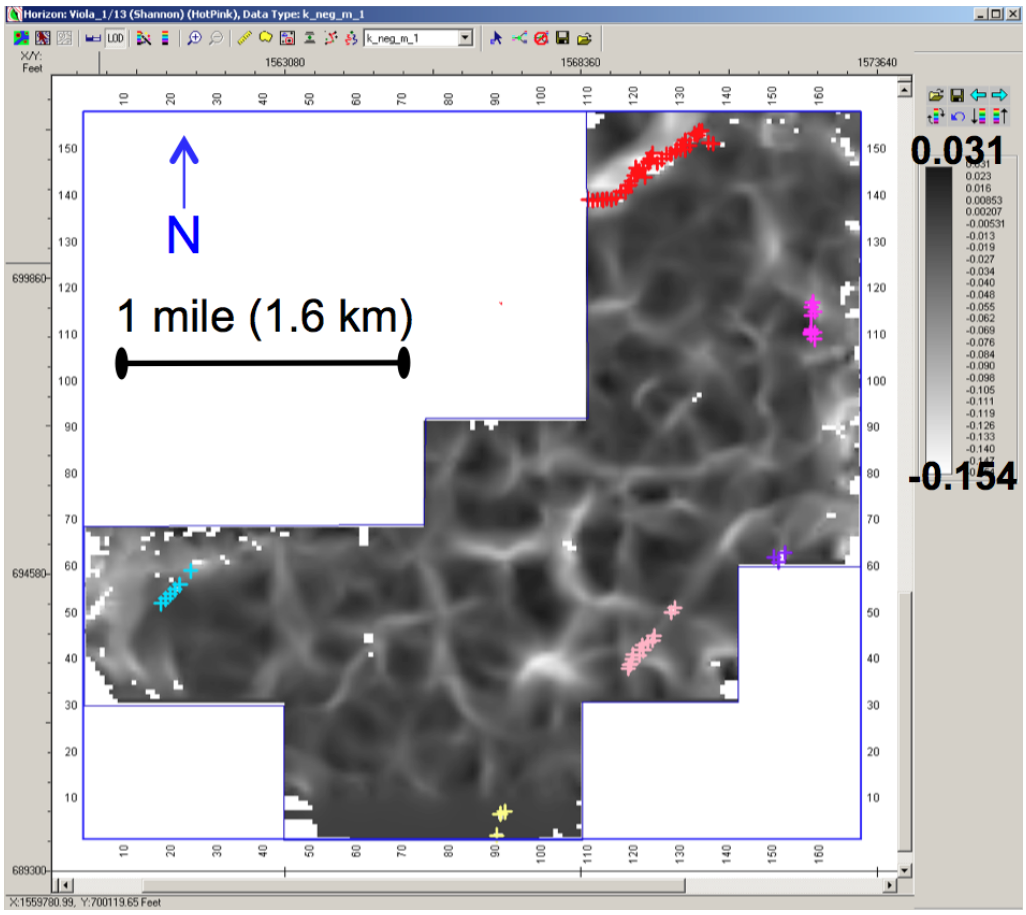

Figure 36: Viola horizon negative curvature map, most lineaments oriented N-S and E-W. Strongest features in vicinity of overlying Mississippian/Pennsylvanian channel.

The maps do contain lineaments oriented from northeast to southwest and northwest to southeast but these lineaments do not stand out as much. Although 3 out of the 6 fault/fracture picks are aligned with the northeast-southwest

orientations. These 3 features also have more extent than the other 3 discontinuity picks. The negative curvature map of the Viola has a maximum value (dark) of 0.031 and a minimum (light) of -0.154.

Negative and positive curvature maps of the Gilmore City (Figure 37) are very similar to those of the Viola. The orientations and their locations are the same although there are a few more lineaments that show on the Viola maps that are not present in the Gilmore City curvature maps. Again, the highest area of curvature is located in the center portion of the map, in the vicinity of the Miss./Penn. channel above. One slight difference observed in the Gilmore City curvature map (Figure 37) is that the lineaments in the negative curvature map seem thicker than those in the Viola (Figure 36), which is a result of the Gilmore City being in closer proximity to the overlying Miss./Penn. channel.

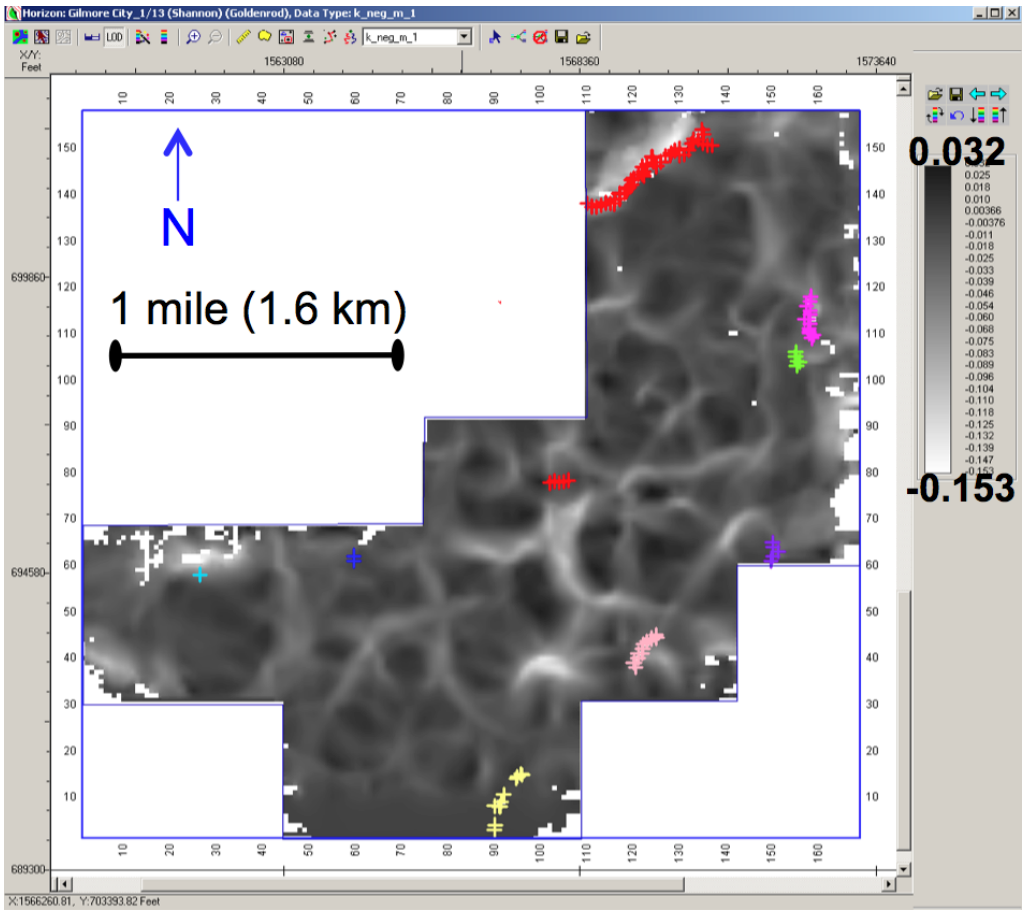

Figure 37: Gilmore City horizon negative curvature map, strong lineaments oriented N-S and E-W. Strongest features are in vicinity of overlying Mississippian/Pennsylvanian channel.

Almost all the discontinuity picks for the Gilmore City curvature maps align with areas of high curvature. Fault/fracture pick 12, in the most southern portion of the map (refer to Figure 16 for exact location), does not align and the reason for this is most likely due to the edge effects. From inlines 0-10 (southern portion) there is no observed curvature information as was the case in the Viola curvature maps as well. 4 out of the 9 fault/fracture picks in this map have extent, one being the pick (12) in the most southern portion of the map where there is minimal curvature

information. The Gilmore City negative curvature map has a maximum of 0.032 and a minimum of -0.153.

As with the Viola and Gilmore City curvature maps, the Osage curvature map in Figure 38 portrays very similar characteristics. The orientation of lineaments is similar as is the quantity of lineaments. The areas of high curvature in the Osage negative curvature map seem thicker than in the Gilmore City. The Osage curvature maps do not display as sharp of a contrast as the Viola or Gilmore City maps. This is due to the broader range in scale. The Osage negative curvature map has a maximum of 0.048 and a minimum of -0.137. Most all of the faults align with areas of high curvature and the same 4 extensive discontinuities at the Gilmore City curvature map are also present in the Osage curvature map. About 3 out of the 9 fault/fracture picks on the Osage negative curvature map are on or near the edge of the survey.

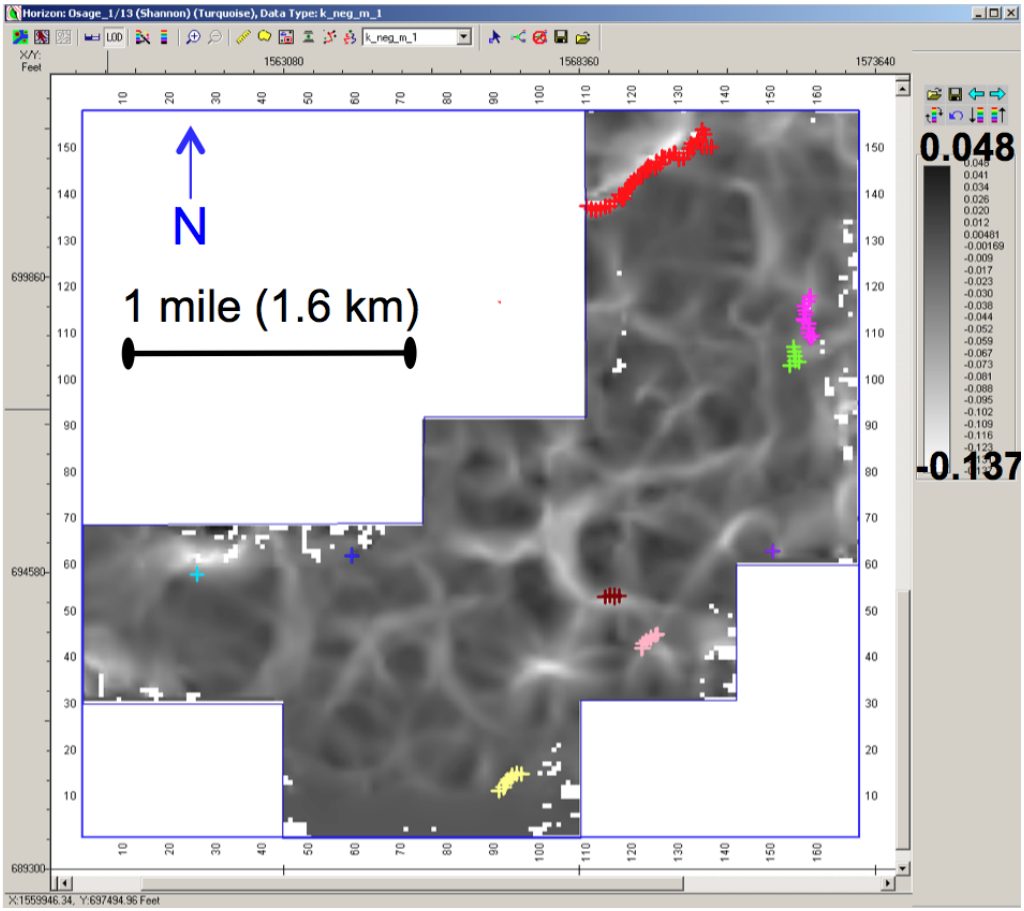

Figure 38: Osage horizon negative curvature map, most lineaments are oriented N-S and E-W. Strongest features are in vicinity of overlying Mississippian/Pennsylvanian channel.

SPICE

SPICE (spectral imaging of correlative events) is a recent attribute that "relates to spectral shaping during wave propagation and reflection" (Liner et. al., 2004). This attribute is especially useful in highlighting discontinuities in that the interpreter can pick fault/fractures in a vertical section using SPICE as the data type. The SPICE attribute contributed to almost half of the fault fracture picks (in vertical section) in this project and was additionally analyzed extracted from each horizon.

Figure 39 shows the Viola SPICE map, like most of the previous attributes (excluding curvature), displays several anomalous areas within the survey area. Most of these areas are in the same locations as anomalous features from previous attributes analyzed. Though, surprisingly these anomalous features do not display as noticeable of a signature as does variance or coherence. Like variance and coherence, several karst depressions are observed in this map, the most obvious being in the center of the map. This karst feature in the center of the map was the same U-shaped feature in the Osage coherence map and the extreme low in the Osage amplitude map.

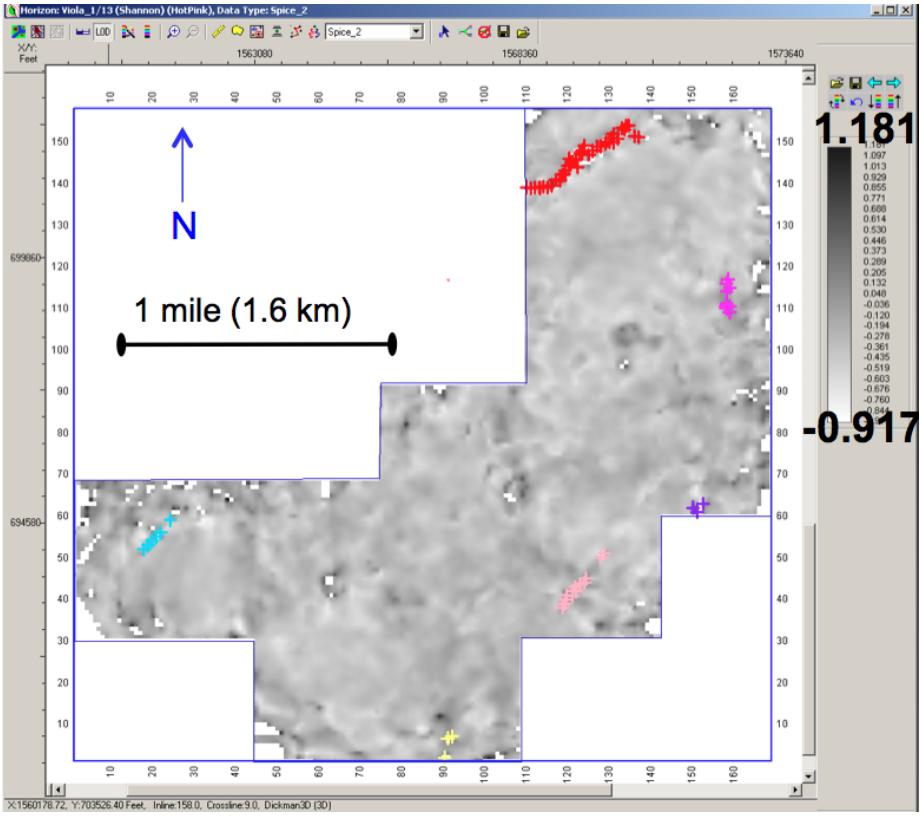

Figure 39: Viola horizon SPICE map, Strongest features in vicinity of overlying Miss./Penn. channel but have no corresponding discontinuity picks.

The discontinuity picks align with the less obvious features of the map. The stronger features have no corresponding faults although all fault/fracture picks do align with an anomalous features rather it be a strong or a weak feature. The maximum value on the Viola SPICE scale is 1.181 and the minimum value is -0.917.

When analyzing the SPICE map for the Gilmore City (Figure 40), the first observation made was that the strongest feature in the center of the Viola map is no longer present in the overlying Gilmore City horizon.

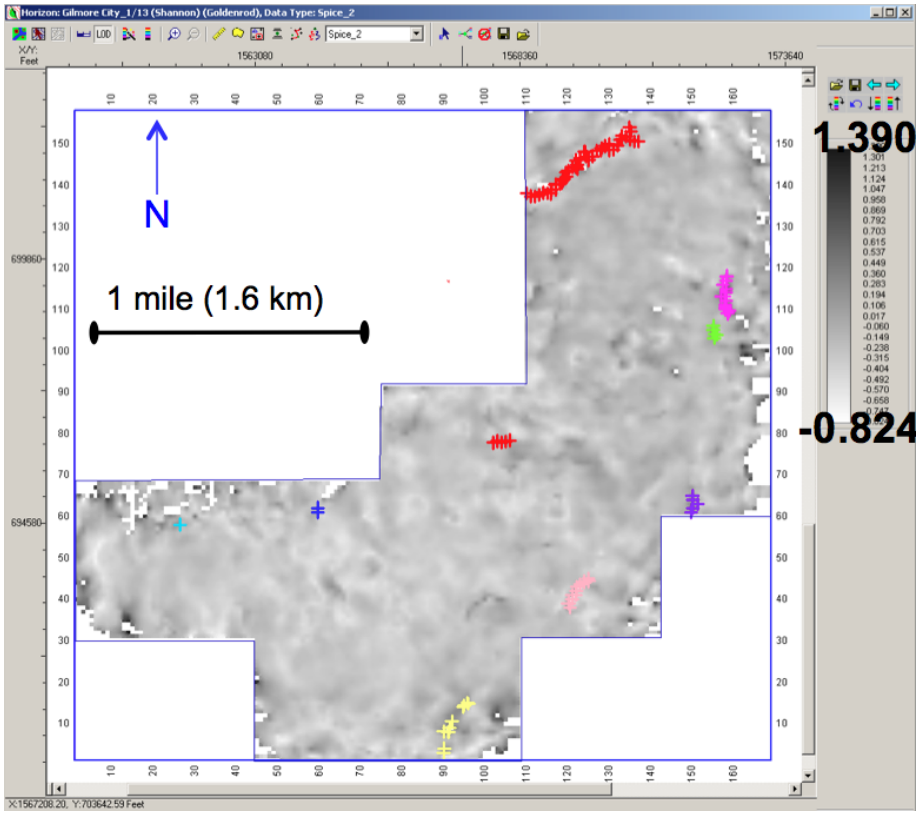

Figure 40: Gilmore City horizon SPICE map. Quantity of anomalous features is less than in the Viola horizon SPICE map.

In fact, there are not many features in this map that were as evident as those in the Viola SPICE map. Most of the discontinuity picks align with anomalous features although 3 out of the 9 fault/fracture picks of the Gilmore City SPICE map did not align with any obvious features. The scale for this map had a maximum value of 1.390 and a minimum value of -0.824, a slightly broader range than the Viola SPICE map. This might give some explanation to why we do not see as obvious features and as sharp of a contrast in the Gilmore City as we do with the Viola. Another explanation could be that the Viola contains more karst features than the overlying Gilmore City.

Figure 41 shows the Osage SPICE attribute map displays more evident anomalous features than the Gilmore City. Still, the Viola takes the lead with the most obvious and most abundant features. The exact locations of these distinct features differ from the Gilmore City and the Viola SPICE map features. The most prominent features reside in the center to northeastern portion of the map, which is analogous with the trend of the overlying Miss./Penn. channel. Almost all of the discontinuity picks align with the dark features present in the Osage SPICE map, fault/fracture pick 13 and 11 are skeptical. The scale for this map has a maximum value of 1.193 and a minimum of -0.061.

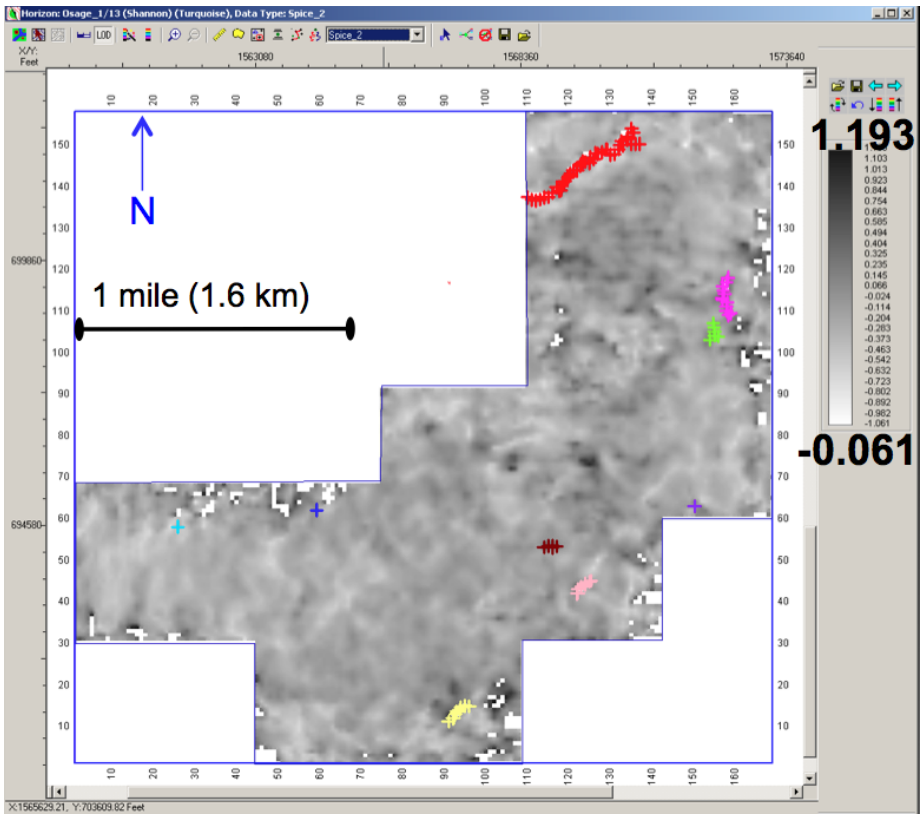

Figure 41: Osage horizon SPICE map, strongest features in vicinity of overlying Mississippian/Pennsylvanian channel.

ANT (from Variance) Tracking

The ANT Tracking attribute produced some of the most significant maps for interpretation because these maps deliver a visual of the so called pluming system within each horizon. Both ANT from SPICE and ANT from variance were observed but I chose only to make interpretations for the ANT from variance. The main reason for this preference is because the variance attribute was more correspondent with the alignment of discontinuities to anomalous features than the SPICE attribute.

The ANT attribute map for the Viola horizon (Figure 42) shows the darkest lineaments to be oriented in a north to south (same orientation as receiver array) and west to east orientation, the same orientation displayed in curvature maps.

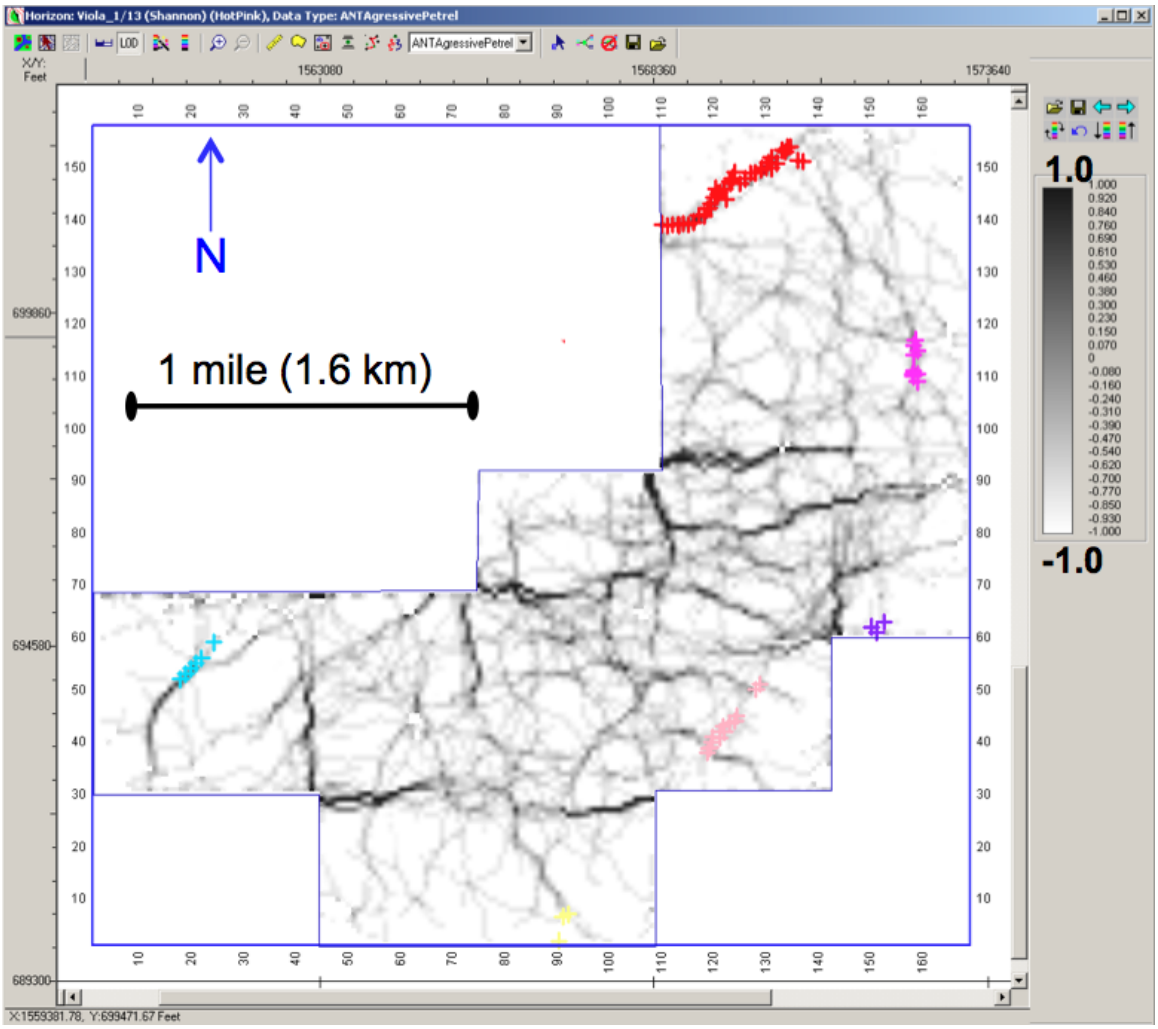

Figure 42: Viola horizon ANT map extracted from Variance map (see Figure 33).

Most of these features are located around the center portion of the map. There are northeast-southwest and northwest-southeast oriented lineaments but they do not have as much standout as north to south and west to east. All fault/fracture picks

are aligned perfectly with only a select amount of the lineaments present in map. 3 out of the 6 discontinuity picks are aligned with the northeast-southwest lineaments and 1 aligned north to south. Feature 12 (most southern portion of map) is aligned with a northwest-southeast lineament but the orientation of 12's fault surface is northeast to southwest. There are many other lineaments with no corresponding fault fracture picks and these areas were investigated once more in vertical section to confirm that there were indeed no faults or fractures in these areas. The minimum and maximum values for all three ANT horizon attribute maps were -1.0 and 1.0 respectively.

Figure 43 shows the Gilmore City ANT attribute map generally has the most prominent features in the same locations as the Viola. The darkest lineaments are also in a north to south orientation as was the Viola. It is not surprising that all fault/fracture picks align perfectly with selected lineaments in the Gilmore City ANT attribute map. Over half of the Gilmore City discontinuity picks are aligned with the northeast-southwest orientation but one of these picks is different from its lineament orientation in the Viola. This pick (12) is located in the most southern portion of the map and was previously oriented with a northwest-southeast lineament in the Viola which peculiar since the orientation of the fault pick is the exact opposite. It is more valid in the Gilmore City ANT map that the fault/fracture pick aligns with the same orientation as the lineament. 3 out of the 9 picks are in a north to south orientation and 1 is in the west to east orientation.

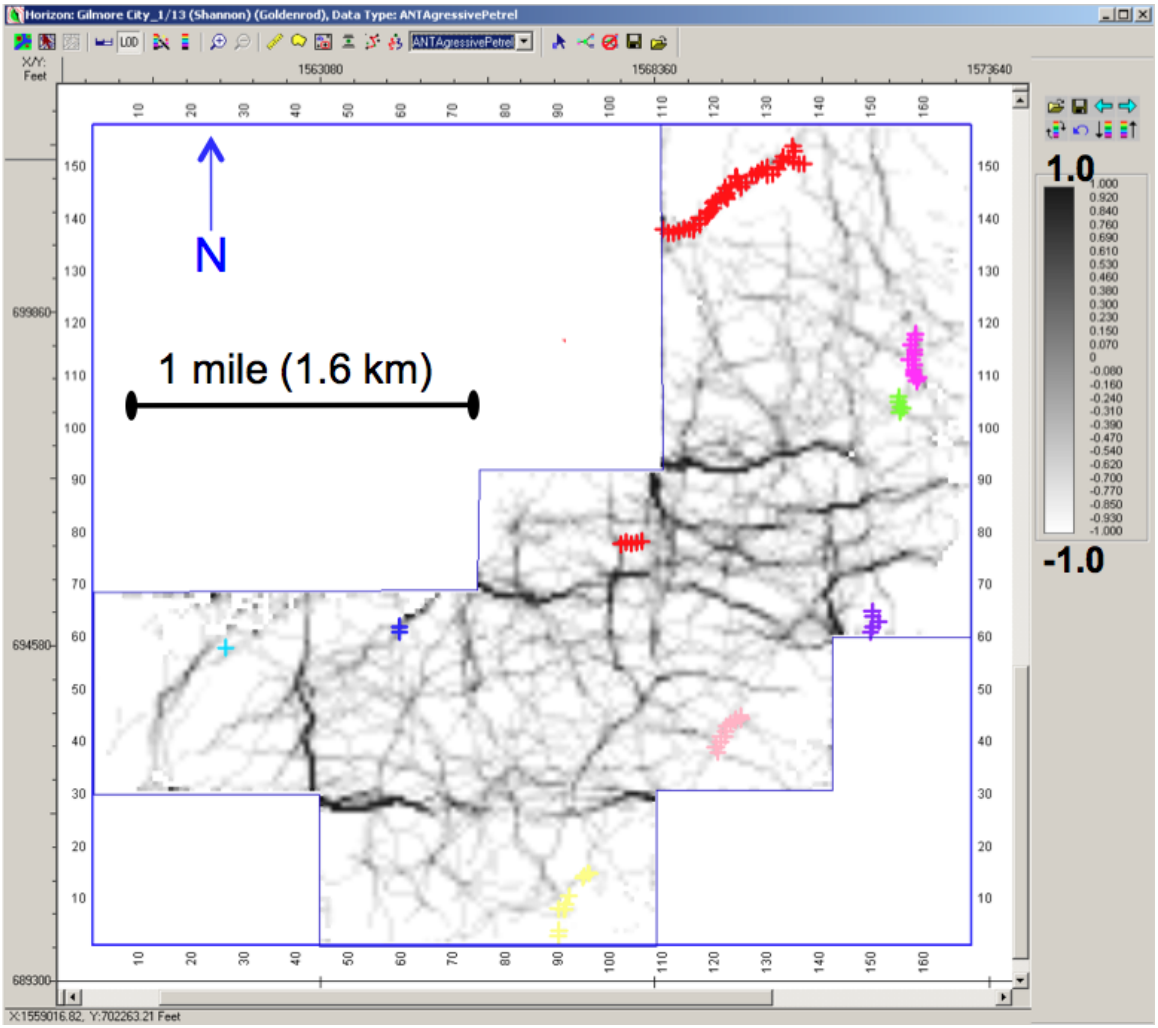

Figure 43: Gilmore City horizon ANT map, extracted from Variance map (see Figure 34).

The ANT attribute map for the Osage horizon (Figure 44) has a larger quantity of dark lineaments than the previous underlying horizons. These features once more have the same orientation with north to south being the most common and darker in color than the other features. 5 out of the 9 lineaments are oriented in the northeast-southwest direction, 3 (8, 10, and 14) are oriented north to south and 1 is oriented west to east. As with the underlying horizons, most of these dark

lineaments are located in the center portion of the map but there is one particular dark lineament, present in all horizons, that is located in the western most portion of the map. This lineament becomes even more convincing due to the extent of its corresponding discontinuity pick (13, refer to Figure 16 for location of discontinuity pick).

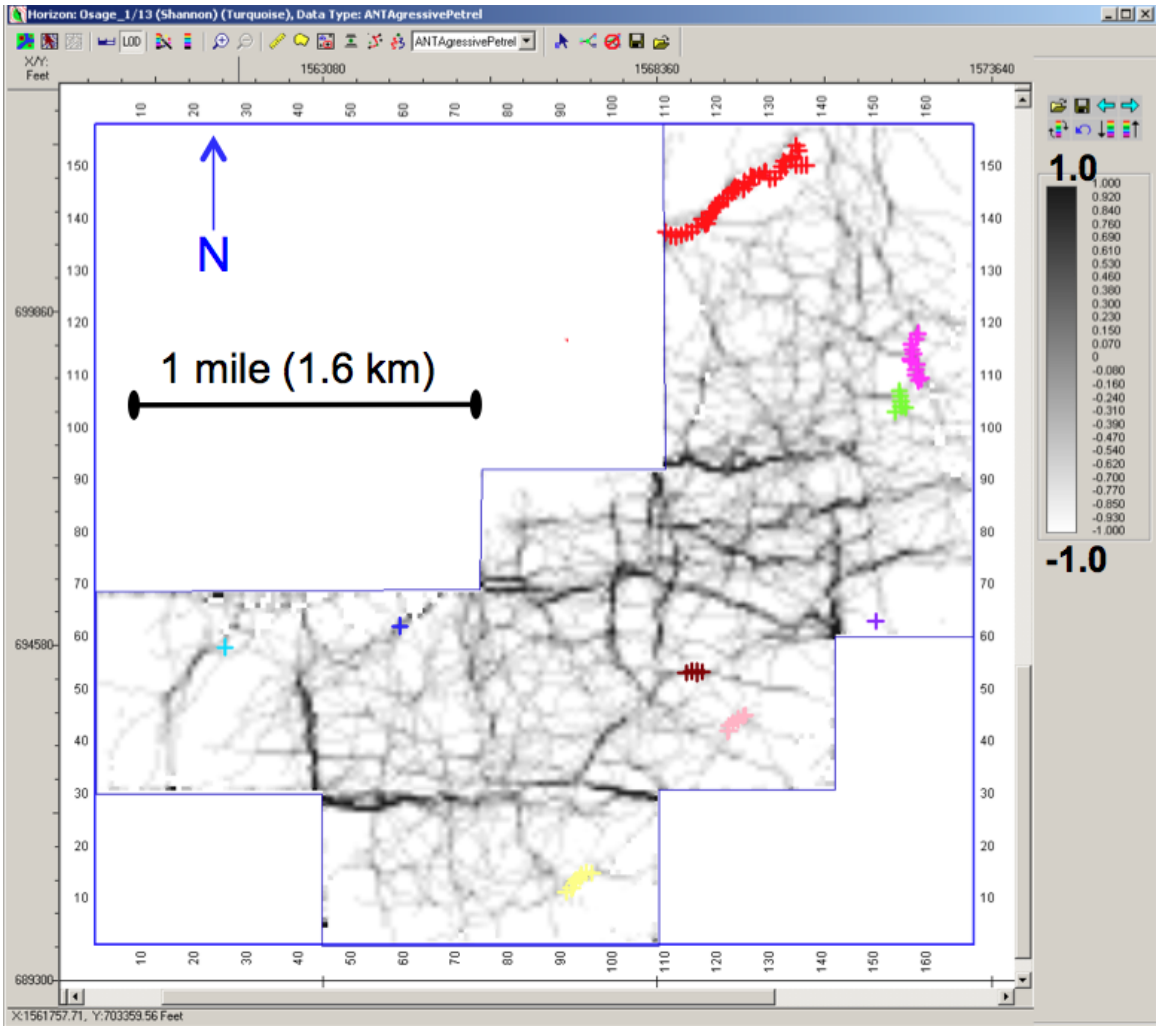

Figure 44: Osage horizon ANT map, extracted from Variance map (see Figure 33).

DISCUSSION

Using 3D seismic data and attributes, I have mapped deep formations at the Dickman field, including Viola (deepest), Gilmore City, and Osage. Time and depth maps alone display rather laterally continuous horizons. The only obvious change in topography is in the vicinity of the channel at the Mississippian-Pennsylvanian boundary. The imprint of the channel is vaguely observed in the Viola but as we move up to the Gilmore City and then the Viola it becomes easily recognizable, especially the meandering portion of the channel in the center portion of the map. This channel imprint is also evident in the Osage amplitude map. In addition, a velocity sag theory has been tested (Figure 29) in order to confirm that the channel imprint is indeed true geology and not a result of sag. Therefore, the karst topography that is present in the Viola must extend all the way up to the Mississippian-Pennsylvanian boundary.

Well logs assisted with the interpretation of amplitude maps. The random clusters of amplitude anomalies are most likely representative of karst areas. Well logs confirm the presence of dolomite and other carbonate minerals that may contribute to the sign (positive/negative) of each amplitude map. Many of the amplitude anomalies, especially at the Osage level, follow the trend of the Miss./Penn. channel imprint. Interpretation of the attribute maps, along with observing and picking discontinuities in both amplitude and SPICE, aided in the verification of

faults/fractures and their classification. Each of the attributes had a different value in highlighting these discontinuities. For instance, the SPICE attribute was much more helpful for fault/fracture identification in vertical section rather than in map view. Only amplitude and SPICE could be analyzed in vertical section. Variance seemed to display the best correlation with discontinuity picks and produced better visualization of karst features than SPICE or coherence. Curvature maps showed us more or less the orientation of lineaments. ANT tracking (from variance) generated better accuracy of correspondence with the fault/fracture picks than curvature while also displaying orientation of strong lineaments. All attribute maps had one common characteristic, they all showed anomalous features that did not have corresponding discontinuity picks. These anomalous features were further investigated in vertical section to confirm that there was no corresponding fault or fracture. Therefore, we must not rely solely on surface attributes to locate possible discontinuities; we must analyze several surface attributes in order to validate and classify picks made in vertical section using both amplitude and SPICE.

Table 6-a shows fault/fracture classification characteristics. Each feature is checked if it had extent, if it was observable on a particular attribute and if it was affected by noise or edge effects. Discontinuities are classified (Table 6-b) as probable if they have significant extent and were seen on most attributes analyzed. Table 4 lists the fault classification criteria. The main fault (1), and discontinuities 7, 10 and 13 were all considered probable faults. Some of these were near the edge of the survey,

including the main fault, but none were likely to be an artifact or noise. Extent was the main factor that enabled a discontinuity to be classified as a probable fault or fracture.

Feature #	Extent	Amplitude Vertical Section	SPICE Vertical Section	SPICE	ANT	Coherence/ Variance	Curvature	Noise Induced	Edge Effects
Main-1	√	√	√	√	√	√	√		√
3*		√	√			√		√	
5*			√		√	√	√	√	
6		√	√	√	√	√	√		
7	√	√	√	√	√	√	√		√
8		√	√	√	√	√		√	√
10	√	√	√	√	√	√	√		√
11		√	√		√	√			√
12	√	√	√	√	√	√			√
13	√	√	√	√	√	√	√		√
14		√	√			√	√		√
15*			√		√	√	√		
16		√	√		√	√	√	√	√
17*			√		√	√	√		
18*			√				√		
19*		√	√			√	√		
20*		√	√		√	√			√

a)

Probable	Possible	Doubtful
Main Fault 1 Fault/fracture 7 Fault/fracture 10 Fault/fracture 13	Fault/fracture 6 Fault/fracture 12	Fault/fracture 5 Fault/fracture 8 Fault/fracture 3 Fault/fracture 11 Fault/fracture 15 Fault/fracture 16 Fault/fracture 17 Fault/fracture 18 Fault/fracture 19 Fault/fracture 20 Fault/fracture 14

b)

Table 6: Discontinuity classification. (a) shows each attribute that corresponded with discontinuity picks, *denotes fault/fractures that are not displayed on horizons but are seen in time-slice and/or VuPack. Faults 2, 4 and 9 were deleted due to interpretation errors. (b) Classification results.

Only two fault/fracture picks (6 and 12) were placed into the “possible” category. Discontinuity pick 6 was seen on all attributes and was not near the edge of the survey, but it did not have extent. Discontinuity pick 12 had extent, corresponded with four out of five of the analyzed attributes but it was located near the edge of the survey and looked as though it could have been picked as a result from edge effects. The remaining fault/fracture picks did not have extent, corresponded with four or less attributes and were either noise induced, had edge effects or both. These discontinuities were all classified as doubtful. Figure 46 (a, b, and c) shows the probable fault/fracture picks on the ANT horizon attribute maps since the ANT attribute has demonstrated the best correspondence of lineaments to discontinuity picks.

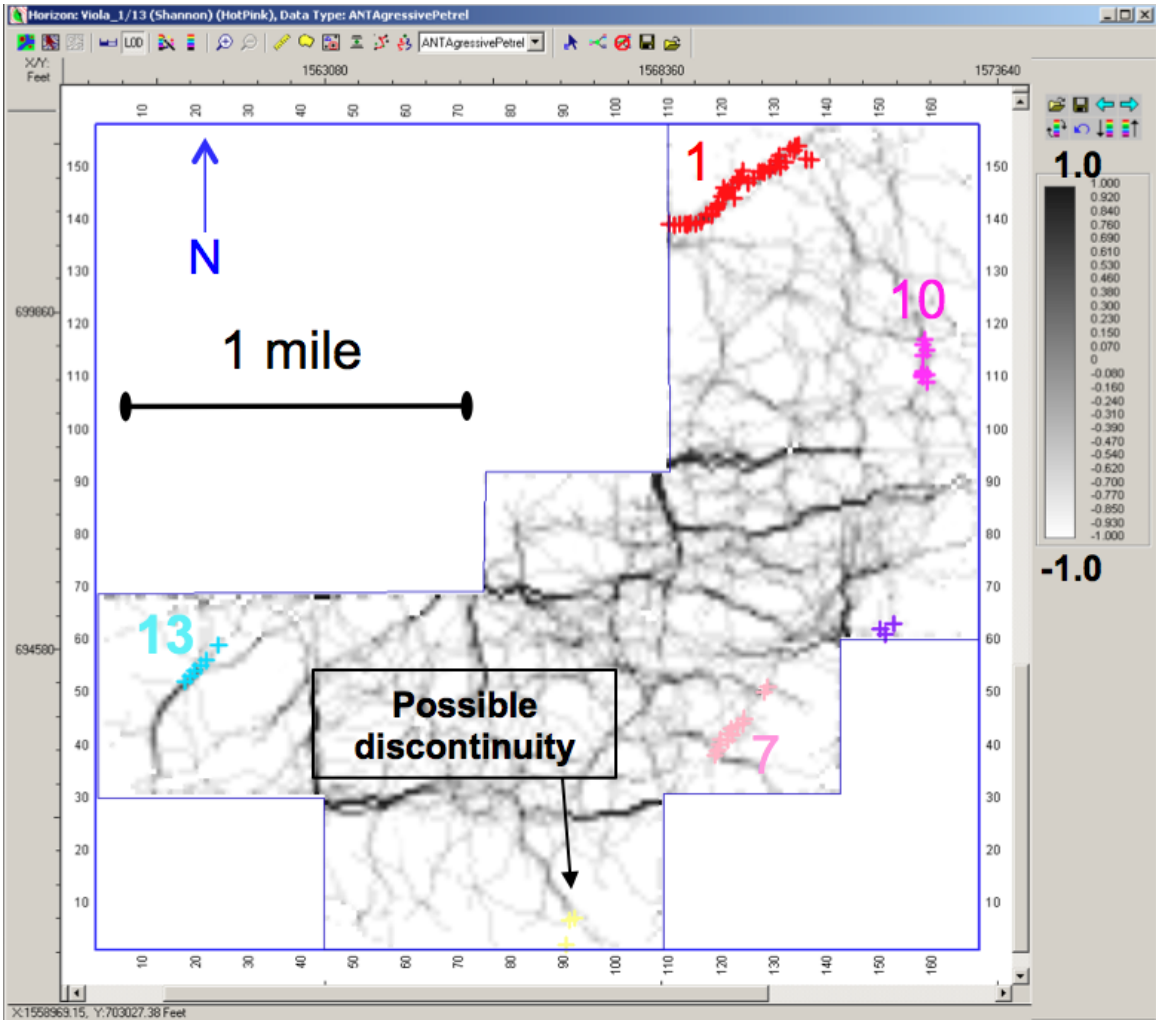

Figure 46 a: Viola ANT map with labeled probable discontinuities.

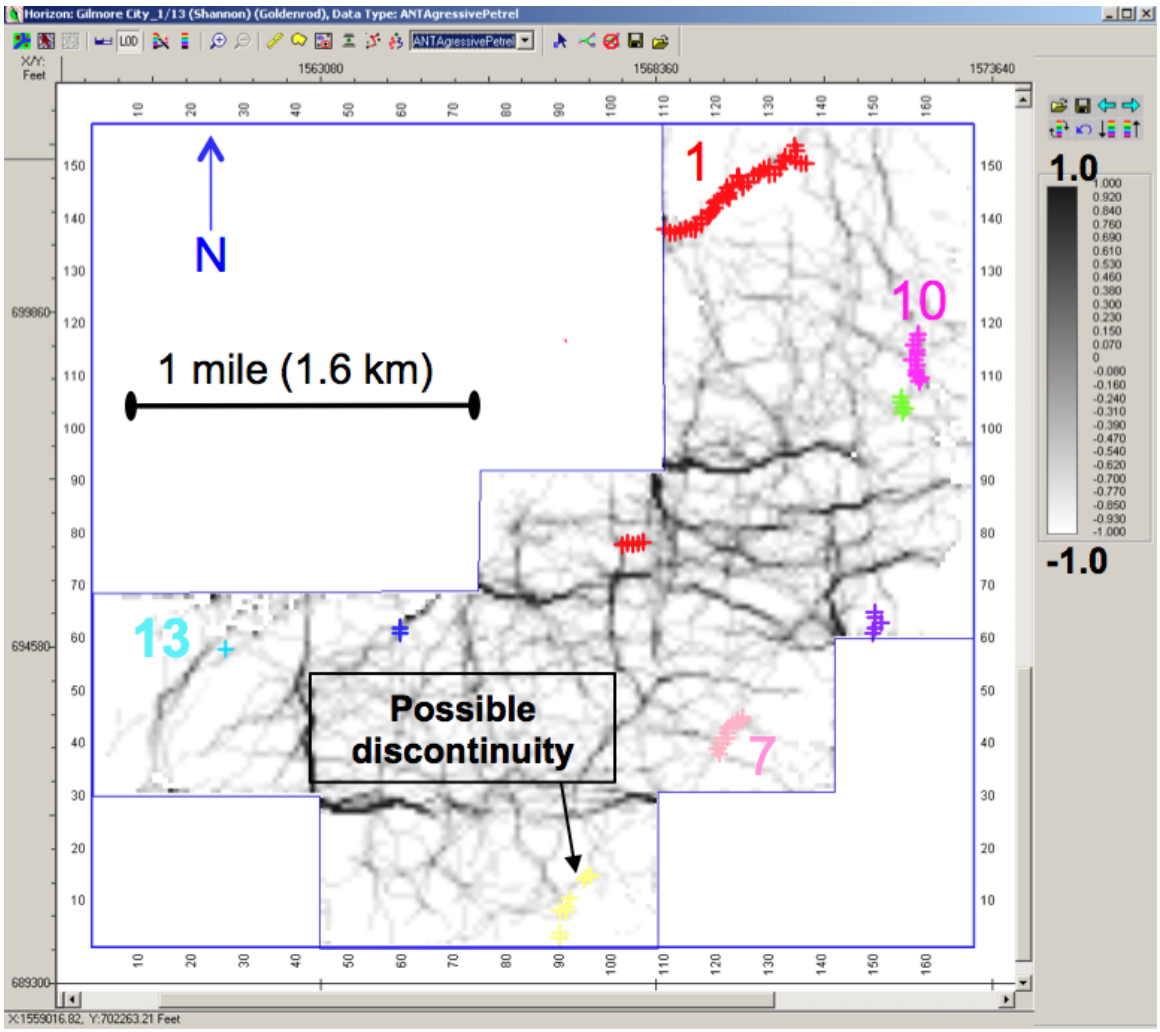

Figure 46 b: Gilmore City ANT map with labeled probable discontinuities.

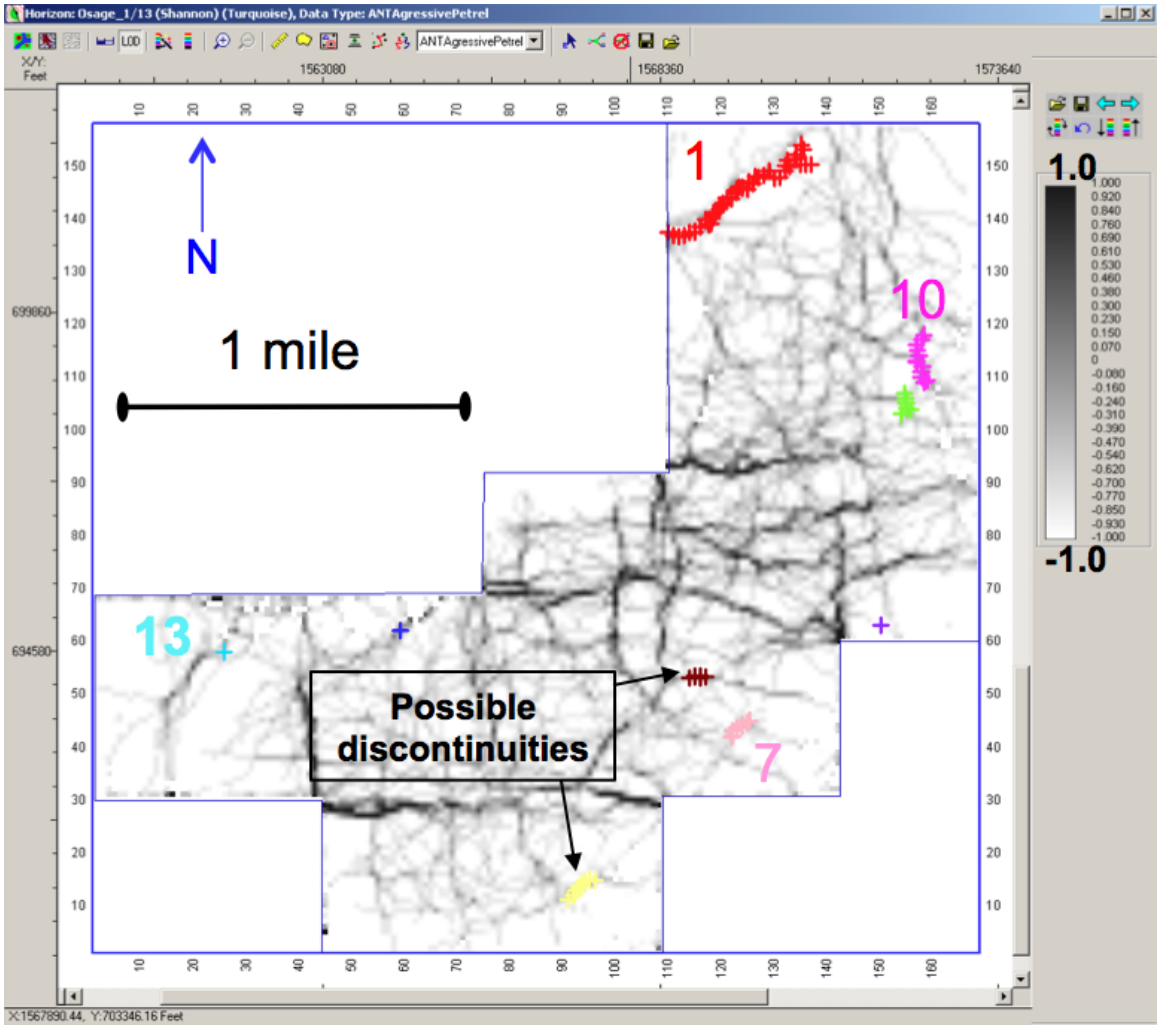

Figure 46 c: Osage ANT map with labeled probable discontinuities.

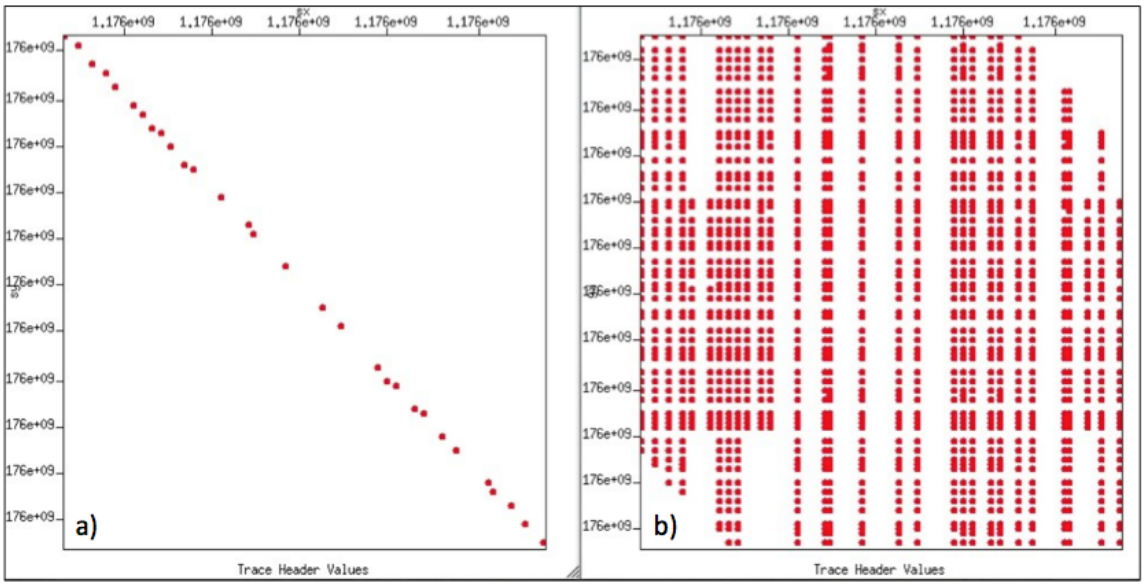

Figure 47: Dickman Field seismic acquisition geometry. (a) Source orientation. (b) Receiver orientation.

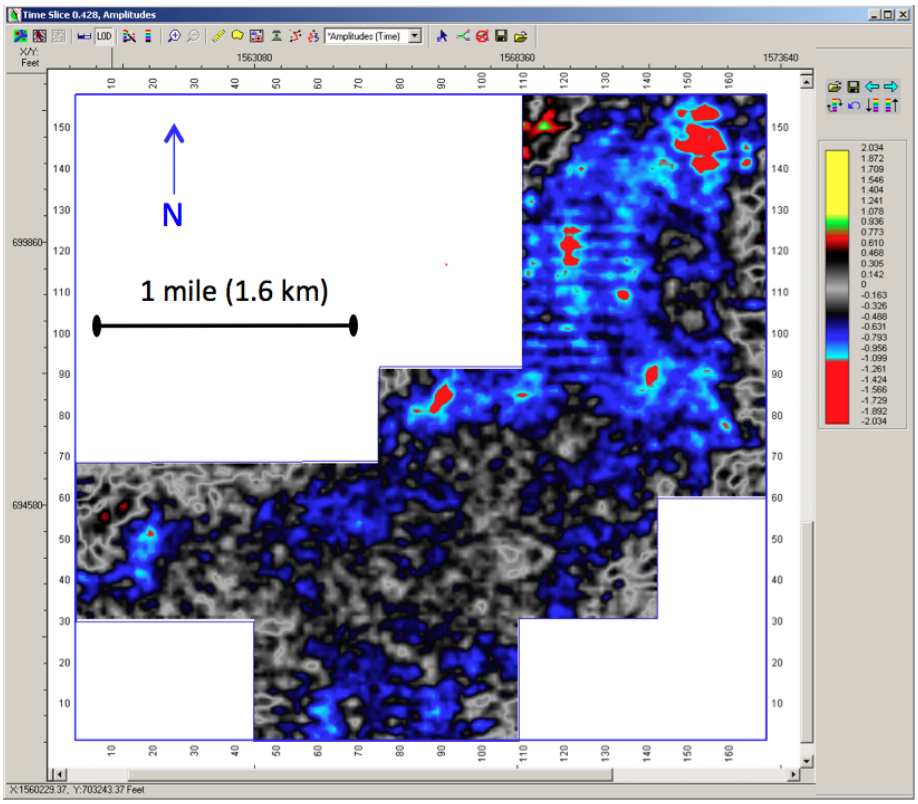

Figure 48: Acquisition footprint (E-W) is clearly observed at shallower depths, timeslice 0.428 sec.

CONCLUSION

Carbon Capture and Storage (CCS) is a developing technology that requires detailed subsurface characterization. The Dickman field serves as a pilot project for CCS with a porous saline aquifer at the Osage formation. Deep formations were mapped in the Dickman field to evaluate structure, faults, and possible fractures. The methods for this investigation included use of several seismic attributes to highlight small faults or fractures. It is important to know the validity and location of these features as they could serve as possible CO_2 leakage pathways.

Amplitude and SPICE data were both carefully examined in vertical section to pick discontinuities and several different attributes were investigated to confirm these features. Surface attributes should not be used alone to located discontinuities, they should be used in order to validate and classify picks made in vertical section using either amplitude or SPICE. The quality of seismic data limited the accuracy of seismic mapping. The vertical resolution in our area of interest was approximately 113 ft. (34 m) and the aquifer is estimated to be less than that in some areas. Stronge edge effects have interfered with interpretation of the Dickman data.

REFERENCES

Blumentritt, C.H., Marfurt, K.J. and Sullivan, C.E., 2006, Volume-based curvature computations illuminate fracture orientations – early to mid-Paleozoic, Central Basin Platform, West Texas: Geophysics, **71**, B159-166

Brown, A.R., 2001, Understanding seismic attributes: Geophysics, **66**, 47-48

Castagna, J., 2011, Personal communication: direct hydrocarbon indicators class

Chopra, S. and Marfurt, K., 2007, Seismic attributes for prospect identification and reservoir characterization: SEG Geophysical Developments Series No. **11**

Chopra, S. and Marfurt, K., 2008, Seismic attributes for stratigraphic feature characterization: Back to Exploration-CSPG CSEG CWLS Convention

Fang, Y., Baojun, B., Dazhen, T., Dunn-Norman, S. and Wronkiewcz, D., 2010, Characteristics of CO_2 sequestration in saline aquifers: Pet. Sci. **7**, 83-92

Jewett, J.M., Bayne, C.K., Goebel, E.D., O'Connor, H.G., Swineford, A. and Zeller, D.E., 1968, The stratigraphic succession in Kansas: Kansas Geological Survey Bulletin, **189**

Liner, C., Zeng, J., Geng, P., King, H., Li, J., Califf, J. and Seales, J., 2010, 3D seismic attributes and CO_2 sequestration: DOE Final Report

Liner, C., Li, C.F., Gersztenkorn, A., and Smythe, J., 2004, SPICE: A new general seismic attribute: SEG Int'l Exposition and 74th Annual Meeting

National Energy Technology Laboratory, 2010, Best practices for: geologic storage formation classification: understanding its importance and impacts on CCS opportunities in the United States, DOE/NETL-2010/1420

Nissen, S.E., Carr, T.R., and Marfurt, K.J., 2006, Using New 3-D seismic attributes to identify subtle fracture trends in mid-continent Mississippian carbonate reservoirs: Dickman field, Kansas: Search and Discovery Article #**40189**

Nissen, S.E., Carr, T.R., Marfurt, K.J., and Sullivan, E.C., 2009, Using 3-D seismic volumetric curvature attributes to identify fracture trends in a depleted Mississippian carbonate reservoir: implications for assessing candidates for CO_2 sequestration: AAPG Studies in Geology **59**, 297-319

Plasynski, S, D. Deel, L. Miller, and B. Kane, 2007, Carbon sequestration technology roadmap and program plan: U.S. Department of Energy, Office of Fossil Energy, National Energy Technology Laborator, e-report

Sawyers, C. and Wilson, T., 2010, An introduction to this special section: CO_2 sequestration: The Leading Edge, **29**, p. 148-149

Sheriff, R. E., 1991, Encyclopedic dictionary of applied geophysics, third edition

Smythe, J. and Gersztenkorn, A., 2004, Gulf of Mexico shelf framework interpretation using a bed-form attribute from spectral imaging: The Leading Edge, **23**, p. 921-926